

Tuo Peter Li
tuo.p.li@gmail.com

Education

- 2009-present **M.D., Ph.D. candidate**
University of Maryland School of Medicine MSTP
Graduate Program in Life Sciences, Program in Neuroscience
Baltimore, MD
- 2005-2009 **Bachelor of Science in Biomedical Engineering**
Focus in Imaging Science
The Johns Hopkins University, Baltimore, MD

Honors

- 2016-17 Nataro MD-PhD scholarship
- 2016 Authored the cover art for an issue in the Journal of Neuroscience (13 April 2016; volume 36 issue 15)
- 2015 Student poster award, 3rd place in the Cellular and Molecular category, the Greater Baltimore Chapter of Society for Neuroscience Meeting, hosted by the University of Maryland, Baltimore
- 2015 The Glaser Prize in Imaging, Department of Physiology, University of Maryland, Baltimore
- 2013-present National Research Service Award of NIMH (F30MH102891) for project on "The Influence of Binding and Crowding on Synaptic Protein Mobility"
- 2013-14 The Leslie B. Barnett Memorial Medical Student Research Fellowship, University of Maryland School of Medicine
- 2013-14 Siddique Award for Medical Student Research, University of Maryland School of Medicine
- 2011-12 Program in Neuroscience Institutional Training Grant 5T32NS063391-09, University of Maryland Baltimore
- 2009 Richard J. Johns Award for Academic Excellence in Biomedical Engineering, Johns Hopkins University
- 2005-9 Dean's List, The Johns Hopkins University

Advanced learning

- 2014 Physics of Living Cells Summer School, Urbana-Champaign, Illinois.
- 2014 Workshop on Computational Methods for Spatially Realistic Microphysiological Simulations in the Pittsburgh Supercomputing Center, Pittsburgh, Pennsylvania

Teaching

- 2014-15 Teaching assistant/student mentor for Proseminar, graduate level class proper methods of scientific inquiry. Program in Neuroscience of the Graduate Program in the Life Sciences at the University of Maryland, Baltimore
- 2014-15 Teaching assistant for an advanced microscopy course, contributed to planning and leading imaging demonstrations, Graduate Program in the Life Sciences at the University of Maryland, Baltimore

Professional affiliations

- 2014-present Society for Neuroscience
2014 American Society for Cell Biology

Conferences attended

- 2016 Molecular Mechanisms in the Synapse: Experiments and Modeling. Janelia Research Campus of Howard Hughes Medical Institute, Ashburn, VA
2015 Annual Meeting of the Society for Neuroscience. Chicago, IL
2015 Gordon Research Seminars and Conference: Excitatory Synapses & Brain Function. Newport, RI
2014 Annual Meeting of the American Society for Cell Biology. Philadelphia, PA
2014 Annual Meeting of the Society for Neuroscience. Washington D.C.
2013 Annual Meeting of the Society for Neuroscience. San Diego, CA
2011 Advanced Course on the Pathophysiology of Basal Ganglia, Cortona, Tuscany, Italy
2011 Annual Meeting of the Society for Neuroscience. Washington D.C.

Service to community, volunteer work, and mentorship

- 2014-15 Promoted neuroscience research for Brain Awareness Week to local high school students. Baltimore, MD
2013 Student Panelist for National Research Service Award Workshop, University of Maryland School of Medicine, Baltimore, MD
2012-14 MSTP Student Mentorship Program: Student mentor to an incoming MD/PhD student throughout their first year to provide support and advice through regular meetings.
2010-11 A Bridge to Academic Excellence. Tutor for disadvantaged primary school children. University of Maryland School of Pharmacy. Baltimore, MD

Committee appointments

- 2014 Selection committee for selecting potential speakers for Stephen Max Memorial Lecture, University of Maryland School of Medicine MSTP, Baltimore, MD
2013 Student judge of oral presentations at the MSTP Summer Research Symposium, where pre-graduate MSTP students presented the results of their summer rotations
2011-13 Interviewer for University of Maryland School of Medicine MSTP
2011-12 Student Council Member, University of Maryland School of Medicine Medical Scientist Training Program

Selected abstracts

- Li TP**, Yu S, Blanpied TA, Raghavachari S. "Postsynaptic crowding can impede the escape of membrane proteins." Conference on the Molecular Mechanisms in the Synapse: Experiments and Modeling. Janelia Research Campus of Howard Hughes Medical Institute. Ashburn, Virginia. May 2016.
Moreira TH, **Li TP**, Jafri MS, Krause GB, Tang CM. A high resolution, 3D atlas of the fiber tracts near the human STN based on optical anisotropy. Program No. 51.12. 2011 Neuroscience Meeting Planner. Washington, DC: Society for Neuroscience, 2011.
Zhuo J, Mullins J, Hazelton J, Simon J, Xu S, **Li T**, Fiskum G, Gullapalli R. Diffusion Kurtosis - A sensitive marker for Traumatic Brain Injury (TBI). Proc. Intl. Soc. Mag. Reson. Med. 19 (2011). 703.

Selected oral presentations

- Li TP.** "Super-resolved neuroscience: light microscopy at the smallest possible scales." A 15-minute talk in a newly implemented one-hour series named New Methods in Neuroscience, at Program in Neuroscience annual retreat. Baltimore, MD. June 2015.
- Li TP.** "Anisotropic Scattering Imaging: an approach to map the human connectome." Award reception talk for the Barnett and Siddique research awards. Baltimore, MD. June 2014.
- Li TP, Yu S, Raghavachari S, Blanpied TA.** "The influence of binding and crowding on synaptic protein mobility." Poster presentation at the Society for Neuroscience annual regional meeting, Baltimore, MD, November 2013.
- Li TP.** "The influence of binding and crowding on synaptic protein mobility." Oral presentation at the MSTP annual retreat, Baltimore, MD, August 2013.
- Li TP, Kvarita MD, Wied H, Wilson K.** "Surviving and thriving in graduate school: on selecting lab and applying for NRSA." [Panel discussion for MSTP medical students who are transitioning into graduate school]. MSTP annual retreat, Baltimore, MD, August 2013
- Li TP, Kvarita MD.** "Transitioning from medical school to graduate school" [Presentation]. UMSOM 3rd Annual MSTP Retreat. Baltimore, MD, 2012
- Li TP, Kvarita MD.** "MS1 Survival Guide" [Presentation]. UMSOM 3rd Annual MSTP Retreat. Baltimore, MD, 2011
- Li TP.** "A novel approach to mapping human brain connectivity." The MSTP Research Symposium, University of Maryland School of Medicine, Baltimore, MD, August 2011.

Publications

- Li TP, Blanpied TA** (2016). Control of transmembrane protein diffusion within the postsynaptic density assessed by simultaneous single-molecule tracking and localization microscopy. *Frontiers in Synaptic Neuroscience* (in press).
- Tang AH, Chen H, **Li TP**, Metzbowser SR, MacGillavry HD, Blanpied TA (2016). A transsynaptic nanocolumn aligns neurotransmitter release to receptors. *Nature* (in press).
- Li TP, Song Y, MacGillavry HD, Blanpied TA, Raghavachari S** (2016). Protein crowding within the postsynaptic density can impede the escape of membrane proteins. *The Journal of Neuroscience*, 36(15), 4276–95.
- Shin RK, Qureshi RA, Harris NR, Bakar D, **Li TP**, Jafri MS, Tang CM (2014). Wilbrand's knee. *Neurology*, 82(5), 459–60.
- Kvarita M, **Li TP** (2013). MSTP matches coast-to-coast for residency training. *Dual Decree* (the periodic newsletter of UMSOM MSTP). Vol IV:2.
- Gehlbach PL, Benson BC, Cortes HM, Davenport MS, Harrison RM, Hwang K, Kapp GM, Lee CY, Lerman JA, **Li T**, Wong JC (2008). Multifunctional neck brace. *US Patent Application Publication*. Pub. No. 2008/0004556 A1. Jan 2008.

Abstract

Title of dissertation: The influence of binding and crowding on the mobility and organization of transmembrane proteins within the synapse

Tuo Peter Li, Doctor of Philosophy, 2016

Dissertation directed by Thomas A. Blanpied, Associate Professor, Department of Physiology and Program in Neuroscience

Postsynaptic transmembrane proteins are important elements of synapses. Positioning and mobility of each member of this large class of proteins dictate their individual function at the synapse. One critical example is that the position of glutamate receptors within the postsynaptic density (PSD) strongly modulates their function by aligning or misaligning them with sites of presynaptic vesicle fusion. However, factors that control receptor mobility and spatial organization within the synapse are not well understood. Scaffold proteins in the PSD are abundant receptor binding partners, and electron microscopy suggests that the PSD is highly crowded, potentially restricting the diffusion of receptors regardless of binding. I complemented computational approaches with empirical data to test the effect of synaptic crowding on receptor movement and positioning in rat hippocampal neurons. Simulation of receptor diffusion in synapses containing previously measured distribution of scaffold proteins predicted that the variation of receptor size and the organization of scaffold proteins each strongly influences the positioning and mobility of receptors within the synapse. Using high-resolution and super-resolution imaging of custom-designed transmembrane (TM) probes, I found that a single-pass TM protein with a single PDZ binding motif was more mobile than the much larger AMPAR. Moreover, either the single binding motif or an increase in bulk slowed the synaptic movement of the small TM probe, suggesting that both crowding and binding can limit the escape of

AMPARs from the synapse. By measuring synaptic architecture and TM protein movement simultaneously, I found that the TM probe that does not bind PSD-95 could be as stabilized as the binding variant in regions of high PSD-95 density, suggesting that crowding by scaffold molecules and perhaps other proteins is sufficient to stabilize receptors even in the absence of binding. Interestingly, single-molecule mapping showed that excitatory neurotransmitter release preferentially occurs over these regions. Using a deterministic computer modeling approach, I found that this type of release-receptor alignment can modulate the synapse potency by 20-30%. Altogether these results demonstrate that tight protein packing within the PSD may organize TM proteins within the synapse by modulating their dwell times, thereby tuning synaptic strength.

The influence of binding and crowding on
the mobility and organization of transmembrane proteins within the synapse

by
Tuo Peter Li

Dissertation submitted to the Faculty of the Graduate School of the
University of Maryland, Baltimore in partial fulfillment
of the requirements for the degree of
Doctor of Philosophy
2016

©Copyright 2016 by Tuo Peter Li
All rights reserved

To Bingqing “Amanda” Ye, who put up with the author for the past four years, and arranged a comfortable climate to write in.

Preface

Neuropsychiatric disorders are the leading cause of disability in the United States. In fact, neurological disorders, mental, and behavioral disorders combined account for nearly a fifth of the disability burden in the U.S. quantified by the counting the total number of years lost to illness, disability, or premature death (Murray et al., 2013). The neuropsychiatric disorders that are severely debilitating affect about 6 percent of the adult U.S. population, and are very costly to society. In fact, a conservative estimate of the costs due to disability benefits, health care expenditures, and earnings lost exceeds \$300 billion dollars per year for the U.S.A. (NIMH, 2002). International estimates including both the adult and pediatric populations is even graver. Sadly, medications do not exist to treat the core symptoms of, much less cure, many of these disorders.

Neuropsychiatric disorders manifest in many different forms. They are believed to result from poorly wired connections among neurons in the developing brains, or from disrupted connections in the matured brains. In fact, before macroscopic changes in brain morphology or slightly more subtle alterations like brain cell loss and cell death can be observed, many types of neuropsychiatric disorders are associated with microscopic changes such as alterations in the number and function of brain connections (Glantz et al., 2006; Hutsler and Zhang, 2010; Penzes et al., 2011). Further supporting this theory, genetic studies have shown that genes encoding proteins important to the functions of brain connections are altered in neurological and psychiatric disorders (Betancur et al., 2009; Hall et al., 2015). Thus, these diverse forms of disorders could involve a common microscopic feature that is fundamentally important in brain circuit performance: the microscopic juxtapositions between brain cells, also known neuronal synapses. It is possible that altered synaptic structure and function contributes to abnormalities in specific brain circuits, which in turn may underlie the symptoms characteristics in the patients suffering from these disorders.

I believe that understanding the normal synapse structure and function is indispensable before diving into the more complex and diverse realm of abnormalities. Sadly, mechanisms that regulate these structures are still poorly understood even in healthy synapse assembly. This dissertation is an attempt to unravel a few but important aspects of how synapses are put together with their many molecular components that are critically important for synapse function. An ultimate aim of my career is to identify subtle synaptic pathology when it occurs, and develop ways to intervene.

The project had a tortuous beginning, but at least one unifying theme: biomedical imaging. In the summer of 2012, I completed the first two years of medical school and began graduate training in neuroscience. I wanted to approach neuroscience research using imaging techniques as I had long been fascinated by the beauty of the central nervous system and the technologies that can capture it. As I rotated through labs that employed macroscopic imaging techniques such as magnetic resonance imaging or a finer-scale imaging approach that could trace out the pathway of axons, I had initially envisioned mapping out the brain better than my predecessors had. However, I soon realized that the goal was overly ambitious and I lacked the resources for such a large undertaking. Most importantly, I realized that a map is only as useful as how well we understand the structure and function of the elements within it. Fortunately, I was guided into a more manageable project in which I employed exciting and informative imaging techniques.

Significance statement

Small alterations to the distribution of key transmembrane proteins within individual neural synapse can dramatically change the strength of synaptic transmission. Indeed, many diseases are thought to unbalance neural circuit function in this manner. However, processes that regulate this in healthy synapses are unclear. By combining computer simulations with imaging methods that examined protein organization and dynamics at multiple scales in space and time, we showed that both steric effects and protein-protein binding each regulate the distribution and mobility of transmembrane proteins in the synapse. *Our findings extend our knowledge of the synapse as a crowded environment that counteracts molecular diffusion, and support the idea that both molecular collisions and biochemical binding can be involved in the regulation of neural circuit performance.*

Acknowledgements

First and foremost, I want to thank my thesis advisor, Thomas Blanpied. He was a great teacher. I sincerely appreciated that he tried to teach me how to fish rather than feeding me fish when I was drafting a grant, manuscripts, or slides for talks. He questioned many things. His way of questioning inspired me not to accept findings at their face values and encouraged me to dig deeper about techniques I and others used, so that I can see their limitations and make proper interpretations. He was humorous. Silly anecdotes of his time as a graduate student helped me relax during stressful times. He did not take himself too seriously, and had a joke for almost every situation. However, he was not all about jokes. His timely anecdotes of feats by his colleagues challenged me to push myself. Importantly, he took the science very seriously. I will not be able to imitate his sense of humor, but I hope to be as self-critical, if not more, in my future career. Tom genuinely cared about my well-being, and gave ample attention to me (and everyone else in the lab). Every time I went to his office, he stopped what he was doing nearly every time to listen to what I had to say. He also ensured that I did not miss any career opportunity to challenge and grow me, whether it be a summer course, a conference, or workshop. Tom was fun to be around. His genuine curiosity and willingness to try new things and learn about a different culture have made my many interactions with him entertaining. He has great time management and organizational skills, with which he has been able to set himself up to spend quality time both with his lab and his family. He also taught me a few things outside the lab like the sport of squash, which is a much more efficient exercise than rock climbing and just as physically demanding. This has enabled me to spend more time in the lab but also with my wife. I believe that he has influenced me to become a better scientist and person. It was truly a privilege to work and play with him. I will consider myself lucky if I can be half as good of a mentor as he is.

A proverb has it that “it takes a village to raise a child.” I certainly agree and believe that it takes more than a lab to raise a graduate student. Fortunately, I found myself in a fun and inspiring lab. Tom Blanpied had knack for attracting people with exceptional work ethics, creativity, and personality. His entire lab has influenced how I do science and how I approach life inside and outside the lab. Harold MacGillavry's tireless work ethics and strong devotion to family inspired me to follow suit. He embodied a rarely followed aphorism, “Don't put off 'til tomorrow what you can do today.” I thank him on my wife's behalf that I will change my future children's diapers just as he did for his. I thank Harold for many of the timesaving lab tips (e.g. keeping a searchable digital lab notebook and using an automated referencing software for writing) which helped me maximize time designing and doing experiments. Hsiangmin Emily Lu took time out of her busy schedule to teach me some of the experimental techniques that were foreign to me, and for this I am very grateful. More importantly, I thank her for encouraging me to take an impromptu trip abroad, where I met the love of my life. In addition, I thank Sarah Metzbower, Haiwen Chen, Sai Sachin Divakaruni, and Aihui Tang for their honest and constructive criticisms on my many practice presentations, draft documents, and preliminary ideas. In particular, I thank Sai for many sessions of squash and for inspiring me to eat less meat and more vegetables. I thank Minerva Contreras and Tamar Davis for all the beautiful cells they have cultured, and for helping me to develop proper lab habits. I thank Minerva in particular on behalf of soon-to-be-my-dog, Elmer, for tips and tricks on caring for a Labrador.

Two approaches stand at the epicenter of this dissertation--both complement each other very well. The first is computer simulation, which would not be possible without Sridhar Raghavachari and Yu Song. Sri's brilliant ideas launched the project. The second is imaging of molecular organization and dynamics, and the technical details can be quite involved and demanding. I owe much of my technical competence to Harold McGillavry and Hsiangmin Emily Lu, Aihui Tang, and Thomas Blanpied.

My thesis committee members have been very helpful. Scott Thompson truly cared about not only the quality of my training but also my personal well-being. I believe all of his trainees would say the same. I went through a rough patch in the graduate program and almost quit, but Scott sat me down, looked me in the eyes, and said "Let me know if there is anything I can do." Knowing that the chair of Physiology was my advocate gave me a boost I needed to keep going. I thank Paul Welling for challenging me to think more broadly on the implication and the applicability of my research for clinical medicine, and for teaching me the nuances of protein-protein interactions involving in transmembrane protein trafficking. I thank Bruce Krueger for engaging me in the off-the-cuff, stimulating scientific discussions during Friday social hours. He cared about my well-being and reminded me to think ahead about my career. I thank Sridhar Raghavachari for the many in-person and Skype discussions, which informed a great deal about my experiments.

Besides these professors, at least several other faculty members in the University deserve dedicated acknowledgement. I thank Norbert Myslinski for accepting my late application for a summer research program in 2004. I am grateful that he introduced me to Ramón y Cajal and gifted me one of his books, "Advice for a Young Investigator." It has been an invaluable guiding force ever since. I thank Samir Jafri and Cha-Min Tang, my first research co-mentors. Even though I had no research experience whatsoever before entering their lab, they exhibited tremendous patience on my very amateur writing, presentation, and reasoning skills. Importantly, they taught me to see problems as opportunities to innovate instead of nuisances that impede progress. Later in my research training, I am very fortunate to have met Tom Abrams and Brad Alger. They taught and challenged me to practice the proper ways of scientific inquiry. I thank Brad in particular on showing me a simple and logical way to present science. I thank Tom Abrams for numerous discussions, which helped hone my scientific reasoning skills. Importantly, I thank Tom Abrams for arranging a short rotation in the Blanpied lab—I would not have met so many great scientists without him.

I want to thank two former members of the Thompson lab, Mark Kvartha and Adam Van Dyke. They were always ready to listen whenever I needed to vent on those unproductive days. In particular, I thank Mark for the many evening walks to the garage when we shared our ups and downs.

I thank the Medical Scientist Training Program at the University of Maryland for the training opportunity. Terry Rogers took a chance on me and I am still grateful he did. He was an encouraging and caring director for as long as I was under his directorship and beyond. Even though he has now moved to a different leadership position, he continues to care and check up on all of his recruits.

Renee Cockerham who runs the Program in Neuroscience (and Jenn Aumiller who used to) were indispensable during my training. I thank them for helping me stay on top of student responsibilities such that I may maximize my time being productive in the lab.

I am grateful for the Grace Life Church, a non-denominational church under the leadership of Pastor Roger Kim. The church family has helped me to appreciate many of the difficulties I have faced and helped me to see them as opportunities to grow. And they helped me to shift much of my attention away from my self and into the problems of people around me, and be a solution instead of a problem.

I will forever be indebted to my parents, who gave up their flourishing careers in China so that I may have the best possible education and the most possible number of opportunities in the United States. I sincerely appreciate that they provided me with all the resources they could to enable me to explore all sorts of career options. Though my parents initially advised against my decision to go through the long process of obtaining two advanced degrees, they nonetheless supported me through this journey. As soon as I was old enough to taste the sweetness of winning and the bitterness of losing a competition, my father taught me that becoming better than myself is more important than being better or farther along than others. This has certainly helped me stay level-headed throughout the course of my graduate studies, particularly when my cohort of medical students moved onto the next phase of medical training while I remained at the lab bench.

Most importantly, I want to thank my beautiful better half, Bingqing “Amanda” Ye. She is responsible, and inspires me to use my time wisely. She is optimistic, and gleans important lessons from failures. She is empathetic, and makes stressful times seem not so bad. She is smart and curious, and makes our conversations interesting and fun. She has been with me through thick and thin, and seen the best and the worst of me over the past four years; yet, she has stayed and brings out the best in me. I feel extremely blessed to have her as a teammate for life.

Table of contents

Chapter 1 General introduction.....	1
The role of synaptic structure in its function	4
Receptor distribution within the synapse dictates synaptic strength	7
Receptor trafficking	13
Factors that could control the distribution of receptors and other TM proteins in the PSD	16
Techniques to measure transmembrane protein diffusion	17
Receptor dynamics within individual synapses	22
Retaining synaptic proteins through steric hindrance	26
Chapter 2 Protein crowding within the postsynaptic density can impede the escape of membrane proteins.....	29
Abstract	29
Introduction.....	30
Materials and Methods.....	32
Results.....	47
Discussion.....	77
Chapter 3 Control of transmembrane protein diffusion within the postsynaptic density assessed by simultaneous single-molecule tracking and localization microscopy	83
Abstract	83
Introduction.....	84
Materials and Methods.....	86
Results.....	90
Discussion.....	101
Chapter 4 Quantifying the effect of sub-synaptically aligned neurotransmitter release and receptors on synaptic strength.....	105
Abstract	105
Introduction.....	105
Materials and Methods.....	108
Results.....	111
Discussion.....	116
Chapter 5 Limitations	121
Abstract	121
Overexpression of chimeric proteins	121
Automatic identification of PSDs and extrasynaptic tracks	123

Agents other than PSD-95 which can contribute to postsynaptic crowding.....	126
Receptors as crowding agents	126
Disadvantages of PALM-PAINT.....	128
Chapter 6 General discussion.....	130
The role of probe-scaffold binding interaction	130
The role of TM protein size in the mobility and distribution of synaptic TM proteins	131
The role of PSD architectural organization in the arrangement and stability of synaptic TM proteins.....	133
What kind of proteins can participate in crowding?	135
The role of PSD architectural dynamics	138
Implications for synapse function.....	139
Potential regulators of crowding within the synapse.	143
Relation to disease mechanisms.....	144
References.....	147

List of tables

Table 2.1. <i>Simulation parameters</i>	33
Table 2.2. <i>Correlation between FRAP and either PSD area or spine enrichment of various TM probes</i>	71

List of figures

Figure 1.1. <i>Functionally important elements of an excitatory synapse.</i>	1
Figure 1.2. <i>The PSD structure is diverse.</i>	6
Figure 1.3. <i>Synaptic strength can be modulated by changing the organization of AMPARs without changing the total number of receptors</i>	8
Figure 1.4. <i>Both membrane trafficking and lateral diffusion determine synaptic AMPAR content.</i>	15
Figure 1.5. <i>Multiple protein-protein interactions at the PSD.</i>	16
Figure 1.6. <i>Schematic of fluorescence recovery after photobleaching experiment.</i>	18
Figure 1.7. <i>Different modes of diffusion detectable by single particle tracking.</i>	21
Figure 1.8. <i>Three conceptual models for receptor diffusion within the synapse.</i>	24
Figure 2.1. <i>Synaptic crowding can retain membrane proteins in a size-dependent manner.</i>	50
Figure 2.2. <i>The arrangement of PSD-95 molecules can prolong the retention of synaptic AMPAR.</i>	51
Figure 2.3. <i>Small and large membrane proteins exchange differently on the surface membrane of dendritic spines.</i>	54
Figure 2.4. <i>The surface mobility of AMPAR in spines is unrelated to synapse size or spine-dendritic concentration gradient; that of the small probe is weakly related to synapse size.</i>	57
Figure 2.5. <i>Small membrane probe has higher subsynaptic mobility than AMPAR.</i>	60
Figure 2.6. <i>Diffusion of small membrane protein and AMPAR within and near the excitatory synapse.</i>	64
Figure 2.7. <i>PDZ-mediated binding is partly responsible for stabilizing the synaptic mobility of a small membrane probe.</i>	69
Figure 2.8. <i>Intracellular protein bulk can influence the mobility of small membrane protein.</i>	73
Figure 2.9. <i>Divalent PDZ-binding motifs can stabilize TM proteins within the synapse more than monovalent binding can.</i>	75
Figure 3.1. <i>PALM-PAINT, single-molecule tracking during PALM imaging.</i>	91
Figure 3.2. <i>Better discrimination of PSD border reveals strong reduction of mobility within synapses.</i>	92
Figure 3.3. <i>PSD size and density do not correlate with intrasynaptic mobility.</i>	93
Figure 3.4. <i>Nanoscale regional density of PSD-95 within the synapse correlates with probe diffusion coefficient.</i>	96
Figure 3.5. <i>A non-binding transmembrane protein enters and slows within the synapse, but not as much as if it can bind PSD-95.</i>	97
Figure 3.6. <i>Subsynaptic regional density of PSD-95 influences the mobility of a probe that does not bind PSD-95.</i>	98
Figure 3.7. <i>Estimating how dense PSD-95 is when protein mobility is slowed sterically.</i>	100
Figure 4.1. <i>Sites of glutamate release preferentially align with regions of high PSD-95 density</i>	107
Figure 4.2. <i>Preferential release in nanocolumns can increase synaptic strength.</i>	115

Figure 5.1. *The AMPARs and small membrane probes diffuse similarly in unenriched nonsynaptic regions.* 125

List of abbreviations and symbols

AChR	acetylcholine receptor
AD	Alzheimer's disease
AMPA	α -amino-3-hydroxy-5-methyl-4-isoxazolepropionic acid receptor
ASD	Autism spectrum disorder
AZ	active zone
CA1	cornu ammonis area 1
CaMKII	Ca ²⁺ /calmodulin-dependent protein kinase II
cDNA	complementary
CNS	central nervous system
Deff	effective diffusion coefficient
dsDNA	double stranded deoxyribonucleic acid
ECM	extracellular matrix
EM	electron microscopy
EPSC	excitatory postsynaptic current
FKBP	FK506 (Tacrolimus) binding protein
FRAP	fluorescence recovery after photobleaching
FRB	FKBP and rapamycin binding domain of a protein called mammalian target of rapamycin
GFP	green fluorescent protein first isolated from the jellyfish <i>Aequorea victoria</i>
GKAP	guanylate kinase-associated protein
GluA2	glutamate receptor of AMPA-type subunit 2
GluK2	glutamate receptor of kainate-type subunit 2
Kflip	the rate at which photobleached receptors get replaced by fluorescent receptors when they encounter the boundary of simulation
Koff	rate of dissociation between receptor and scaffolding molecule
Kon	rate of association between receptor and scaffolding molecule
LRRTM	leucine-rich repeat transmembrane protein
LTD	long-term depression
LTP	long-term potentiation
MAGUK	membrane-associated guanylate kinase
mCerulean3	monomeric GFP variant that emits blue fluorescence
mCherry	monomeric red fluorescent protein derived from a protein isolated from <i>Discosoma</i> coral
mEos-TM	single-pass transmembrane chimeric protein made with the mEos fluorescent protein on the extracellular domain and the transmembrane domain of platelet derived growth factor receptor

mEos-TM-Bind	single-pass transmembrane chimeric protein made by fusing the cytoplasmic tail of stargazin on the intracellular domain of mEos-TM
mEos-TM-Cerulean	single-pass transmembrane chimeric protein made by fusing the mCerulean protein on the intracellular domain of mEos-TM
mEos-TM-Nonbind	single-pass transmembrane chimeric protein made by fusing the nonbinding mutant variant of cytoplasmic tail of stargazin on the intracellular domain of mEos-TM
mEos2/3	monomeric photoswitchable fluorescent protein derived from a protein isolated from the coral <i>Lobophyllia hemprichii</i>
mEPSC	miniature excitatory postsynaptic current
MSD	mean squared displacement
mTagBFP	monomeric blue fluorescent protein derived from a protein isolated from sea anemone <i>Entacmaea quadricolor</i>
NMDAR	N-methyl-D-aspartate receptor
OCD	obsessive-compulsive disorder
PALM	photoactivated localization microscopy
PALM-PAINT	PALM combined with uPAINT
PDZ	protein-protein interaction motif. The acronym combines the first letters of three protein which were first discovered to share the domain: postsynaptic density protein (PSD-95), Drosophila disc large tumor suppressor (Dlg1), and zonula occludens-1 protein (zo-1)
PSD	postsynaptic density
RIM1/2	regulating synaptic membrane exocytosis protein
SAP102	synapse-associated protein 102
SDS	sodium dodecyl sulfate, an anionic surfactant
SDS-FRL	SDS-digested freeze-fracture replica labeling
SEP	superecliptic phluorin, a pH sensitive variant of GFP
SEP-TM	same as mEos-TM except the mEos is replaced by SEP
SEP-TM-Bind	same as mEos-TM-Bind except the mEos is replaced by SEP
SEP-TM-Cerulean	same as mEos-TM-Cerulean except the mEos is replaced by SEP
SEP-TM-Nonbind	same as mEos-TM-Nonbind except the mEos is replaced by SEP
SMT	single-molecule tracking
SPT	single-particle tracking
Stg	Stargazin
StgCtail	the cytoplasmic tail of stargazin
STORM	stochastic optical reconstruction microscopy
TARP	transmembrane AMPAR regulatory protein
TM	transmembrane

uPAINT universal point accumulation imaging in nanoscale topography
ZDC2 Z drift compensation, a fully motorized Olympus module to correct focal drift in the axial plane

Chapter 1

General introduction

The proper execution of complex human behaviors such as learning is mediated by exquisitely regulated performance of neural circuits. Changes in the strength of synaptic connections was first speculated to be the mechanism underlying learning and memory more than a century ago (Ramón Y Cajal, 1894) (as interpreted by Jones (1994) and Berlucahi and Buchtel (2009)). More concrete synaptic models were proposed decades later (Konorski, 1948; Hebb, 1949), but it was not until the discovery of long-term potentiation (LTP) (Bliss and Lomo, 1973), in which a brief high frequency synaptic stimulation results in a long lasting increase in synaptic strength, that this model was supported by empirical evidence. Since then, a large number of studies have been devoted to clarifying the mechanisms that mediate and modulate synaptic strength.

At the synapses, or near-physical contacts between brain cells, electrical signals from one neuron are converted to chemical signals when chemical neurotransmitters released from the presynaptic terminal diffuse across the cleft to activate receptors on the postsynaptic neuron. The neurotransmitters open postsynaptic receptor channels which

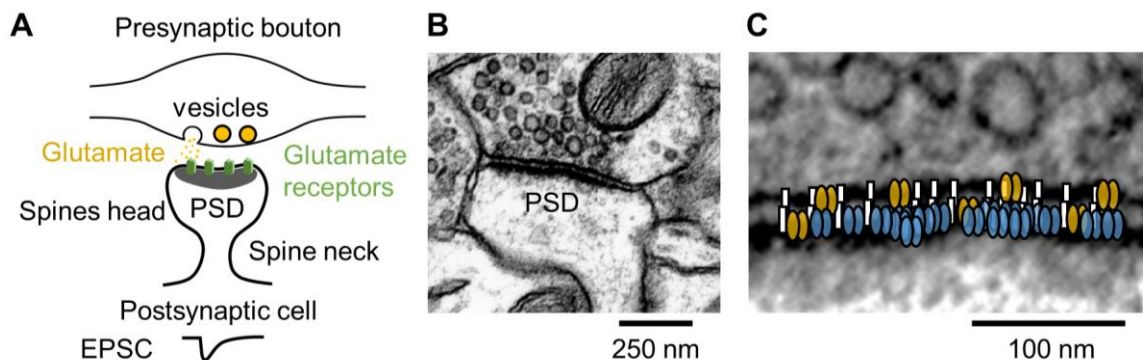


Figure 1.1. Functionally important elements of an excitatory synapse.

(A) Cartoon illustrating the release of glutamate (yellow) from a presynaptic terminal onto postsynaptic receptors (green) in the postsynaptic density (grey) on a dendritic spine. A typical excitatory postsynaptic current (EPSC) response. (B) Electron micrograph (EM) of an excitatory synapse in a rat hippocampus (Kristen Harris). (C) Cartoon illustrating transmembrane proteins such as adhesion molecules (white), ion channels (yellow), and neurotransmitter receptors (blue) superimposed on an EM of a synapse.

allow the passage of ions and propagate the electrical signal in the postsynaptic neuron (Fig. 1.1A,B). Changing the number or the conductance of postsynaptic receptor channels tunes the synaptic strength (Benke et al., 1998; Malinow and Malenka, 2002; Song and Huganir, 2002). However, it is becoming increasingly clear that synaptic strength is the net result of numerous factors; an important general principle is that transmembrane (TM) proteins establish the basis for this function. Adhesion molecules link the pre- and postsynaptic membranes; ion channels on each side of the synapse initiate and control signaling; neurotransmitter receptors gate both chemical and electrical responsiveness (Fig. 1.1C). Thus, in an important sense, the precise architectural organization of TM proteins at a single synapse determines how the synapse will operate (Sheng and Hoogenraad, 2007). Indeed, mutations of many of these TM proteins have been identified as causes of autism spectrum disorder, Tourette's syndrome, learning disability, and schizophrenia (Bear et al., 2004; Sudhof, 2008).

The excitatory synapses are arguably the best characterized among many types in the mammalian brain. They play critical roles in information processing and experience-dependent plasticity which are believed to underlie many forms of learning and memory (Martin and Morris, 2002; Kessels and Malinow, 2009). This type of plasticity involves increases in the strength of synaptic connections, and this potentiation can last any duration from tens of minutes up to a year (Bliss and Gardner-Medwin, 1973; Bliss and Lomo, 1973; Abraham et al., 2002). In this way, long-lasting synaptic plasticity at excitatory synapses are believed to convert experiences into stored information that can be retrieved later.

The association between persistent potentiation in synaptic strength and the formation of a kind of memory is best understood in the hippocampus (Squire, 1992)

Neuropsychological studies of the patient H.M. who became amnesic after the surgical removal of both medial temporal lobes (Scoville and Milner, 1957) preceded a number of studies on the hippocampus and its connected regions. Further studies in rodents with hippocampal lesions (Hirsh, 1974) and patients with hippocampal damage (Squire, 1982) indicate that the hippocampus is essential for a type of memory. Two important studies strongly support that LTP in the hippocampus mediates spatial memory formation and retrieval. Firstly, Whitlock et al. (2006) found that rats which were conditioned to avoid a specific chamber by electric shock developed a specific set of potentiated synapses as measured by *in vivo* electrical recordings; importantly, a LTP induction protocol which could normally boost synaptic strength failed to further increase the synaptic strength in these synapses, suggesting that the learning-induced potentiation and the electrically stimulated potentiation utilize the same pathway. Secondly, studies from the group of Todd Sacktor (Pastalkova et al., 2006; Tsokas et al., 2016) showed that injecting a peptide inhibitor into the hippocampus which abolishes LTP was sufficient to reverse the shock-conditioned memory in rats that learned to avoid a section of a moving platform. These data indicate that changes in synaptic strength play a causal role in hippocampal learning and memory.

Given the clinical and fundamental importance of excitatory synaptic transmission and plasticity, intensive efforts have been devoted to understanding their mechanisms of action and regulation. Nonetheless, many aspects of how synapses perform chemico-electrical conversion of information remain poorly understood, even in the absence of plasticity during basal synaptic transmission. Particularly, it remains for the most part

unclear precisely how critically important transmembrane proteins get to the synapse, and once there how they are retained and positioned appropriately.

One reason for the slow progress was due the lack of tools to study the precise movement and spatial organization of individual proteins, in living neurons. However, there has been a renaissance of synaptic neuroscience as more advanced imaging methods have enabled us to see the internal structure of the living synapse and test how it can influence the organization of transmembrane proteins.

In this general introduction, I will highlight major findings related to how the internal architectural structure of excitatory synapses could modulate synaptic function. I will also focus on how the organization of transmembrane proteins and its regulation within the synapse are less well understood. I will argue that the spatial organization of a protein is just as important as its number or composition in modulating synaptic strength. This introduction sets the stage for the results of this dissertation in advancing the current knowledge on the mechanisms that regulate the mobility and positioning of TM proteins within the synapse and its implications in regulating synaptic transmission and plasticity.

The role of synaptic structure in its function

Excitatory synapses in the mammalian brain form at specialized plasma membrane compartments at the tip of femtoliter (μm^3) sized protrusions called dendritic spines (Fig. 1.1A,B). In the adult brain many mature spines resemble the shape of a bulbous mushroom. This type of morphology supports the autonomy of individual synapses by promoting the retention of intracellular signaling molecules (Koch and Zador, 1993; Bloodgood and Sabatini, 2005; Tonnesen et al., 2014) and transmembrane proteins (Ashby et al., 2006; Simon et al., 2014) within the spine head. The compartmentalizing function of the spine

structure has motivated much investigation on the relationship between spine size and synaptic strength. In fact, multiple independent groups have found—by uncaging a photo-sensitive glutamate directly over spines while measuring synaptic strength via whole-cell patch clamp recording—that there was a robust, direct association between spine size and synaptic strength (Matsuzaki et al., 2001; Beique et al., 2006; Noguchi et al., 2011). Furthermore, this relationship is supported by studies on opposing forms of synaptic plasticity. Diverse protocols of LTP induction lead to a concomitant increase in the spine size and the amplitude of AMPAR-mediated synaptic transmission (Lang et al., 2004; Matsuzaki et al., 2004; Kopec et al., 2006). The converse was true for low-frequency stimulation protocols of long-term depression (Okamoto et al., 2004; Zhou et al., 2004). Importantly, however, exceptions have been reported where synaptic strength can change in the absence of morphological change in the spine structure (Bagal et al., 2005; Sdrulla and Linden, 2007; Wang et al., 2007). Altogether, the evidence suggests there might be a more consistently reliable structural correlate of synaptic strength.

Within the synapse, critically important transmembrane proteins such as glutamate receptors accumulate at the postsynaptic plasma membrane and are kept in register with the presynaptic terminal through association with a proteinaceous structure called the postsynaptic density (PSD). In electron micrographs, PSDs appear as electron-dense material at the tip of the spine or on the shaft of the dendrite (Fig. 1.1B), and they are on average disk-shaped, measuring 300-400 nm in the lateral plane (Harris and Stevens, 1989) and 20-30 nm in the axonal-dendritic axis (Valtschanoff and Weinberg, 2001). The range of sizes and shapes, however, are remarkably variable (Spacek and Hartmann, 1983; Harris et al., 1992). An individual PSD can be oval or amorphous, and can contain perforations

where protein density is low (Fig. 1.2). In addition to concentrating TM proteins at the synapse, the PSD connects postsynaptic signaling molecules, kinases and phosphatases in close proximity to their substrates, positions trans-synaptic adhesion complexes that bridge the cleft between communicating neurons.

Given central role of PSD in compartmentalizing proteins and keeping pre- and post-synaptic components in register, its size and structure were hypothesized to correlate with synaptic strength much more reliably than spine size. In fact, PSD diameter correlates with the number of synaptic AMPARs (Harris and Stevens, 1989; Takumi et al., 1999); PSD surface area correlates with the area of apposed presynaptic AZ and the number of glutamate vesicles docked there (Schikorski and Stevens, 1997); and the LTP induction protocols increased the fraction of complex and perforated PSDs (Stewart et al., 2005; Connor et al., 2006). Therefore, the PSD structure is tightly correlated with synaptic

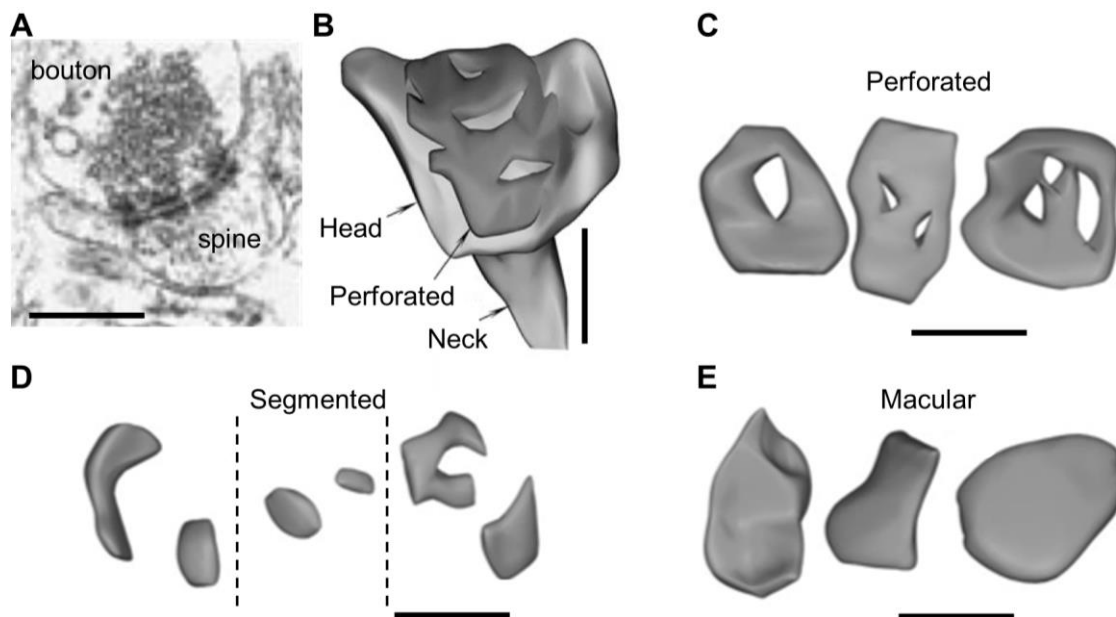


Figure 1.2. The PSD structure is diverse.

(A) A serial electron micrograph representative of a perforated postsynaptic density. (B) 3D reconstruction of PSD on a mushroom spine from serial thin sections in the CA1 region of a mouse hippocampus. Three categories of PSDs located on mushroom spines: (C) perforated PSDs, (D) segmented PSDs (dashed lines separate PSDs from separate spines), and (E) macular PSDs. Every scale = 500 nm. Adapted from Stewart et al. (2005) with permission from the publisher Wiley-Blackwell.

strength, likely because different architectural organizations within the PSD dictate distributions of glutamate receptors and other important TM proteins that either boost or reduce response to pre-synaptic glutamate release.

Receptor distribution within the synapse dictates synaptic strength

Several landmark studies in synaptic physiology were indispensable for our current understanding of the factors that could determine the amplitude of synaptic response. In 1950, Fatt and Katz first reported the existence of ‘biological noise’ when recording the endplate potential at the amphibian neuromuscular junction with an intracellular micro electrode. They, and other groups of investigators, later gave more detailed accounts of these “miniature potentials,” showing that evoked compound postsynaptic responses were the summation of multiple simultaneous miniature events and that these quantal miniature events could be detected action potential blockade (Del Castillo and Katz, 1954; Boyd and Martin, 1956; Liley, 1956). These observations motivated the use of quantal analysis and subsequently its application to study excitatory synapses in the mammalian central nervous system. Thus, numerous experiments have asked what determines the amplitude of the postsynaptic response at these synapses (quantal size). Until the turn of the 21st century, it remained to be determined—even in the case of a single release event—whether the limiting factor which determines the amplitude of the postsynaptic response was the number of postsynaptic receptors available for activation or whether the vesicular glutamate content is limiting. Asked differently, does glutamate release saturate the number of available receptors on the postsynaptic membrane? The short answer is no, and thus the total number of receptors within a synapse does not determine the synaptic strength. The support comes from numerical modeling and empirical evidence.

Known biophysical parameters of the synapse, when considered together, support the notion that not all receptors within the synapse are activated and the synaptic strength can be modulated by either tuning the amount of glutamate released or the density of receptors encountered by the glutamate released. When glutamate is released from a presynaptic vesicle, glutamate concentration within the synaptic cleft rises up to 1-3 mM constrained to narrow spatial distribution (<200 nm) (Clements et al., 1992) and dissipates substantially due to diffusion and buffering within ~100 μ sec (Diamond and Jahr, 1997; Bergles et al., 1999). Importantly, the concentration of glutamate required for half-maximally activating AMPARs is at most 2 mM (Traynelis et al., 2010), and thus receptors displaced a small distance from the site of release likely cannot open due to insufficient glutamate concentration. Indeed, numerical modeling which incorporates these

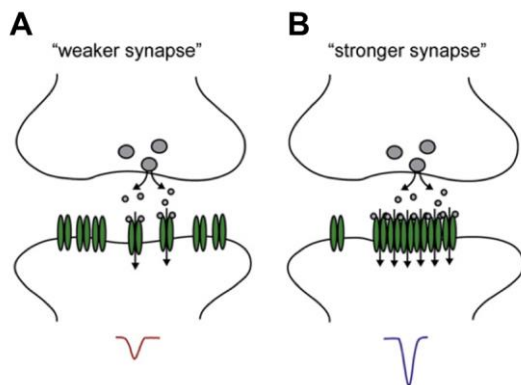


Figure 1.3. Synaptic strength can be modulated by changing the organization of AMPARs without changing the total number of receptors

(A) Presynaptic release of glutamate onto a region of two AMPARs produces a small excitatory postsynaptic current (EPSC)

(B) Release onto a highly dense region of receptors can enhance EPSC.

Adapted from MacGillavry et al. (2011) and printed with permission from the publisher.

parameters indicate that while AMPARs directly across from the site of release open with fairly high probability (~0.5-0.6), receptors laterally displaced by even 50 nm are much less likely to open (Xie et al., 1997; Franks et al., 2003; Raghavachari and Lisman, 2004). This translates to as little as 25% of receptors activated by single release within a medium to large synapse (Lisman and Raghavachari, 2006; Lisman et al., 2007). Importantly, this model assumed that receptors were uniformly spaced on the lateral face of the PSD. Heterogeneity in receptor distribution could enhance or limit AMPAR activation

depending the density of receptors directly across from the site of release. Thus, not just the total number of AMPARs in a synapse, but also the local density of AMPARs within synapse subdomains may determine the efficiency of synaptic transmission (Fig 1.3).

Multiple empirical studies were designed to test whether glutamate receptors at excitatory synapses are saturated by glutamate release following a single action potential. At the calyx of Held in acute brainstem slices, in which both the presynaptic terminal and the postsynaptic neuron are amenable to patch-clamp electrophysiology recordings, adding exogenous glutamate via presynaptic patch pipette further increases the postsynaptic response to spontaneous vesicle fusion (Yamashita et al., 2009), demonstrating that the concentration of glutamate in the presynaptic terminal is limiting. However, the multi-active-zone structure of this large compound synapse may differ in important ways from other excitatory synapses composed of single active zones. Further evidence of receptor non-saturation was also demonstrated at cerebellar mossy fiber–granule cell connections which, like hippocampal excitatory synapses, contain a single release site. At this synapse, receptors appear well below saturation, and the quantal variance is very high (Sargent et al., 2005). While the situation for hippocampal excitatory synapses has been somewhat more difficult to dissect, there is good evidence that many synapses of this type operate below AMPAR saturation during quantal transmission. One approach has been to compare postsynaptic currents in dissociated hippocampal neurons evoked by local electrical stimulation with those resulting from direct application of glutamate to that identified synapse by iontophoresis. In these studies, the amplitude was greater for iontophoretically evoked responses even while the variance was lower (Liu et al., 1999; McAllister and Stevens, 2000). This suggests that when vesicular glutamate is

released at hippocampal synapses during synaptic transmission it is not saturating. Instead, quantal release stochastically activates a subset of synaptic AMPARs giving rise to the high variability in responses. It is conceivable that this variance could arise because of continual adjustment postsynaptic AMPAR distribution with respect to presynaptic release location. As a result, an important first step is to understand how receptors are positioned within the synapse and whether these processes are dynamic in living synapses.

Historically, the best available approach to measure receptor distribution has been electron microscopy following immunogold labeling of AMPARs. As informative as it is, a major disadvantage with this approach is that the very high spatial precision requires limiting the density of antibody labeling in order to maintain specificity. Consequently, this approach can only be used across a population of synapses to determine population-averaged views of synaptic AMPAR distribution. Nevertheless, this approach has revealed that with excitatory synapses of neocortical tissue and striatum AMPARs tend to be located more peripherally (Bernard et al., 1997; Kharazia and Weinberg, 1997). This is particularly striking when compared with the distribution of NMDARs in the same neocortical synapses where their distribution is opposite, tending to be centrally concentrated (Kharazia and Weinberg, 1997). In another study, Somogyi et al. (1998) performed similar experiments focused on CA1 pyramidal excitatory synapses and found additional evidence for a central concentration of NMDARs but only a uniform distribution of AMPARs measured as the single dimensional distance from the PSD center. Again, while this approach has suggested trends in AMPAR distribution across synapse populations, the interpretation of the results from these studies is limited by the necessity of averaging across synapses.

Several technological developments have advanced the ability to map the entire receptor population within individual synapses without averaging, improving the ability to map these receptors fully in two dimensions. First, an alternative preparation method for EM called SDS-digested freeze-fracture replica labeling (SDS-FRL) has been applied to several excitatory synapse types by the Shigemoto lab. The special tissue preparation involved in this method allows for high-density, stoichiometric, immunogold labeling of synaptic receptors. In cerebellum, an initial study of immature Purkinje cells (climbing fiber to Purkinje cell synapses) indicated a uniform distribution of AMPARs within synapses (Tanaka et al., 2005). An additional study with more mature tissue, where Purkinje cells have an additional type of excitatory synapses, showed that the climbing fiber synapses maintained a uniform receptor distribution consistent with the previous study (Masugi-Tokita et al., 2007). However, AMPAR distribution on the parallel fiber synapses onto Purkinje cells had a much more variable density (comparing different synapses), and within any individual synapse AMPARs appeared in irregularly organized clusters. This indicates that complex organization of synaptic AMPARs is certainly possible and can even be a characteristic feature of certain synapse types.

Two additional approaches offered the possibility to map receptor distribution within single synapses with the additional advantage of simultaneously mapping the distribution of other synaptic proteins. First, EM tomography is yet another refinement of EM-based approaches. In this case, like other forms of tomography, a series of images are made to virtually section through the tissue. These tomographic images can then be used to reconstruct a 3-dimensional representation of electron dense synaptic constituents at a level that can resolve the general shape of individual proteins and receptors. Utilizing this

approach the Reese lab has identified the relative distribution of AMPARs and NMDARs based on the particular electron-dense profiles of each and found the distribution of AMPARs to be considerably more peripheral than NMDARs (Chen et al., 2008; Chen et al., 2011). Though the results of this approach are compelling, it should be noted that technological limitations still restrict these experiments to one or a few synapses per study. Many receptors of each type were associated with “vertical filaments” which were identified as MAGUK family members, prominently PSD-95 (more on these in the next section. These vertical structures are then interlinked by horizontal structures which are presumably GKAP and Shank molecules, though a more confident identification of horizontal filaments remains to be completed. From these early studies, it is clear that EM tomography will be a powerful approach to pursue a more comprehensive understanding synapse organization in the future.

Complimentary to EM tomography, super-resolution light imaging approaches called STORM (stochastic optical reconstruction microscopy) (Dani et al., 2010) and PALM (photoactivated localization microscopy) (Betzig et al., 2006) utilize fluorescence-conjugated antibody labels or expressible proteins fused to photoswitchable fluorescent proteins to resolve the precise locations of multiple synaptic proteins simultaneously within the synapse. Briefly, after labeling fixed tissue or cells, low-level excitation of fluorophores is used to stochastically excite limited numbers of labeled proteins, and their precise position in 2-D or 3-D space; this process is repeated until a large population of synaptic proteins has been sampled (Huang et al., 2008). Using STORM, Dani et al. found a broad range of distribution patterns for AMPARs and NMDARs in excitatory synapses in the accessory olfactory bulb (Dani et al., 2010). In some cases, they found a central

concentration of NMDARs and peripheral AMPARs (even tending toward perisynaptic enrichment) while in other cases they found very uniform receptor distributions which were uniformly organized across PSDs labeled by Shank or Homer antibodies. Further studies by multiple groups found that the AMPARs are often arranged non-uniformly in multiple dense regions across the lateral face of an individual synapse (Nair et al., 2013) and these dense receptor regions co-localize with dense regions of PSD-95 (MacGillavry et al., 2013). This application of superresolution light imaging is powerful in mapping synaptic proteins in two and three dimensions and at high density within single synapses. Together these data suggest the possibility that receptor organization could be quite diverse among synapses and highlights the need for further investigation including the development of live-cell imaging approaches to study how the organizations of AMPARs and other TM proteins are controlled.

Receptor trafficking

AMPAR content within the synapse results from multiple steps that regulate subunit synthesis, forward trafficking from intracellular compartments to the plasma membrane, and lateral diffusion from the location of exocytosis to synapses. Messenger RNAs coding for AMPAR subunits are present throughout the neuron, in the dendrite and the nucleus (Huang et al., 2006; Irier et al., 2009). Quality control in the endoplasmic reticulum ensures proper folding and tetramer assembly and association with auxiliary subunits such as Stargazin, which promotes export (Tomita et al., 2003; Vandenberghe et al., 2005), permitting passage to the Golgi and subsequent packaging into intracellular storage vesicles.

In the endosomal storage pool, AMPARs become subject to regulated cycling between intracellular compartments and the plasma membrane. GluA2-containing AMPARs constitutively cycle between these two pools via rounds of endocytosis and exocytosis. The rate of reinsertion and degradation can be regulated by activity (Ehlers, 2000; Lee et al., 2004). In fact, increased AMPAR endocytosis mediates long-term depression (Man et al., 2000; Ashby et al., 2004; Lin and Huganir, 2007), and increased exocytosis mediates long-term potentiation (Lledo et al., 1998; Hayashi et al., 2000; Park et al., 2004). Thus, AMPAR content within the synapse is subject to constitutive and activity-dependent trafficking between intracellular and surface membrane compartments.

The simplest model for changing AMPAR content in the synapse would be direct endocytosis or exocytosis of receptors at the synapse. However, all experimental evidence so far suggests that receptors are delivered to extrasynaptic locations. Exocytosis can occur at the cell body, the dendritic shafts (Yudowski et al., 2007; Lin et al., 2009; Makino and Malinow, 2009), or in the spine head (but still outside the synapse) (Kennedy, 2010; Park, 2006). Similarly, endocytosis takes place at specialized sites called endocytic zones away from the synapse (Blanpied et al., 2002; Racz et al., 2004). Between 15 and 50 AMPARs (Yudowski et al., 2007; Tao-Cheng et al., 2011) are packaged into each exocytic vesicle (~0.15 μm measured by Racz et al. (2004)); fewer AMPARs (1-2) are immunolabeled by at individual endocytic zones (Petralia et al., 2003; Tao-Cheng et al., 2011). These results indicate that additional steps are needed for AMPARs to travel between synapses and

locations of membrane trafficking in order to populate synapses with the appropriate number of AMPARs (Fig 1.4).

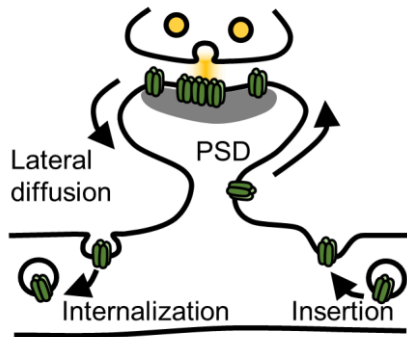


Figure 1.4. Both membrane trafficking and lateral diffusion determine synaptic AMPAR content.

The diffusion of AMPARs within the plasma membrane facilitates the exchange between synaptic and extrasynaptic pools of receptors. Receptor endocytosis and exocytosis occur outside the synapse and determine the AMPAR content in the extrasynaptic pool.

As demonstrated by techniques that measured the diffusion of receptors on the plasma membrane (to be discussed shortly), AMPARs are mobile on the lateral plane of the plasma membrane. And this mobility allows AMPARs to explore large area on the dendritic plasma membrane, to enter and exit dendritic spines, and most importantly to encounter synapses where they can become incorporated. However, factors that control synaptic incorporation and organization of receptors remain poorly understood and will be addressed by experiments presented in this dissertation.

Factors that could control the distribution of receptors and other TM proteins in the PSD

Given that the PSD is highly abundant in the brain and that it can be enriched by a few steps of centrifugation, the composition of the PSD has been studied extensively by biochemical analysis. Within the PSD, the most common class of proteins are the multi-domain scaffolding proteins. These provide means of retaining TM proteins within the synapse. Among these, the MAGUKs are the best characterized. Of four members in this family, PSD-95 is particularly relevant for regulating the accumulation, retention, and organization of TM proteins, as it lies closest to the postsynaptic membrane

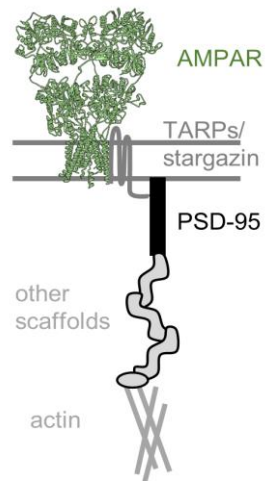


Figure 1.5. Multiple protein-protein interactions at the PSD. AMPARs (green) directly bind to TARPs (dark grey), which interact directly with PSD-95 (black), which interacts with multiple layers of scaffolding proteins (light grey), and they ultimately interact with the actin cytoskeleton.

by associating with the membrane through N-terminal palmitoylation, and thus well positioned as a scaffold to interact with TM proteins that contain sizable cytoplasmic protein domains (Fig. 1.5). The structure of some synapses can be maintained over a time of days, weeks, and even years, although the lifetime of a receptor or TM protein is at most on the order of days. The fixed snapshot of postsynaptic membrane through biochemical or electron-micrographic analysis cannot account for the rapid structural modifications. An increasing amount of experimental evidence in living synapses has demonstrated the role of PSD-95 as a PSD-resident protein binding partner in regulating the trafficking of TM proteins to the synapse and accumulation within it.

The most studied role of PSD-95 as a binding partner is in the regulation of the number of postsynaptic AMPARs (Malinow and Malenka, 2002; Granger et al., 2013) and their distribution across the face of the postsynaptic density (PSD) (Kennedy, 2000; MacGillavry et al., 2011). At excitatory synapses, AMPARs are concentrated in the PSD, but diffuse laterally throughout the surface of the neuronal membrane, and they enter and exit the PSD via this mechanism (reviewed by Opazo et al. (2012)). Thus, in order to sustain or tune synaptic strength at rest or during activity, the synapse must capture receptors and slow their mobility in order to retain them. However, despite intensive efforts, the mechanisms that govern intrasynaptic AMPAR mobility and organization remain surprisingly unclear. My general contention is that some of these mechanisms will be receptor-specific, but others may hold very broadly for a large number of TM proteins.

Techniques to measure transmembrane protein diffusion

Particles suspended in a liquid are pushed in different random directions owing to their collision with thermally agitated surrounding molecules (e.g. water). Brown (1828) first observed this phenomenon while looking through a microscope at particles trapped inside pollen grain cavities suspended in water; the precise mechanism of Brownian motion was elegantly described later by Einstein (1905) and confirmed empirically by Perrin (1909). In a similar process, transmembrane (TM) proteins in a typical cell membrane undergo Brownian or free diffusion, but also exhibit motions that cannot be described by this process alone. Many techniques to measure protein diffusion have been developed to understand additional factors that could control protein motion in the plasma membrane of living cells, including fluorescence recovery after photobleaching (FRAP) and single particle tracking (SPT). Results so far suggest that the motion of TM proteins could be

influenced by physical obstacles and reversible biochemical interactions (Kusumi et al., 2005).

Fluorescence recovery after photobleaching

Fluorescence recovery after photobleaching (FRAP) (Axelrod et al., 1976) has been used for measuring two-dimensional lateral mobility of fluorescent particles. In this technique, a small region containing fluorescent molecules is irreversibly, photochemically bleached by a brief intense pulse of light (Fig. 1.6) (Reits and Neefjes, 2001; Chen et al., 2006). The rate of exchange in and out of the bleached region is determined by measuring the rate of

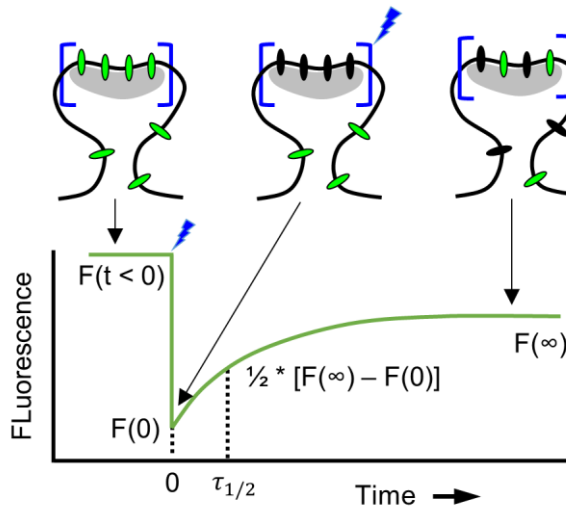


Figure 1.6. Schematic of fluorescence recovery after photobleaching experiment.

First, the fluorescence $F(t < 0)$ in a region of interest (e.g. tip of a dendritic spine) is measured to establish that fluorescence change due to imaging alone does not substantially bleach fluorescence over time. Second, an intense pulse of laser is applied on the same region to bleach fluorescence in that region. Then, the fluorescence $F(0)$ in the same region is measured again and this is defined as time zero. Last, the recovery of the fluorescence within the bleached area is recorded as a function of time. Green ovals represent fluorescent TM proteins, black ovals the bleached proteins.

fluorescence recovery from naive fluorescent parts of the membrane. The proportion of receptors that are exchangeable in a given area can be estimated by quantifying the extent of recovery. The transmembrane proteins of interest are commonly tagged with a fluorophore (e.g. green fluorescent protein, GFP) to enable FRAP (Ashby et al., 2004; Ashby et al., 2006; Kopec et al., 2006; Park et al., 2006; Heine et al., 2008).

FRAP provides information on the ensemble of many proteins as a whole, yielding the estimate of protein mobility as the movements of hundreds or thousands of molecules are averaged. It can uncover the difference in movement of two different proteins in the

same kind of environment or the same kind of protein in different kinds of environment. A slow rate and extent of fluorescence recovery of a tagged TM protein can indicate the presence of physical barriers, reversible chemical interactions, restricted membrane geometry, or both (Kusumi et al., 1993; Ashby et al., 2006; Choquet and Triller, 2013).

Single particle tracking

Single particle tracking (SPT) is a powerful tool to distinguish the movement TM proteins with high temporal and spatial resolution. The major advantage of SPT is capability to measure the diffusion of individual TM proteins as opposed to the ensemble measurement in FRAP. This enables the investigation of the diffusion and organization of a subpopulation of TM proteins within submicron confines of the plasma membrane, ideally suited for the questions at hand.

SPT employs sub-micron-sized particles that can bind to the protein of interest through ligands that recognize the receiving extracellular domain on the protein. The particle is distinguishable by increased light contrast through various means (e.g. differentially scattered visible light or fluorescence). The ligands can be made of latex (0.1 to 1 μm in diameter) (Meier et al., 2001; Borgdorff and Choquet, 2002), gold (40 nm at the smallest), quantum dots (8-20 nm), or organic dyes (< 1 nm). Colloidal gold is a strong light scatterer that acts as a light sink rather than a light source. After background subtraction and contrast enhancement, the label appears darker than the surrounding image. Particles are deposited onto cells by passive incubation or are directly placed onto specific cell areas with laser tweezers. The movement, and therefore TM protein diffusion, is then imaged by video-enhanced differential interference microscopy or fluorescence imaging.

The use of latex beads and gold beads in neurons limited SPT study to extra synaptic receptors, as the size of the particles prevents access to receptors in the synaptic cleft (~20 nm). An improvement of latex bead tracking was the use of antibodies conjugated to organic dyes (e.g., Cy3, Cy5). The smaller size of organic dyes allows for optical tracking of receptor diffusion in more restricted regions. The experimental results have demonstrated that extra-synaptic AMPA receptors exchange laterally in and out of the PSD and are less mobile within the PSD (Tardin et al., 2003). The major limitation of using organic dyes is their fast photobleaching, which is limited to short (\ll 1 sec) recording particle trajectories, limiting the precision of estimating diffusion coefficients.

The introduction of semiconductor quantum dots has circumvented many of the limitations (Dahan et al., 2003). Quantum dots are nanometre-sized semiconductor fluorescent particles that practically do not photobleach (Michalet et al., 2005; Triller and Choquet, 2005). However, the smallest quantum dot made so far, when combined a nanobody, is ~14 nm (Cai et al., 2014), still close to the average size of a synaptic cleft gap. These ligands likely preferentially label TM proteins that exit or hover near the periphery of the PSD, making difficult the precise interpretation of their location in relation to the synapse. In some SPT experiments of this study, I used a nanobody conjugated to a highly stable organic dye, which is small enough to access the synapse easily but also bright enough to enable second-long tracking of diffusion.

The goal of SPT data analysis is to sort trajectories into various modes of motion and to quantify metrics characterizing the motion, such as the diffusion coefficient and confinement area. Both of these parameters can be determined by fitting characterizing the mean squared displacement (MSD) over time, which is an estimate of the area explored of the diffusing protein over time. The instantaneous diffusion coefficient can be calculated from the initial linear slope of the MSD curve, and the confinement area can be calculated

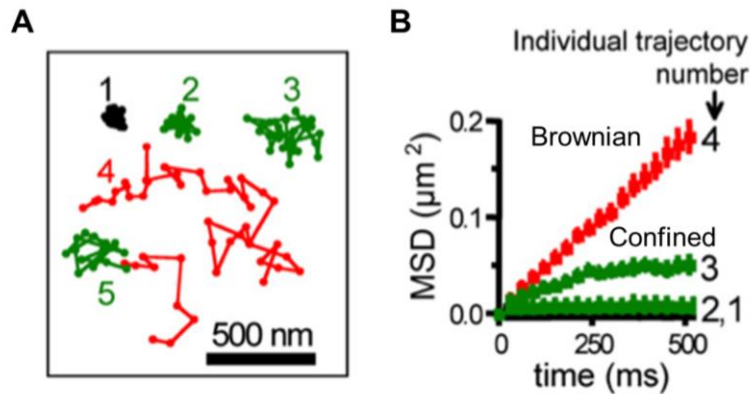


Figure 1.7. Different modes of diffusion detectable by single particle tracking.

(A) AMPAR trajectories within synaptic and extrasynaptic area. Examples 2-5 are trajectories from tracking single Cy5-anti-GluR2 on living dendrites. The trajectories within synaptic domain are labeled green and those in extrasynaptic area red. Track 1 was an immobilized antibody fixed onto a coverslip as control. Track 2 and 3 remained within synaptic sites, track 4 remained in the extrasynaptic site, and track 5 began in the extrasynaptic area and entered into synaptic region, where it appeared more confined.

(B) Mean squared displacement (MSD) curves plots corresponding to tracks shown in (A). Track 2 and 3 in the synaptic regions showed varying degrees of confinement and were less mobile than track 4.

Both panels adapted from Newpher and Ehlers (2008), with permission from the publisher Elsevier Inc.

from the end point of MSD curves if they plateau (for more theoretical and mathematical treatment of these calculations, please see Saxton and Jacobson (1997). A few modes of motion have been observed on the plasma membrane: Brownian diffusion and varying degrees of confined diffusion (Fig. 1.7). A major result of this technique is that motion in the membrane is not limited to pure Brownian diffusion.

Receptor dynamics within individual synapses

The diffusion of proteins on the plasma membrane has received increasing attention, not only due to the availability of experimental methods to study the diffusion process but also given that this motion can influence the function of neurons and heterologous cells. Decades ago, Axelrod et al. (1976) examined the fluorescence recovery after photobleaching (FRAP) of acetylcholine receptors at the surface of cultured muscle cells and found distinct pools of mobile and immobile receptors. Further experiments by Young and Poo (1983) showed that AChRs rapidly diffuse on the muscle membrane outside of neuromuscular junctions, and they first proposed that the nerve contacts serve as a trap for rapidly diffusing receptors in the membrane. By monitoring the motion of individual receptors using single-molecule tracking techniques, Daniel Choquet and colleagues (Borgdorff and Choquet, 2002; Tardin et al., 2003) elegantly demonstrated that excitatory synapses can confine the diffusion of AMPARs, indicating that, similar to neuromuscular junctions, central synapses can also stabilize the motion of receptors.

AMPARs on the plasma membrane diffuse laterally at a high rate ($\sim 0.02 \mu\text{m}^2/\text{s}$) as measured by SPT (Ehlers et al., 2007; Groc et al., 2007). FRAP of fluorescently tagged GluA2 subunits of AMPARs on the plasma membrane showed that in both intact hippocampi and cultured neurons, 30% of spine and 60% of shaft-localized AMPARs are exchangeable (Heine et al., 2008). Reducing the mobility of these receptors by antibody-mediated cross-linking impaired the fidelity of synaptic transmission during high frequency stimulation (Heine et al., 2008), indicating that rapid exchange of glutamate receptors on the plasma membrane provides the basis of acute changes in synaptic strength.

The movement of rapidly diffusing receptors and other TM proteins must be slowed down and stabilized to permit synapses to accumulate and arrange these proteins for proper response to neurotransmitter release. However, mechanisms that stabilize TM protein diffusion within the synapse are poorly understood. The rapid lateral diffusion of various transmembrane proteins critical for synaptic function can be interrupted by periods of stability at synaptic sites as previously demonstrated using single-molecule tracking studies (Borgdorff and Choquet, 2002; Biermann et al., 2014; Schneider et al.; Chamma et al., 2016). The constraints on the diffusion of membrane dynamics have been first studied in non-neuronal cell types. In the model proposed by Singer and Nicolson (1972), the membrane is considered as a two-dimensional solution of integral membrane proteins embedded in a viscous phospholipid bilayer solvent. However, this model cannot explain the later findings as the measured diffusion coefficients in the biological membranes were found to be more than one order of magnitude lower than those predicted from theory or from measurements in reconstituted lipid bilayers (Saxton and Jacobson, 1997), indicating that the structure of the membrane is quite complex.

The great variability in diffusion exhibited by TM proteins on the cell surface suggested that the plasma membrane is composed of diverse micro-domain architectures that can hinder TM protein diffusion (Edidin et al., 1991; Jacobson et al., 1995; Simson et al., 1998; Kusumi et al., 2014). Extensive studies of glutamate receptor dynamics in the PSD have inspired a few conceptual models (Fig. 1.8). One class of models, arguably the most investigated, considers PSD-95 as slots which stabilize receptors by binding to them

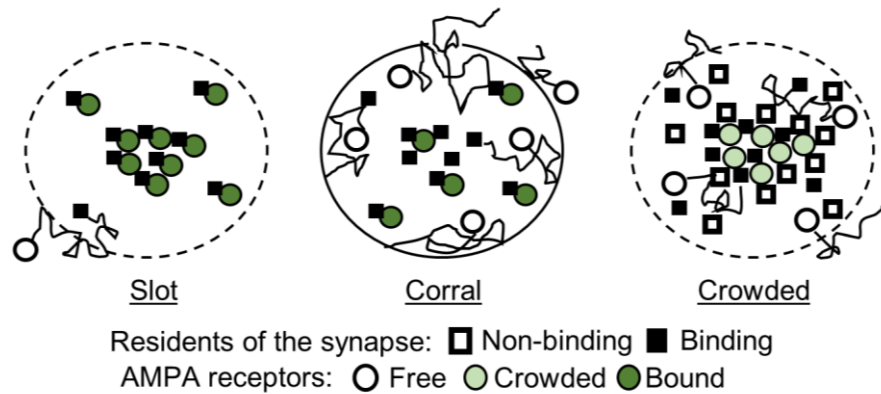


Figure 1.8. Three conceptual models for receptor diffusion within the synapse.

The slot model proposes that receptors within synapses are strongly bound and stabilized by slot proteins (e.g. PSD-95). In the corral model, receptors diffuse within the synapse, can bind to scaffolds and have narrow escapes frequently. In the crowded model, receptor diffusion is confined due to obstacles and receptors can also bind to scaffolds.

(Opazo et al., 2012). This scaffold protein contains multiple protein interaction domains (Cho et al., 1992; El-Husseini Ael et al., 2002), the most relevant of which are the PDZ domains. PSD-95 interacts with AMPARs via their auxiliary subunits known as TM AMPAR regulatory proteins (TARPs) (Chen et al., 2000) through PDZ-mediated binding (Schnell et al., 2002; Xu et al., 2008; Hafner et al., 2015). TARPs not only promote surface expression of AMPARs (Tomita et al., 2004), but their interaction with PSD-95 is required for synaptic enrichment of AMPARs (Tomita et al., 2005). Furthermore, overexpression or acute knockdown of PSD-95 respectively increases or decreases synaptic AMPAR content (El-Husseini et al., 2000). These results suggest that changes in PSD-95 content determine alterations in synaptic AMPAR numbers during synaptic plasticity, but there is

no clear evidence for an increase in synaptic PSD-95 during induction of long-term potentiation, the well-studied cellular model of learning.

On the other hand, activity-dependent phosphorylation of the cytoplasmic tail of the TARP stargazin (Stg) by CaMKII α increases AMPAR interaction with PSD-95 and augments the ability of AMPARs to accumulate in the synapse (Opazo et al., 2010; Sumioka et al., 2010). These results suggest that disrupting the interaction between PSD-95 and TARPs would prevent the synaptic retention of most receptors. However, results of experiments to test this prediction have been equivocal. Overexpression of Stg with its PDZ-binding c-terminus deleted reduces the fraction of immobilized AMPARs within the synapse, but only by 50% (Bats et al., 2007). Similarly, direct interference of the Stg-PSD-95 interaction with carefully optimized peptides that interfere with PDZ binding at both PDZ1-2 does reduce EPSC amplitude, but only by 25% (Sainlos et al., 2011). Thus, though binding may be required for a subset of AMPARs to be slowed in the synapse, the plentiful remaining receptors suggest that it may not be the only mechanism for synaptic immobilization of receptors. Remarkably, many critically important proteins other than AMPARs contain forms of PDZ binding ligands at their cytoplasmic domains which can bind to PSD-95 as well. In Chapters 2 and 3, I test whether a specific form of PDZ binding is sufficient to slow and dictate the organization of a TM protein representative within the synapse by using single-molecule tracking.

A second class of models treats the synapse as a corral with a gate that opens and closes to permit the entry and escape of receptors (Sako and Kusumi, 1995; Sheets et al., 1997; Simson et al., 1998; Fujiwara et al., 2002). However, this model quickly lost steam

as the candidates for the “fence” and “gate” have yet to be identified despite intensive search.

Retaining synaptic proteins through steric hindrance

Mounting evidence suggests that another binding-independent mechanism may complement binding to regulate mobility of receptors or TM proteins in general within the synapse. Single-particle tracking demonstrated that receptors explored only an area smaller than the synapse (Ehlers et al., 2007). Moreover, a high-resolution FRAP study found that most AMPARs do not freely diffuse within the synapse and exchange minimally within the PSD (Kerr and Blanpied, 2012). These data suggest a more complex picture of receptor trapping, in which the spatial organization of the PSD can influence the stability of receptors. The role of synaptic spatial organization in the regulation of TM protein mobility and retention is addressed by both simulation and experiments presented in this dissertation.

The PSD accumulates so many protein in such a small volume (Husi et al., 2000; Sheng and Hoogenraad, 2007) that PSD-native proteins could influence the mobility of AMPARs by acting as a series of physical barriers to sterically hinder lateral diffusion within the synapse. The idea that structural proteins sitting just below the plasma membrane can serve as barriers and impede the TM protein motion has been proposed long ago (Jacobson et al., 1995). The extent of this effect was first quantified through computational modeling, in which PSDs densely packed with protein obstacles retained receptors for minutes or even hours, even in the absence of binding interactions (Santamaria et al., 2010). In support of this view, tomographic electron microscopy (EM) of synapses indicates that PSDs are likely highly crowded (Fig take from Chen et al 2008 Xiaobin) (Chen et al., 2008). The presence of large numbers of high molecular weight

proteins significantly restrict protein diffusion within cells, a process known as macromolecular crowding (Ryan et al., 1988; Saxton, 1994; Minton, 2006). Single-molecule tracking studies in living neurons support this view by revealing that not just receptors but also membrane lipids display confinement and reduced diffusion within the synapse (Renner et al., 2009). However, these limited findings are difficult to interpret, because they used a variety of molecules (lipids or their protein ligands which, though conveniently available, have strongly different characteristics that fundamentally alter diffusion through membrane which contains heterogeneous distributions of other lipids (Lajoie et al., 2009)). In addition, more direct mobility measures of AMPARs themselves have been carried out via many other tags, ranging from antigen-binding antibody fragment to full antibodies carrying synthetic dyes, quantum dots, or beads as reviewed by Opazo et al. (2012). But these labeled AMPARs by definition are much larger than the receptors themselves, and so are of unclear relevance to the synaptic steric mechanism that may govern receptor mobility. Thus, whether the size of the TM protein itself influence mobility and the positioning of the TM proteins is poorly understood. The role of TM protein size in the regulation of TM protein mobility and retention is addressed by both simulation and experiments presented in this dissertation.

The advent of super-resolution imaging methods have made it possible to visualize protein distribution within the PSD with nanometer precision (Fukata et al., 2013; MacGillavry et al., 2013; Nair et al., 2013). These studies have revealed a heterogeneous and nonuniform distribution of scaffold proteins and receptors within the PSD, consistent with EM studies (Chen et al., 2008). EM studies further made it possible to discern the specific orientations of scaffold proteins such as PSD-95 within the PSD (Chen et al 2011).

Together these spatial maps of PSD-95 within the synapse make it possible to investigate how the size of the TM proteins and the organization of scaffold proteins can control the mobility and positioning of TM proteins.

I hypothesize that macromolecular crowding in the PSD and receptor-scaffold interactions act together to facilitate the retention and to modulate the distribution TM proteins within the synapse. One key goal of this project is to test empirically the predictions generated by computer models which incorporate measured aspects of PSD organization. The other key goal is to simulate the functional consequence of the experimental data and motivate further studies to test the impact of macromolecular crowding on synaptic function.

Chapter 2: Protein crowding within the postsynaptic density can impede the escape of membrane proteins¹

Abstract

Mechanisms regulating lateral diffusion and positioning of glutamate receptors within the postsynaptic density (PSD) determine excitatory synaptic strength. Scaffold proteins in the PSD are abundant receptor binding partners, yet electron microscopy suggests that the PSD is highly crowded, potentially restricting the diffusion of receptors regardless of binding. However, the contribution of macromolecular crowding to receptor retention remains poorly understood. We combined experimental and computational approaches to test the effect of synaptic crowding on receptor movement and positioning in Sprague Dawley rat hippocampal neurons. We modeled AMPA receptor diffusion in synapses where the distribution of scaffold proteins was determined from photoactivated localization microscopy experiments, and receptor-scaffold association and dissociation rates were adjusted to fit single-molecule tracking and fluorescence recovery measurements. Simulations predicted that variation of receptor size strongly influences the fractional synaptic area the receptor may traverse, and the proportion that may exchange in and out of the synapse. To test the model experimentally, I designed a set of novel transmembrane (TM) probes. A single-pass TM protein with one PDZ binding motif concentrated in the synapse as do AMPARs, yet was more mobile there than the much larger AMPAR. Furthermore, either the single binding motif or an increase in cytoplasmic bulk through addition of a single GFP slowed synaptic movement of a small TM protein. These results

¹ Li TP, Song Y, MacGillavry HD, Blanpied TA, Raghavachari S (2016) Protein Crowding within the Postsynaptic Density Can Impede the Escape of Membrane Proteins. *The Journal of Neuroscience*, 36:4276-4295.

suggest that both crowding and binding limit escape of AMPARs from the synapse. Moreover, tight protein packing within the PSD may modulate the synaptic dwell time of many TM proteins important for synaptic function.

Introduction

Synaptic strength is modulated by both the density and positioning of AMPARs within the synapse (Xie et al., 1997; Franks et al., 2003; Raghavachari and Lisman, 2004; Lisman et al., 2007; Kessels and Malinow, 2009), so determining the mechanisms that establish their synaptic entry, exit, and distribution is of great interest. We argue here that key mechanisms controlling AMPAR dynamics in the synapse are likely also to apply to the many other transmembrane (TM) proteins that establish synapse structure and function.

Receptors and other critical synaptic TM proteins are highly mobile in the dendritic plasma membrane (Meier et al., 2001; Borgdorff and Choquet, 2002; Serge et al., 2002; Breillat et al., 2007; Biermann et al., 2014; Chamma et al., 2016). This mobility is generally sufficient to permit TM proteins to explore large expanses of the dendrite on the time scale of minutes, to enter and exit spines efficiently, and perhaps most importantly, to encounter numerous synapses where they may be incorporated (Giannone et al., 2010; Masson et al., 2014). It is now well-established in particular that AMPARs enter and exit the synapse via lateral diffusion (Borgdorff and Choquet, 2002; Heine et al., 2008). Given this, it is widely expected that synapses maintain steady state enrichment of receptors by presenting binding sites that slow receptor diffusion (Gerrow and Triller, 2010). Indeed, a large fraction of AMPARs within the synapse are highly constrained and nearly immobile (Ehlers et al., 2007; Kerr and Blanpied, 2012; Choquet and Triller, 2013). In addition, PDZ-mediated interactions between transmembrane AMPAR regulatory proteins (e.g. Stargazin) and the

major synaptic scaffolding protein PSD-95 play a key role in reducing the lateral mobility of AMPARs at synapses (Bats et al., 2007). However, peptides that acutely disrupt their binding decrease synaptic currents by only 20 to 50% (Sainlos et al., 2011). This suggests that Stargazin-PSD-95 binding cannot solely determine AMPAR number and mobility at the synapse.

Macromolecular crowding could be a key mechanism that complements receptor-scaffold interactions to regulate the mobility of TM proteins in the synapse. The density of proteins in the PSD is extremely high near the cell membrane (Husi et al., 2000; Sheng and Hoogenraad, 2007; Burette et al., 2012), likely imposing a series of physical barriers to hinder lateral diffusion of TM proteins (Trimble and Grinstein, 2015). Indeed, diffusion of extracellularly labeled lipids in the synapse is affected by the extent of the protein bulk used for labeling (Renner et al., 2009), suggesting a role for excluded volume interactions in regulating molecular mobility. However, because lipids can preferentially sample membrane regions not accessible by most TM proteins and extracellularly labeled lipids are most likely not influenced by the cytosolic environment, it is unclear whether these observations apply in general to TM proteins containing extended intracellular domains. Computational modeling of receptor diffusion in crowded PSDs showed that even in PSDs devoid of receptor-binding proteins, synaptic receptors could be retained for minutes or even hours merely because hindrance by transmembrane and membrane-proximal proteins reduced their mobility (Santamaria et al., 2010). Furthermore, proteins in the PSD are not just densely packed but are heterogeneously distributed with notable clustering (MacGillavry et al., 2013; Nair et al., 2013) that may accentuate steric effects. Despite

these observations, the influence of intracellular protein bulk in determining synaptic mobility of TM proteins has not been directly tested.

To address this, we distilled a receptor to its barest essence, a single-pass transmembrane domain and a cytosolic tail that can bind to PSD-95. This probe accumulates in synapses yet is dramatically smaller than AMPARs, allowing us to manipulate protein bulk and binding capacity independently. Combining dynamic imaging with theoretical modeling, we show that mobility of these probes within the PSD is affected in a size-dependent manner by both steric effects and biochemical binding. Our results suggest that steric effects may regulate the mobility of a large diversity of synaptic TM proteins, with implications for synaptic transmission and plasticity.

Materials and Methods

For simulations

Synapse geometry. We approximated the PSDs as convex hulls, the boundaries of which were extracted from the PSD-95 coordinates directly measured with PALM imaging (MacGillavry et al., 2013). The PSD area ranged from 0.02 to 0.53 μm^2 ($n = 100$). The density of PSD-95 inside each PSD was kept to about 3,000/ μm^2 (Chen et al., 2011). The PSD-95 molecules acted as obstacles to receptor diffusion. Adhesion molecules, NMDA-type glutamate receptors, and other proteins were also added to the system (Table 2.1).

Table 2.1. Simulation parameters.

	Value	Study
PSD-95 radius	2.5 nm	Chen et al. (2008)
NMDAR radius	8 nm	Chen et al. (2008)
Adhesion molecules, radii	3-8 nm	This work ^a
Other immobile proteins, radii	5-10 nm	This work ^a
NMDAR number	20	Cheng et al. (2006)
Adhesion molecule number	48	Cheng et al. (2006)
Other immobile protein number	15	Cheng et al. (2006)
Diameter of PSD	140-400 nm	MacGillavry et al. (2013)
AMPA number within a synapse	100	Matsuzaki et al. (2001)
AMPA diffusion constant	0.2 $\mu\text{m}^2/\text{s}$	Ehlers et al. (2007)

^aRadii of assumed unstructured conformations were deduced from total counts of amino acids based on the radius of gyration estimates of peptide chains by Kohn et al. (2004).

Two-dimensional percolation for receptors within PSD. We adapted methods from computational geometry that were recently used to study percolation (Saxton, 2010). Briefly, transmembrane and juxta-membrane proteins (such as PSD-95) were modeled as disks distributed on a plane. Given the set of points representing the centers of the disks, the Voronoi diagram divides the plane into polygons, each containing a single point. The dual of the Voronoi diagram, known as the Delaunay triangulation, is a set of triangles that tiles the plane, with the vertices at the different points and the edge lengths, D_{ij} representing the distance between the points i and j . The region of polygon belonging to one point is closer to that point than any other point. If a tracer's diameter, d_{trac} is smaller than $D_{ij}-r_i-r_j$ (the edge length minus the radii of the two points), then the tracer can move across the edge between the two particles. The edge connecting the particle centers i and j is then labeled a "conducting edge." Thus, given a distribution of differently-sized disks on a plane, all the conducting edges can be identified for a given tracer diameter. If a tracer can enter, traverse, and exit a distribution of disks at distinct points, then a percolation path exists for those particles.

To investigate the effects of PSD molecular crowding and receptor-scaffolding binding on AMPAR concentration, we considered the two-dimensional movement of a tracer particle in the presence of a set of effectively immobile molecules, such as PSD-95, NMDA receptors, and adhesion molecules. We first placed PSD-95 molecules based on coordinates estimated by PALM experiments (MacGillavry et al., 2013), and then randomly placed a set of transmembrane proteins without spatial overlap within the PSD border. These include AMPA receptors, NMDA-receptors, adhesion molecules, and other ion channels; their numbers were prescribed based on density estimated by EM and mass spectrometry experiments (Sheng and Hoogenraad, 2007). NMDARs and the initial locations of AMPARs were distributed relative to PSD-95 by matching the number distribution of PSD-95 neighbors as determined from measured two-color localizations (MacGillavry et al., 2013) while also ensuring that individual molecules did not overlap. While the other non-PSD-95 proteins were randomly placed, the constraint of non-overlapping spatial arrangement yielded non-random distributions in which most of these proteins were more likely to be excluded from the highly dense PSD-95 regions and thus relatively enriched toward the edge of the synapse. Nevertheless, the occupied volume of these molecules is far less than that of the receptors and PSD-95 combined and would therefore have a smaller effect on receptor mobility. We set the radius of PSD-95 to be 2.5 nm as estimated by EM tomography (Chen et al., 2008). We set the extracellular and transmembrane radii of the AMPAR complex to be 8 and 5 nm, respectively, as estimated by single-particle EM (Nakagawa et al., 2005). To model the yet to be crystallized intracellular bulk of the AMPAR complex, we used estimates from single-particle EM of GluK2 intracellular domain and a mathematical estimate of Stargazin C-tail size based on

its residue count. Schauder et al. (2013) showed that the putative intracellular domain of a full length GluK2 receptor is around 10 nm in width and 5 nm in height. TARP proteins have not been crystallized, but the intracellular tail (N~120 amino acids) of the most studied TARP representative Stargazin is estimated to be around 3 nm in radius assuming an unstructured globule, as calculated from the radius of gyration of a random polymer $R_g^2 \approx \frac{1}{6} N^{6/5} b^2$ (Kohn et al., 2004), where N is the number of amino acids and b is a constant that is a function of the persistent length of the polymer. Given the residue count of GluK2 cytoplasmic portion is intermediate between that of GluA1 and that of GluA2 and that full AMPARs can contain anywhere from 1 to 4 Stargazin subunits (Hastie et al., 2013), we conservatively modeled the intracellular radius of the AMPAR complex to be 8 nm. The radii of adhesion molecules were taken from a random distribution ranging from 3 to 8 nm. The sizes of other immobile proteins (e.g. ion channels) were taken from a random distribution ranging from 5 to 10 nm. The Voronoi diagram was computed in MATLAB (Mathworks). Poisson distributions of PSD-95 were generated by first drawing a convex hull to mark the boundary around the measured positions of PSD-95, and then randomly placing the particles within the hull, while ensuring that two randomly placed particles did not overlap.

The percolation paths were found based on the diameter of the diffusing tracer and the boundaries between the mentioned molecules. We evaluated the conducting area numerically as the area of the Voronoi regions that had at least one conducting edge for different measured PSD configurations used in the percolation calculations. We calculated the conducting area fraction as the ratio of area with conducting paths divided by total PSD area at different tracer sizes.

Simulating AMPAR diffusion and binding. To simulate AMPAR diffusion within the PSD and the surrounding extrasynaptic space, we used Monte Carlo simulations of Brownian dynamics with a discretization time step of 2 μs . For sufficiently small time interval Δt , each time step is simulated based on the following equations:

$$\begin{aligned}\Delta x &= \sqrt{2D\Delta t}\xi_x \\ \Delta y &= \sqrt{2D\Delta t}\xi_y\end{aligned}$$

where ξ_x, ξ_y are Gaussian-distributed white noise. The AMPAR diffusion coefficient outside synapses was chosen to be in the range of 0.2 $\mu\text{m}^2/\text{s}$, based on single-particle-tracking data by Ehlers et al. (2007) and current data. The diffusion space was chosen as a circular domain of 400 nm radius with a central region occupied by the PSD. At each time step, trial position (x, y) coordinates of AMPARs were incremented by the distances (Δx , Δy); however, whether a receptor could diffuse to the new position depended on several rules: 1) whether it bound to PSD-95 upon collision, and 2) whether it collided with nearby immobile obstacles. Once it bound to PSD-95, the particle stopped lateral diffusion but underwent rotational diffusion, which determined its subsequent position of dissociation. A bound receptor molecule could dissociate from a PSD-95 molecule according to a first-order reaction. Receptors underwent free diffusion in extrasynaptic space, which was treated as devoid of any obstacles. Although the PSD is a complex network of scaffold proteins, we pooled all binary and unitary reactions into two first-order kinetic rates, K_{on} and K_{off} . Altogether this model of receptor dynamics accounts for 1) association with scaffolding molecules, 2) dissociation from scaffolding molecules, 3) collision with obstacles when diffusing, and 4) free diffusion outside the PSD. Given that scaffold molecules at the synapse are in excess compared to the number of AMPARs (Sheng and Kim, 2011), we kept K_{on} constant. The dissociation rate K_{off} was taken as the inverse of

mean dwell time of AMPARs within postsynaptic density. Simulation parameters were chosen based on estimates of other studies (Table 2.1).

Simulating full and partial synapse FRAP. Diffusible particles were labeled as fluorescent, and randomly placed in the PSD and in a bigger domain (circle R) surrounding the PSD. The circle R radius was set to 400 nm. Particles were allowed to reach steady state before photobleaching. In case of full PSD bleaching, all particles within the convex hull of the PSD were set to be non-fluorescent while the ones outside remained marked as fluorescent. The number of fluorescent particles within the convex hull of the PSD were recorded as a function of time to calculate the FRAP curve. In case of partial synapse FRAP, particles within half the convex hull of the PSD were considered as bleached. While in simulations in Figs. 2.1-2, the total number of receptors was fixed, FRAP simulations needed to account for the exchange of receptors between the synaptic/perisynaptic region and the rest of the spine. To account for this exchange, a third parameter, K_{flip} , was introduced. K_{flip} was defined as the rate at which photobleached receptors get replaced by fluorescent receptors when they hit the outside boundary circle R. We tried different values of K_{on} and K_{off} and K_{flip} to fit experimental FRAP recovery curves, and we chose the values that fit the experimental FRAP with the least squared error.

For experiments

Neuron culture and transfection. Dissociated hippocampal neuron cultures were prepared from embryonic day 18 rats of both sexes as previously described (Frost et al., 2010). For PALM and uPAINT experiments, cells were plated onto coverslips that were cleaned and coated as reported by MacGillavry et al. (2013). Cells were grown 2-3 weeks in culture and transfected 36-48 h before experiments (unless stated otherwise). Individual coverslips

were transfected with 0.5-1.0 μ g of cDNA for each expression construct using Lipofectamine 2000 (Invitrogen).

Expression constructs. cDNAs were obtained or produced as follows (with original sources): SEP-GluA2 (R. Haganir); mEos3-GluA2 and PSD-95-mEos2 (MacGillavry et al., 2013). SEP-TM and mEos3-TM were constructed by subcloning SEP from SEP-GluA2 and mEos3.1 from mEos3.1-N1 (S. McKinney), respectively, into the pDisplay vector (Invitrogen) at XmaI-SacII; SEP-TM-Bind and mEos3-TM-Bind were constructed by subcloning TM-StgCtail into SEP-TM and mEos3-TM at SacII-XhoI. TM-StgCtail was bought as a single dsDNA segment (gBlocks Gene Fragments, Integrated DNA Technologies), in which the TM was derived from the pDisplay vector, and the StgCtail derived from residues D203-V323 of Stargazin peptide sequence (UniProt ID O88602); multiple cloning sites flanking the TM-StgCtail were introduced to facilitate further customization: added features include AgeI and MluI upstream, as well as MluI and a stop codon downstream. Homer1c-mCh was prepared by subcloning Homer1c from Homer1c-GFP (P. Worley) to NheI-AgeI sites of mCh-N1 (R.Y. Tsien).

SEP-TM-Cerulean and mEos3-TM-Cerulean were made by removing StgCtail from SEP-TM-Cerulean-StgCtail and mEos3-TM-Cerulean-StgCtail using MluI-mediated restriction and self-ligation. SEP/mEos3-TM-Cerulean-StgCtail was made by PCR extracting mCerulean3 from mCerulean3-C1 (M.A. Rizzo) and subcloning into SEP/mEos3-TM-StgCtail at AgeI. XbaI and NheI were added immediately up- and downstream of mCerulean3, respectively, during PCR extraction for two purposes: 1) to facilitate verification of the correction orientation of insertion, and 2) to facilitate addition of multiple mCerulean3's in tandem as XbaI and NheI have overlapping sticky ends and

thus a XbaI-NheI-digested mCerulean3 can be cloned into either XbaI or NheI site of a plasmid that contains both, which can be done multiple times without requiring additional restriction sites (adapted from iDimerize protocol of Clontech). However, SEP-TM-Cerulean-StgCtail and SEP-TM fused to multiple mCerulean3's on the intracellular domain, when expressed in neurons, did not show detectable fluorescence under neutral pH but fluoresced in ammonium-chloride-based alkaline bath (Park et al., 2006), indicating that the constructs do not traffic to the surface plasma membrane.

To generate SEP-FKBP-TM-Bind/Nonbind, FKBP was inserted into SacII site of SEP-TM-Bind/Nonbind. To generate TagBFP-FRB-TM-Bind/Nonbind, mTagBFP2-FRB was substituted for the SEP domain in SEP-TM-Bind/Nonbind between restriction sites XmaI and SacII. FKBP and mTagBFP2-FRB flanked by the appropriate restriction enzyme recognition sites were purchased as gBlock dsDNA segments (IDT). The mTagBFP2 sequence was derived from pBAD-mTagBFP2, a kind gift from Vladislav Verkhusha (Addgene plasmid #34632). The monomeric FKBP and FRB sequences were derived from pC₄M-F2E and pC₄-R_{HE}, respectively (Ariad Pharmaceuticals), now available as pHet-Mem1 and pHet-1 (Clontech). All constructs were confirmed by sequencing.

Live-cell imaging conditions. Cells expressing the indicated constructs were imaged in extracellular imaging solution containing the following (in mM): 120 NaCl, 3 KCl, 2 CaCl₂, 2 MgCl₂, 10 glucose, 10 HEPES, pH adjusted to 7.35 with 1N NaOH. Cells remained at 25 °C for no more than one hour per imaging session. In experiments where rapalog (AP21967 or A/C Heterodimerizer, Clontech) was applied, 100 µL of 10X treatment solution was added to the 0.9 mL bath. Rapalog was supplied in ethanol; it was

diluted to 10 μM in the extracellular imaging solution from a 500X stock solution. Thus each application of rapalog resulted in a final concentration of 0.2 % ethanol.

Fluorescence recovery for up to 11 minutes after photobleaching. Short-term FRAP experiments were performed on a spinning disk confocal system using software acquisition control by iQ (Andor Technology) similar to what has been previously described (Lu et al., 2014); however, it was modified to use a sCMOS camera (Zyla, Andor Technology) and a computer-steered, galvo-scanning laser delivery system (FRAPPA, Andor Technology). Imaging was performed with a 100X 1.45 numerical aperture (NA) oil-immersion objective, yielding a final effective pixel size of 65 nm. For recovery up to 140 seconds after photobleaching, images were single optical sections acquired every 2 s for 40 frames (20 before and 20 after bleaching) and subsequently every 5 s for 20 frames. Z stability was maintained by ZDC2 (Olympus) feedback positioning system. For recovery of 11 min after full and partial synapse photobleaching, images were 5-section Z-stacks (0.4 μm / section) acquired four times at variable delays after bleaching (5 s, 1 min 5 s, 6 min 5 s, and 11 min 5 s).

Photobleaching of synaptic SEP-tagged proteins was achieved via the FRAPPA unit using 405 nm laser excitation. (488 nm laser was avoided as it bleached both SEP and mCherry fluorescence regardless of bleaching power, dwell time, or iterations). Bleaching was executed in all cases with 60 μs dwell time, 2 iterations at 40-50% of the available 405 nm laser power. Bleaching parameters were adjusted at the beginning of each experiment to minimize mCherry bleaching. Time = 0 image acquisition followed directly after photobleaching. For full-synapse photobleaching, a rectangular bleaching region was placed around an entire synapse or spine. In contrast for partial synapse photobleaching, a

small rectangular region was placed near the edge of synapses. This resulted in $67\pm 2\%$ bleached for the half of the synapse close to the bleaching spot and $40\pm 4\%$ bleached for the opposite half in the case of SEP-GluA2; $67\pm 2\%$ for half targeted for bleaching and $36\pm 4\%$ for the opposite half in the case of SEP-TM-Bind. On average, $50\pm 3\%$ of the total synaptic SEP fluorescence was lost during partial synapse bleaching. Each experiment contained some synapses that were targeted for partial synapse photobleaching while others were fully bleached.

Fluorescence recovery for 52 minutes after photobleaching. Longer recordings of FRAP to measure the near-equilibrium states were performed on a Zeiss LSM710 laser scanning confocal system using a 20X/1.0 Plan-Apochromat water immersion objective and software acquisition control by Zen. SEP was excited with a 488 nm Ar ion laser, and mCherry with a 561 nm DPSS laser. Selected Homer1c-mCherry containing spines were bleached with 2 scans of the 488 nm laser at elevated power, which achieved 50-70% reduction in synaptic SEP fluorescence with minimal bleaching of mCherry fluorescence. Images were 5-section Z-stacks ($1.0\ \mu\text{m}$ / section) acquired 7 times at variable delays after bleaching (1, 2, 7, 12, 22, 32, and 52 min). Pinhole size was set to 2-3 Airy units, and a 4X optical zoom was used, yielding a pixel size of 104 nm.

FRAP image analysis. Image processing and analysis was performed in ImageJ after export from iQ or Zen. Values measured in ImageJ were output to Prism (Graphpad Software), in which statistics and graphing were done. Image z-stacks at all time points were maximally projected in the z dimension. Values measured in ImageJ were background subtracted before analysis. Baseline fluorescence intensity was normalized to 1.0 and FRAP recovery was calculated as the fluorescence increase between $t = 0$ (immediately

after SEP photobleaching) and the indicated time point. Rectangular regions were drawn to enclose individual spines or synapses while excluding the parent dendrite and minimizing background contribution. In partial synapse photobleaching experiments, the SEP intensity of nine to fifteen randomly selected spines in each field not targeted for bleaching were quantified at each time point; in longer recordings of FRAP, two spines not targeted for bleaching were randomly selected. The SEP signal in unbleached spines served as a control for the bleaching that occurred during imaging acquisition. The recovery curves of the bleached spines were normalized to a linear fit of the average intensity of the unbleached spines over time.

For full synaptic photobleaching, a single region was drawn around the entire synapse using the Homer1c-mCherry image. Averaged fluorescence intensity of SEP-tagged protein was quantified at each time. For partial synaptic photobleaching, two regions were drawn. The bleached region was drawn based on where the original bleaching region of interest was targeted. An additional control region of similar size was placed on the opposite side of the synapse. StackRegJ (Jay Unruh, Stowers Institute for Medical Research in Kansas City, MO) a plugin of ImageJ was used to correct for XY drift. StackRegJ aligns the mCherry channel timelapse based on the first time point in most cases, and then applies the same transformation to the SEP channel.

Synapses that were improperly bleached were discarded from further analysis. Synapses targeted for partial photobleaching could be improperly bleached for several reasons. For example, a single-pixel offset between the bleaching laser and the synapse before bleaching occurs can result in over- or under-bleaching. In addition, synapses can morph so much within a few minutes after photobleaching that the bleached spot cannot

be relocated reliably. To avoid these, we excluded the following cases from further analysis:

1) synapses of which partial bleaching regions were <60% bleached with respect to baseline fluorescence intensity, 2) synapses targeted for partial photobleaching that inadvertently resulted in decreased fluorescence over >3/4 of the synaptic area, and 3) synapses, of which morphology changed so considerably within the 11-minute experiment that analysis regions could not be repositioned with confidence. Using these criteria, 30 of 61 synapses targeted for partial photobleaching were excluded from further analysis.

We measured the areas of individual synapses by counting the image pixels of the Homer1c-mCherry cluster after thresholding the background-subtracted image at the half the peak fluorescence intensity of the PSD. We measured spine enrichment of each SEP-tagged protein by first drawing a rectangular region to enclose the entire spine head with minimal contribution from the background, and then drawing a polygonal region (~3X the width of the spine region) to enclose the parent dendritic segment immediately near the spine. The dendritic region was occasionally offset laterally to avoid dendritic hot spots of Homer1c-mCherry. SEP and Homer1c-mCherry (or TagBFP-FRB-TM-Bind) fluorescence in spines and dendrites were measured as averaged green and red (or blue) fluorescence after background subtraction. Spine enrichment was defined as $(G_{Spine} / R_{Spine}) / (G_{Dendrite} / R_{Dendrite})$, where G_{Spine} and $G_{Dendrite}$ represent the spine and dendritic SEP fluorescence, and R_{Spine} and $R_{Dendrite}$ the spine and dendritic mCherry (or TagBFP) fluorescence. This method was used as a relative, not absolute, means of comparing enrichment levels.

Single-molecule tracking (smt). SmtPALM was performed using a custom-built setup as described previously (Lu et al., 2014). Imaging was conducted at 50 Hz, with 4 ms laser pulses for 5,000-10,000 frames. To account for lateral drift, a 3-plane z-stack (1.5

μm thick) of PSDs marked by fluorescently tagged Homer1c was taken once before and after each single-molecule acquisition, a cross-correlation was calculated on maximum intensity projected images of the two sets, and experiments that yielded a lateral shift of more than one pixel (100 nm) were discarded from further analysis.

Single-molecule tracking method uPAINT was applied as reported by (Giannone et al., 2010). FKBP- and FRB-containing proteins were cross-linked using 1 μM rapalog (AP21967 or A/C Heterodimerizer, Clontech). Neurons were pre-incubated in full culture medium at 37 $^{\circ}\text{C}$ for 1-2 hours with rapalog, and subsequent imaging was performed at 25 $^{\circ}\text{C}$ in extracellular imaging solution. ATTO647N-conjugated anti-GFP nanobodies (GFPBooster-647N, Chromotek) were bath applied to a final concentration of 300-500 pM once the first stretch of synapses was identified for each coverslip. BSA (A7030, Sigma Aldrich) was bath applied to a final concentration of 0.5% to ameliorate nonspecific interactions of nanobodies with untransfected cells and the coverslip surface. A two-color single-molecule imaging setup that splits the emission of red and far-red bands was used as described by MacGillavry et al. (2013), in order minimize mechanical vibration after acquiring the first and before acquiring the last Z-stack of PSDs. To image subsequent fields of the same cell or coverslip, the bound nanobodies were photobleached first.

Single-molecule localization, tracking analysis, and diffusion coefficient calculation. All data analysis was performed offline using custom routines in Matlab (Mathworks). Algorithms for determining molecule locations and criteria for filtering molecules to be considered in further analysis were applied as described previously (MacGillavry et al., 2013). Criteria for defining a track were described by Lu et al. (2014). Using a tracking radius of 500 nm permitted monitoring of molecules with diffusion

coefficients up to $3 \mu\text{m}^2/\text{s}$, the upper bound for AMPARs as estimated by other groups (Bats et al., 2007; Hoze et al., 2012; Nair et al., 2013). Synaptic tracks were defined as tracks or periods of tracks that were within the border of the PSD, defined as in (Lu et al., 2014). Nonsynaptic tracks were defined as tracks or periods of tracks that were within a neuronal border but outside enriched regions or clusters as defined by a Voronoi-based segmentation program, SR-Tesseler (Levet et al., 2015). Briefly, each imaging field was subdivided into a number of polygonal regions centered on the localizations detected in smtPALM or uPAINT. A density metric δ_i^1 was computed for each localization, defined as the localization density within the total area composed of the polygon surrounding the localization and the immediate edge-sharing polygons. Localizations within the neuron were defined by thresholding the localizations with $\delta_i^1 > 2\delta_i$, where δ_i is the average localization density in the whole imaging field. Localizations within clusters were defined by the threshold $\delta_i^1 > 2\delta_N$, where δ_N is the average localization density of neuronal localizations. In general, some of the clustered localizations colocalized with the synaptic marker Homer1c but some did not. Potential contributions include synapses with low Homer1C expression, regions with a high density of endocytic adaptor molecules, sites of plasma membrane-ER apposition, or zones of dense cortical cytoskeleton. Since the precise origins of the clustered nonsynaptic localizations were outside the scope of this study and difficult to distinguish, we discarded them from further analysis. Nonsynaptic tracks were formed from unclustered neuronal localizations.

For PALM, the effective diffusion coefficient (D_{eff}) was calculated for tracks that persisted at least 4 frames on a weighted linear fit of the first four points of the mean square displacement (MSD) plots as described by Lu et al. (2014). For uPAINT in which tracks

are typically longer and MSD plots are linear up to 8-10 frames, D was calculated for tracks that persisted at least 8 frames. Mean squared displacement curves of synaptically located molecules in uPAINT experiments were determined from whole tracks or periods of tracks that spent at least 30 contiguous frames within the PSD borders. Statistical comparisons were done on $\text{MSD}(t = 30 * 20 \text{ ms})$ as a relative, not absolute, means of comparing the explored areas.

Statistics. Where means are presented, the accompanying errors are the standard error of the mean; additionally, these data were normally distributed according to the Shapiro-Wilk normality test. Where box-and-whisker plots are presented, the middle bar represents the median, the upper and lower limit of the boxes denote the interquartile range, and the whiskers extend to 5% and 95% of the distribution; additionally, these data were not normally distributed according to the Shapiro-Wilk normality test. Different sets of statistical tests were used for normally and non-normally distributed data. Pairwise statistical tests were performed using unpaired t test with Welch's correction for normally distributed data; they were performed using Mann-Whitney U test for non-normally distributed data. For experiments with more than two conditions, one-way ANOVA was used to test for overall differences among means of normally distributed data, whereas Kruskal-Wallis one-way ANOVA was used to test for overall differences among medians of non-normally distributed data. For partial and full synapse FRAP experiments, two-way ANOVA was used. For all omnibus tests, a Bonferroni correction was used for post-hoc pairwise comparisons. Kolmogorov-Smirnov tests were applied for cumulative frequency distributions. In all cases, means (or medians) were considered significantly different if the test reported $p < 0.05$.

Results

Transmembrane protein size influences its access to areas within the PSD

Emerging data demonstrate that PSD-95, the most abundant of synaptic scaffolding proteins, can be arranged in multiple well-defined, 80-nm wide clusters within the excitatory synapse (MacGillavry et al., 2013; Nair et al., 2013). To predict how this type of arrangement can influence the mobility and retention of critically important transmembrane proteins, we first developed a minimalist model of the PSD, which incorporated coordinates of PSD-95 molecules (Fig. 2.1A blue dots) measured by PALM (MacGillavry et al., 2013). In addition to PSD-95 molecules, the model PSD map contained a random placement of other abundant synaptic proteins (i.e. NMDARs, adhesion molecules, and other relatively immobile proteins such as potassium channels), the relative concentrations of which were based on mass-spectroscopy estimates (Cheng et al., 2006). We modeled the AMPARs to be hour-glass shaped, its external, transmembrane, and internal radii consistent with sizes measured using EM tomography (Chen et al., 2008) and single-particle EM (Nakagawa et al., 2005). Details on the shapes and sizes of AMPARs, PSD-95, and other components of the PSD model can be found in the Materials and Methods. We calculated the possible diffusion trajectories of AMPARs within the PSD by using two independent modeling methods: Monte Carlo simulation of Brownian dynamics and geometric modeling of potential diffusion paths using percolation theory (see Materials and Methods for programming details). Geometric modeling showed that a significant fraction of the PSD map was excluded from receptor passage (Fig. 2.1A gray lines). Monte Carlo simulation of receptor diffusion showed that a single AMPAR initiated within the PSD can sometimes be trapped (Fig. 2.1A cyan region). Regions of trapped diffusion

overlapped with regions that lacked percolation paths, even in the absence of binding. This initial observation predicted that the PSD could trap receptors even in the absence of receptor-scaffold interaction.

To test this prediction, we allowed receptor concentration to reach steady state through receptor-scaffolding binding, and then turned off the binding interaction ($K_{on} = 0$). In the PSD map shown in Fig. 2.1A, we found that majority (~75%) of AMPARs remained in the PSD, one minute after abolishing receptor-scaffold binding (Fig. 2.1B black curve), consistent with the small reduction in mEPSC amplitude measured in the presence of a peptide that disrupted the interaction between AMPAR and PSD-95 (Sainlos et al., 2011). To investigate whether the retention of AMPARs can be influenced by the protein bulk alone, we repeated the simulation using a “small receptor,” with an intracellular domain radius of 5 nm as opposed to 8 nm in the full AMPAR complex. We found that a much smaller fraction of small receptors remained in the synapse than AMPARs did in the absence of binding (Fig. 2.1B magenta curve). This effect was robust in a randomly selected subset of PSD maps ($n = 9$ maps; mean and s.e.m. of small receptor $20 \pm 0.9\%$; large receptor $68 \pm 1.9\%$; $p = 0.0039$; Fig. 2.1C-D). In a model of cylindrical tracer diffusion on two-dimensional membrane, Saffman and Delbruck (1975) predicted that lateral diffusion coefficient is directly proportional to $\log(1/R)$, where R is the radius of the cylindrical tracer. This relation suggests a weak dependence of diffusion coefficient on particle size, which was experimentally shown by Kucik et al. (1999). The difference of synaptic retention between small and large tracers observed here was larger than what could be explained by obstacle-independent change in diffusion on 2-D membrane,

suggesting that PSD-95 crowding can regulate the mobility and retention of AMPARs and other critically important transmembrane proteins based on the sizes of their protein bulks.

To investigate whether macromolecular crowding can influence the positioning of receptors based on protein size, we estimated all possible moving paths of differently sized cylindrical tracers in measured PSD-95 maps based on Voronoi methods used to study percolation (Saxton, 2010). We found that the smaller the tracer, the larger the synaptic region it was able to traverse (Fig. 2.1E-F), which suggests that the distribution of receptors within the synapse can be regulated in a manner dependent on the sizes of the diffusing proteins.

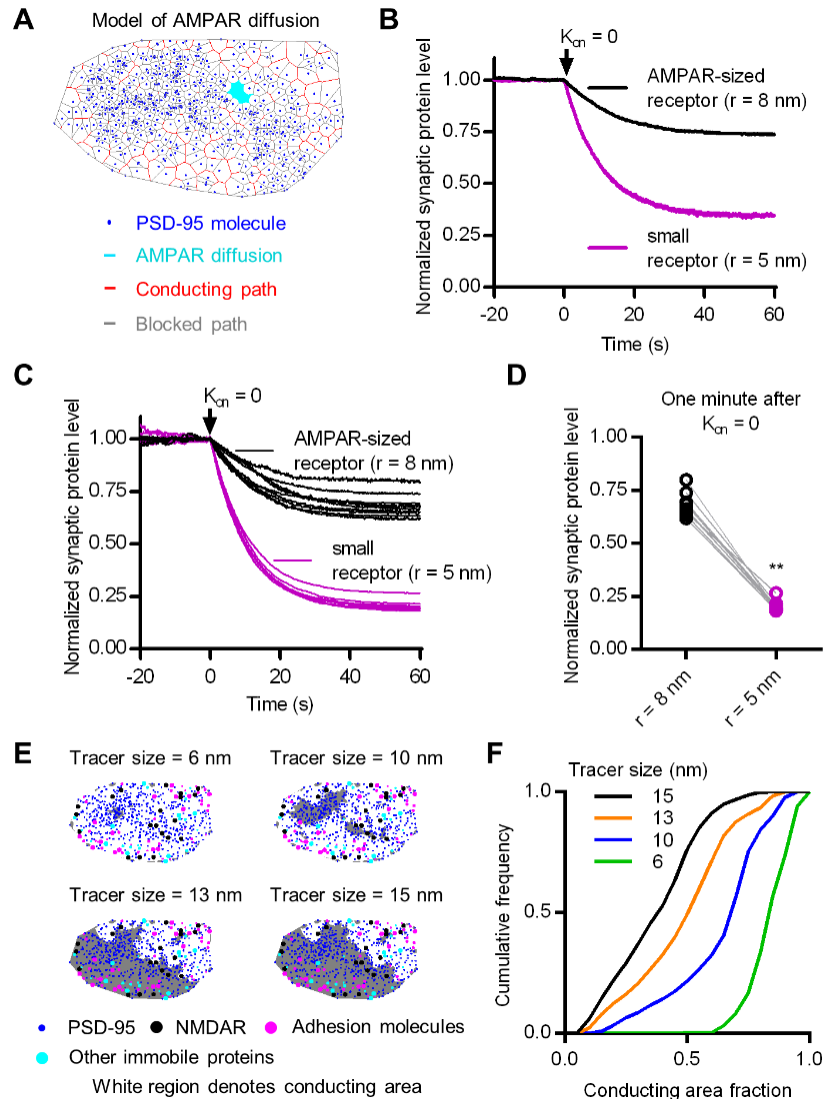


Figure 2.1. Synaptic crowding can retain membrane proteins in a size-dependent manner.

(A) Single example of simulated AMPAR-sized tracer diffusion (cyan) in a measured map of PSD-95 molecules (black) (MacGillavry et al., 2013). Conducting (red line segments) and blocked paths (gray line segments) of diffusion are predicted through percolation theory and Voronoi tessellation of PSD-95 occupied regions. (B) Synaptic level of large (black) and small (magenta) receptor before and after acutely abolishing receptor-scaffolding protein binding ($K_{on} = 0$) in a single measured PSD-95 map. (C) Same simulation as (B) performed for multiple measured PSD-95 maps ($n = 9$). (D) Paired statistical comparison of synaptic levels of large and small receptors one minute after turning off binding in multiple measured PSD-95 maps ($n = 9$ synapses; Wilcoxon matched-pairs signed rank test, $**p = 0.0039$). (E) Conducting area (white) estimated by Voronoi tessellation, predicting all possible paths a tracer of increasing size was allowed to take in an environment filled with PSD-95 molecules measured from PALM, along with other abundant proteins whose relative numbers were estimated from mass-spectroscopy (Cheng et al., 2006). (F) Cumulative likelihood of conducting area fraction of differently sized tracers in 100 measured PSD-95 maps.

We next considered whether the conservative retention of AMPARs is specific to the heterogeneous arrangement of PSD-95 molecules. To test this in the model, we allowed the receptor concentration to reach steady state either in a map of measured PSD-95 locations or in a boundary-matched map of randomly distributed PSD-95 locations (Fig. 2.2A), and then we measured receptor concentrations after turning off receptor-scaffold binding (Fig. 2.2B). Interestingly, receptors escaped quicker and to a larger extent from PSDs with randomized distribution of PSD-95 molecules than from PSDs with measured

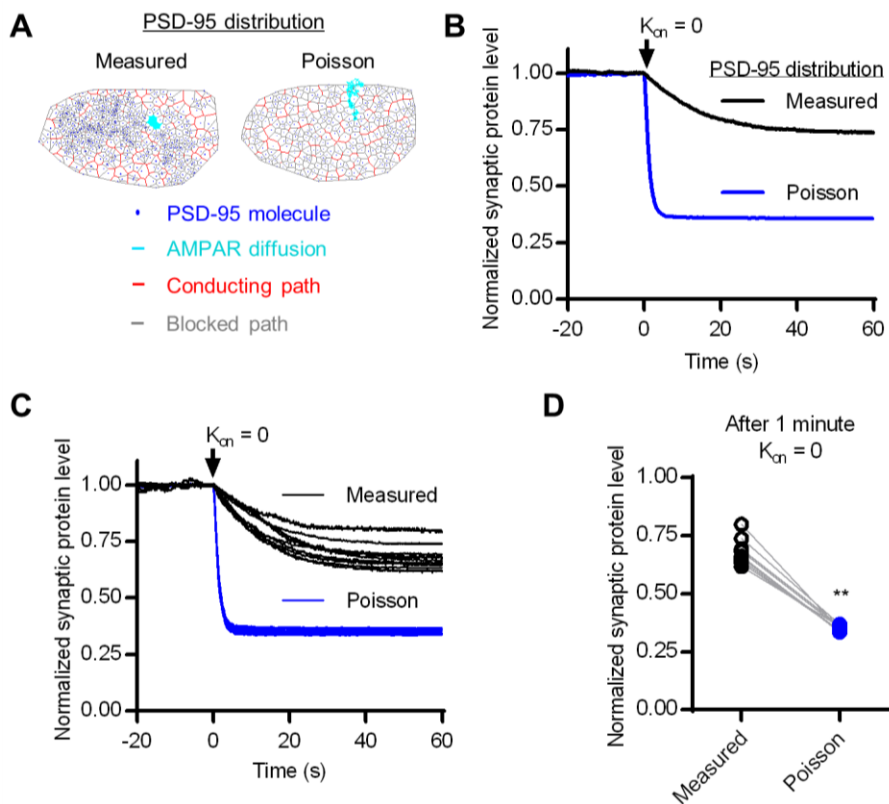


Figure 2.2. The arrangement of PSD-95 molecules can prolong the retention of synaptic AMPAR. (A) Single examples of AMPAR-sized tracer diffusion in a measured distribution PSD-95 molecules (left), and in a random distribution of PSD-95 molecules (right) (MacGillavry et al., 2013). (B) Synaptic receptor level before and after acutely abolishing receptor-scaffolding protein binding ($K_{on} = 0$) in a measured PSD-95 map (black) and its convex-hull matched Poisson distributed PSD-95 map (blue). (C) Simulation as done in (B) repeated for multiple measured PSD-95 maps ($n = 9$) and their convex-hull-matched Poisson distributed PSD-95 maps ($n = 9$). (D) Paired statistical comparison of synaptic receptor levels one minute after turning off binding in measured PSD-95 maps and their hull-matched Poisson PSD-95 maps ($n = 9$ synapses; Wilcoxon matched-pairs signed rank test, $**p = 0.0039$).

distribution of PSD-95 molecules (Fig. 2.2C-D). This result suggests the PSD can tune the density of membrane proteins by modulating the arrangement of PSD-95 molecules.

Transmembrane protein mobility depends on protein size in living synapses

To examine systematically the influence of protein size on protein mobility in synapses of live neurons, I first created a single-pass transmembrane probe molecule containing a superecliptic pHluorin (SEP) on the extracellular domain and the cytoplasmic tail of Stargazin (SEP-TM-Bind) (Fig. 2.3A). Akin to the AMPAR, this minimal probe was prominently trafficked to synapses marked by co-transfected Homer1c tagged with mCherry (Fig. 2.3B). Synaptic accumulation required the Stargazin C-tail, as a second probe lacking this domain (SEP-TM) trafficked with a nearly uniform distribution across the neuronal surface (Fig. 2.3B). More specifically, synaptic accumulation required the PDZ ligand on the Stargazin C-tail, as a third probe (SEP-TM-Nonbind) containing a single point mutation on threonine at position -2 (TTPV to TEPV) trafficked with a uniform distribution across the cell surface as well (Fig. 2.3B bottom), consistent with previous reports which demonstrated that the same mutation abolished the binding between Stargazin and PSD-95 (Chetkovich et al., 2002; Choi et al., 2002). To test the model prediction that transmembrane protein mobility within the synapse depends on protein size, I first measured fluorescence recovery of the small transmembrane probe and AMPAR after photobleaching single spines (Fig. 2.3C-D). SEP-GluA2 recovered on average 21% after 140 sec, similar to previous reports (Ashby et al., 2006; Kerr and Blanpied, 2012); however, SEP-TM-Bind recovered nearly twice this amount (Fig. 2.3E). Both proteins recovered similar amounts in the dendritic shaft (Fig. 2.3E). As it could be the case that smaller synapses correlate with faster recovery, I examined the PSD areas within the

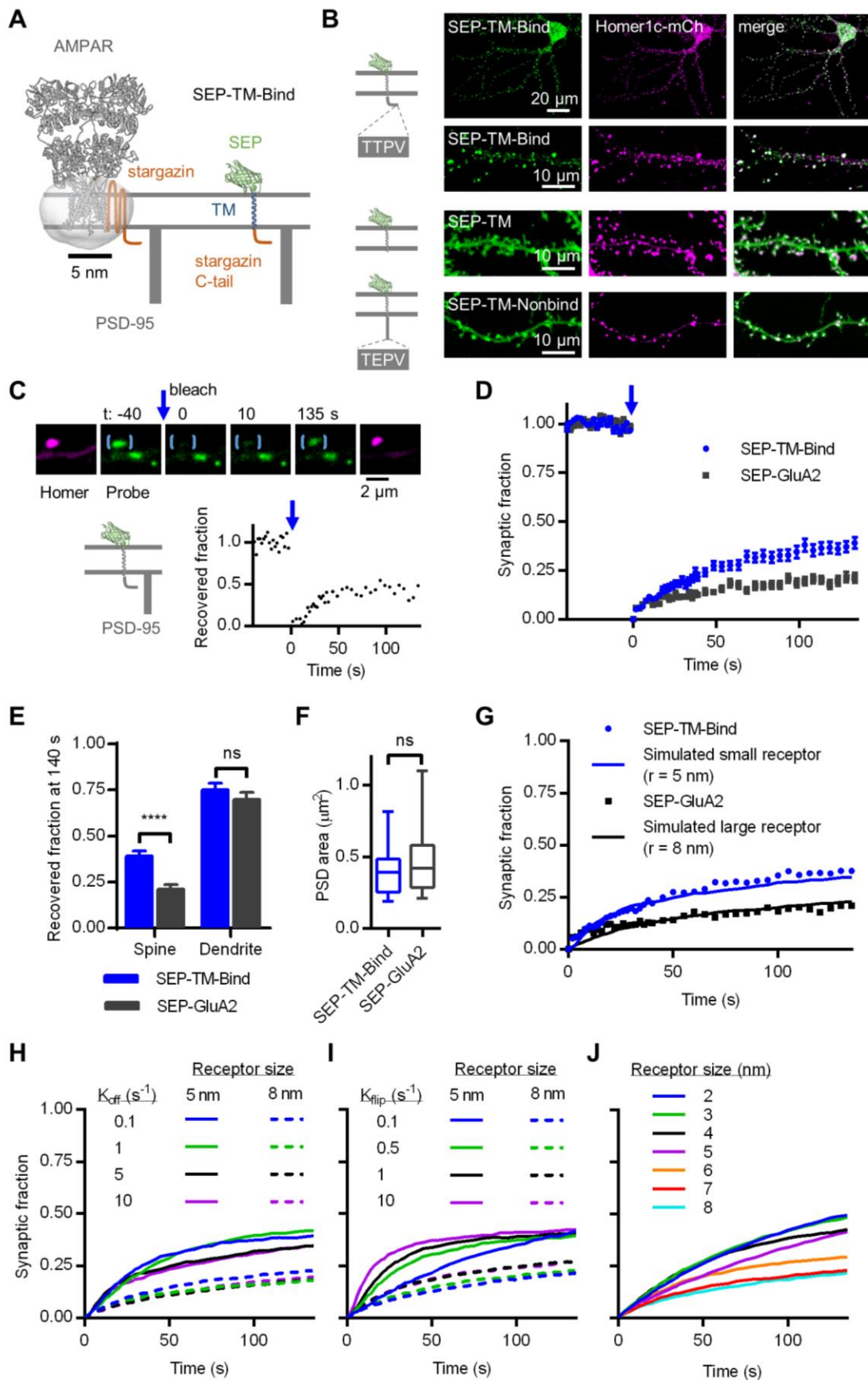
bleached spines by measuring the width of the Homer1c-mCherry image. The PSD areas were not different (Fig. 2.3F), the recovery of SEP-TM-Bind at 140 sec after bleaching was weakly negatively correlated with PSD area ($r^2 = 0.17$, $p = 0.0064$, $n = 42$), and the recovery of SEP-GluA2 at 140 sec after bleaching was not correlated with PSD area ($r^2 \ll 0.001$, $p = 0.97$, $n = 37$), suggesting that a difference in synapse size cannot account for the recovery difference in spines between the two groups.

It is possible that the difference of recovered fractions in spines between SEP-GluA2 and SEP-TM-Bind could be explained by a potential difference in affinity for PSD-95. To examine this notion formally, I turned to computer modeling (and see also Fig. 2.9). The kinetic rates of the model (i.e. K_{off} : receptor-scaffold binding affinity, and K_{flip} : the likelihood to reset photobleached receptors back to fluorescence when they hit the boundary of simulated spine head area) were initialized by minimizing the difference between the simulated and the measured recovery curves (Fig. 2.3G). Varying K_{off} by 2 orders of magnitude had negligible influence on the time-course and steady state of simulated recoveries, but changing the tracer size by a factor of two yielded a consistent difference in recovery for a large range of K_{off} values (Fig. 2.3H). This suggests that the size of the receptor protein is more likely than the receptor-scaffold binding affinity to influence receptor mobility. Altering K_{flip} by 2 orders of magnitude yielded notable change in the recovery speed of the small tracer, but had negligible influence on the steady state of the recovery for both the large and the small tracer (Fig. 2.3I). K_{flip} crudely accounts for factors like spine geometry and synaptic-extrasynaptic protein concentration gradient, and thus the result suggests these factors are unlikely to explain the difference in the mobile fraction after 2 min of exchange. Importantly, tracers that were no more than four times

smaller than the AMPAR recovered more than twice as much after 2 min (Fig. 2.3J), suggesting that membrane protein size can be a major determinant of mobility.

Figure 2.3. Small and large membrane proteins exchange differently on the surface membrane of dendritic spines.

(A) Schematic of AMPAR crystal structure and minimalist membrane protein (SEP-TM-Bind) drawn to scale. SEP-TM-Bind is a fusion protein of three parts: SEP a pH-sensitive GFP protein, TM the transmembrane domain of PDGFR, and the binding component which is the cytoplasmic tail of Stargazin. (B) The SEP-TM-Bind was trafficked to the synapse (top and second row) in dissociated hippocampal cultured neurons; the SEP-TM which lacks any intracellular domain was expressed with uniform distribution across dendritic surface (second to last row); and the SEP-TM-Nonbind (in which Thr at the -2 position is mutated to be Glu) was trafficked with uniform surface distribution as well (last row). (C) An example of FRAP to assess the mobility of SEP-TM-Bind on spines. (D) Averaged recovery curves \pm standard error of the mean for small and large membrane proteins in spines ($n = 42/11/2$ ROIs/neurons/cultures for SEP-TM-Bind, 37/10/2 for SEP-GluA2). (E) Recovered fractions at 140 sec in spines ($p < 0.0001$ unpaired t -test, $n = 42/11/2$ for SEP-TM-Bind, 37/10/2 for SEP-GluA2) and dendritic segment ($p = 0.31$, $n = 27/9/2$ for SEP-TM-Bind, 33/10/2 for SEP-GluA2). (F) Areas determined from confocal images of Homer1c-mCherry co-expressed with either SEP-TM-Bind or SEP-GluA2 in FRAPed spines ($p = 0.18$ Mann-Whitney test, $n = 42/11/2$ for SEP-TM-Bind, 37/10/2 for SEP-GluA2). (G) Simulated FRAP to fit parameters of K_{off} , diffusion, anything else in a measured PSD-95 map. (H) Changing binding dissociation rate (K_{off}) by 2 orders of magnitude did not remarkably alter the simulated FRAP spines containing either small ($r = 5$ nm) or large tracer ($r = 8$ nm). (I) Changing K_{flip} by 2 orders did not significantly alter spine FRAP. (J) Changing the receptor size within one order of magnitude significantly altered spine FRAP. (Corresponding figure shown on the preceding page)



In further experiments, I found that this difference persisted at longer periods following photobleaching (Fig. 2.4A,B). The small binding probe recovered more fully than AMPARs both transiently (2 min after bleaching) and near steady-state (52 min after bleaching) (Fig. 2.4C), suggesting that compared to the larger AMPARs, the small probe diffuses faster and has a smaller proportion stabilized in the spine.

To address whether the spine-to-dendrite concentration gradient or an altered synapse size induced by probe expression might contribute to these observed differences in mobility, I measured the PSD area and spine enrichment (defined in Methods) in the same spines that were followed for FRAP. The PSD areas were not different between spines expressing SEP-TM-Bind and SEP-GluA2 (Fig. 2.4D). The recovered fraction of the small probes 2 min after bleaching was weakly inversely proportional to PSD area ($r^2 = 0.26$), and that of AMPARs was not correlated with PSD area (Fig. 2.4E). Fifty-two min after bleaching, the recovered fractions of both proteins were not correlated with PSD areas (Fig. 2.4F), indicating that the fraction of molecules exchanging in and out of the spine was unaffected by synapse size. The spine enrichment was not different between spines expressing the small probes and AMPARs (Fig. 2.4G). The transient and steady-state recovery levels were not correlated with the spine enrichment in spines expressing either protein (Fig. 2.4H,I). Altogether, both simulated and experimental FRAP results support the notion that receptor size is a prominent factor in limiting receptor mobility in the dendritic spine.

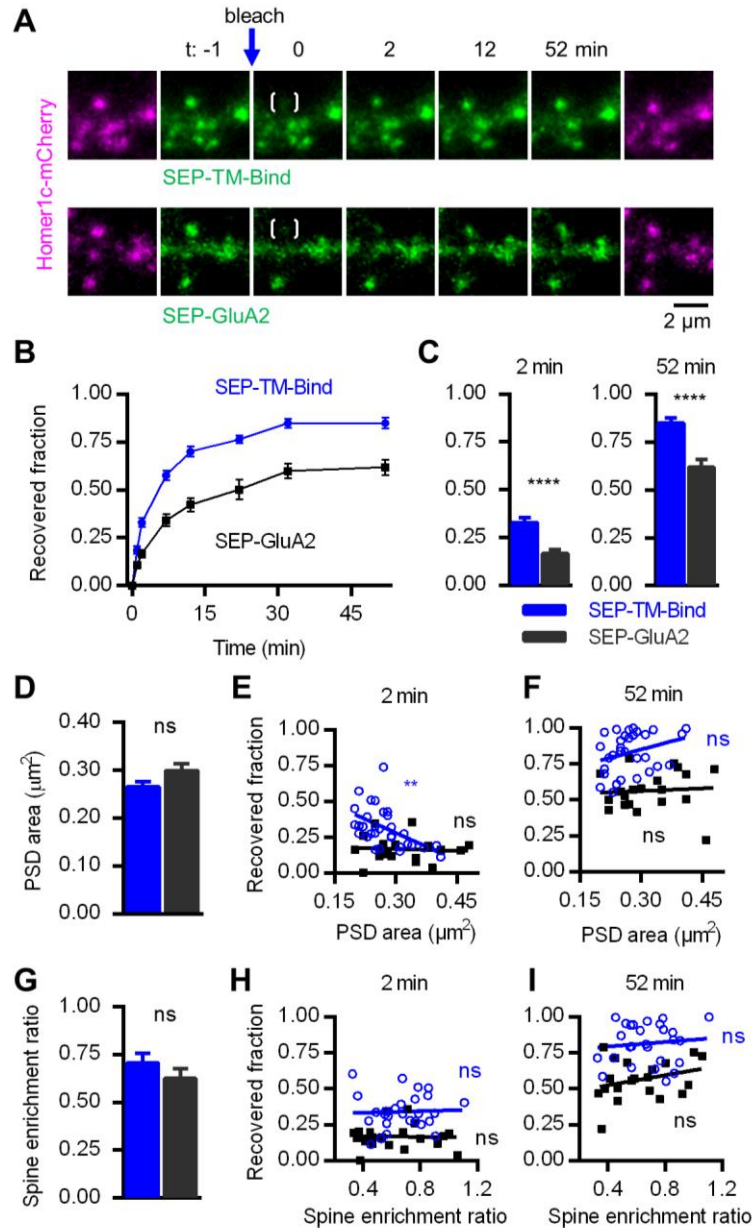


Figure 2.4. The surface mobility of AMPAR in spines is unrelated to synapse size or spine-dendritic concentration gradient; that of the small probe is weakly related to synapse size.

(A) Representative FRAP images of DIV20-21 hippocampal neurons co-transfected with Homer1c-mCherry, and either SEP-TM-Bind or SEP-GluA2. Bracketed spines were photobleached. (B) Recovery curves of bleached SEP-TM-Bind ($n = 35$ spines/5 neurons) and SEP-GluA2 ($n = 20/3$) from 3 separate cultures. (C) Recovered SEP fractions of SEP-TM-Bind and SEP-GluA2 in spines after 2 and 52 min ($p < 0.0001$). (D) PSD areas of bleached SEP-TM-Bind and SEP-GluA2 ($p = 0.0732$). (E) The PSD area and transient (2 min) recovery level of each bleached SEP-TM-Bind (circles, $r^2 = 0.26$, $**p = 0.0038$) and SEP-GluA2 (squares, $r^2 = 0.0051$, $p = 0.77$). (F) The PSD area and near-steady-state (52 min) recovery level of bleached SEP-TM-Bind ($r^2 = 0.091$, $p = 0.10$) and SEP-GluA2 ($r^2 = 0.090$, $p = 0.77$). (G) Spine enrichment of bleached SEP-TM-Bind and SEP-GluA2 ($p = 0.255$). (H) The spine enrichment and transient (2 min) recovery of bleached SEP-TM-Bind ($r^2 = 0.0018$, $p = 0.83$) and SEP-GluA2 ($r^2 < 0.001$, $p = 0.91$). (I) The spine enrichment and near-steady-state (52 min) recovery of bleached SEP-TM-Bind ($r^2 = 0.011$, $p = 0.60$) and SEP-GluA2 ($r^2 = 0.086$, $p = 0.21$). Color-coding in D-I same as in C. Data in B-D, G shown as mean \pm s.e.m, statistical test was unpaired t-test.

Small and large membrane proteins traverse the PSD at different rates in live neurons

Spine geometry will influence recovery after photobleaching the entire spine and synapse together (Ashby et al., 2006; Simon et al., 2014). To assess mobility within synapses, I first utilized photobleaching by targeting just part of single synapses and monitoring recovery within this subregion of the PSD (Kerr and Blanpied, 2012) (Fig. 2.5A). Fully bleached synapses will recover fluorescence via exchange with the extrasynaptic unbleached population. However, in the targeted region of partially bleached synapses, recovery will proceed more quickly than this only if mobility of the probe within the synapse (subs synaptic mobility) is substantial enough to permit the synaptic unbleached pool to distribute to the bleached region.

To formalize our expectations on the subsynaptic mobility of large and small membrane proteins, we first modeled this experiment. To simulate membrane protein dynamics, we modeled tracer diffusion by Monte Carlo simulations of Brownian dynamics (see Materials and Methods) within a measured PSD-95 distribution and in surrounding extrasynaptic space. In the case of full synaptic bleaching, all particles within the convex hull of the measured PSD-95 molecules (synaptic region) were set to be non-fluorescent while ones outside remained marked as fluorescent. The number of fluorescent particles within the synaptic region were recorded as a function of time to calculate the full synapse FRAP curve (Fig. 2.5B, solid lines). In the case of partial synaptic bleach, particles within half of the synaptic region were considered bleached. The number of fluorescent particles within the bleached half were recorded over time to calculate the half synapse FRAP curve (Fig. 2.5B, dotted lines). The recovery dynamics of AMPAR-sized tracers ($r = 8$ nm) were nearly identical after half-synapse bleaching and after full synapse bleaching (17-18% after

40 seconds; Fig. 2.5B, black lines). On the other hand, the smaller tracers ($r = 5$ nm) recovered more after half-synapse bleaching than after full synapse bleaching (45% and 39% at 40 seconds after half and full synapse bleach, respectively; Fig 2.5B blue curves). This result is useful to consider because recovery after photobleaching in synapses depends on several factors. The rate of recovery will depend on the extrasynaptic probe enrichment as well as extrasynaptic mobility. In addition, an important parameter is how quickly synaptic receptors explore the PSD to find an exit route compared to how fast exited receptors get replaced. In this simulation, several key variables that could influence the recovery were kept identical for both tracers: the PSD-95 distribution, the binding affinities, the true diffusion coefficient (D) of the molecule in the synapse, and the total number of tracers. In addition, the enrichment ratio of both tracers at the equilibrated state before photobleaching reached the same value of $\sim 4:1$ (inside:outside the PSD). The only difference was the diameters of the tracers, which thus could access different fractional areas within the synapse. Therefore, the simulated subsynaptic bleaching results indicate that the conduction area or routes of passage within the synapse can contribute significantly to intrasynaptic recovery.

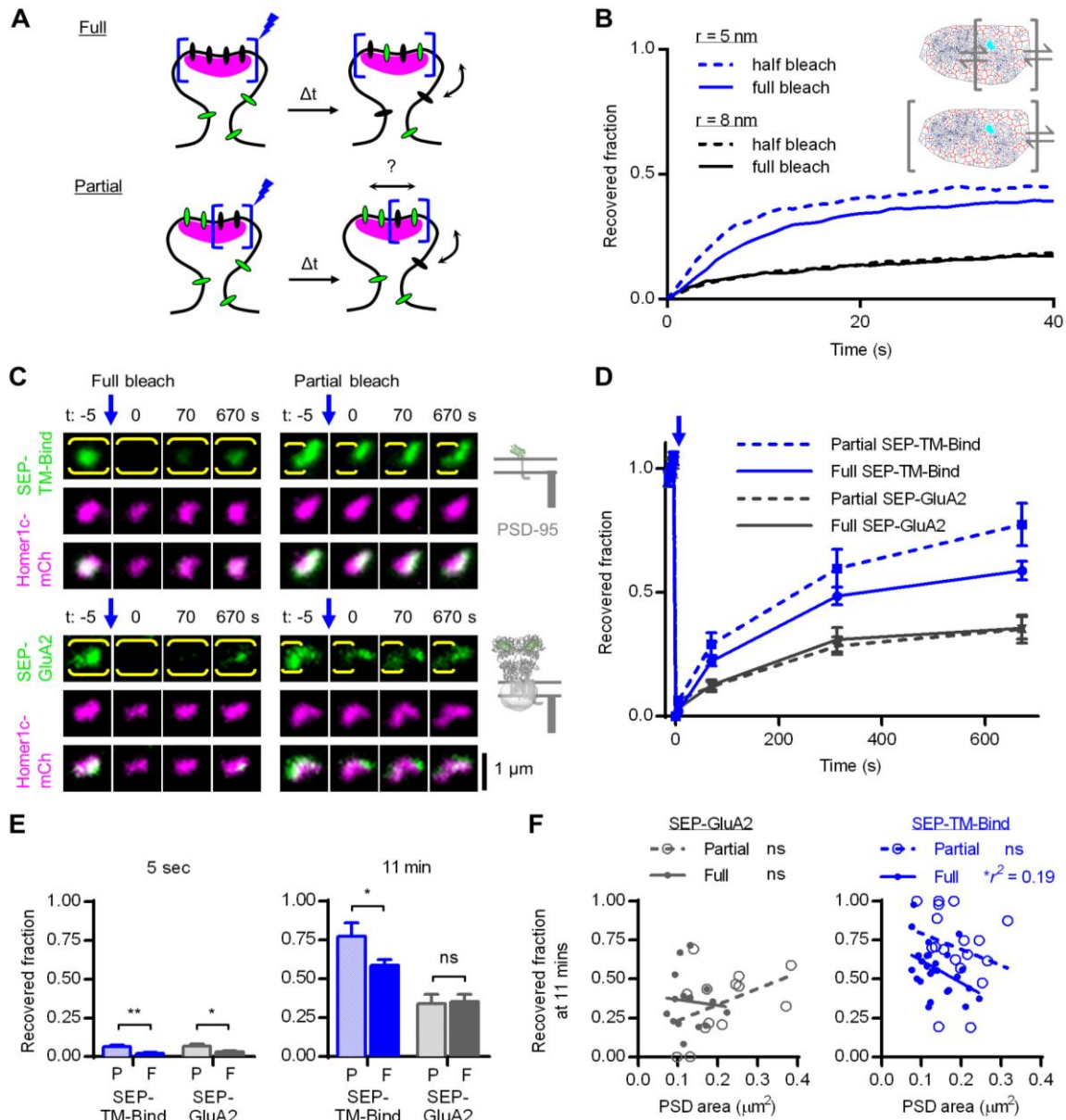


Figure 2.5. Small membrane probe has higher subsynaptic mobility than AMPAR.

(A) Partial synaptic FRAP can assess mobility of membrane proteins within the confine of a synapse. (B) Simulated partial synaptic and full FRAP for small ($r = 5 \text{ nm}$) and large tracer ($r = 8 \text{ nm}$). (C) Example synapses expressing SEP-TM-StgCtail or SEP-GluA2 and Homer1c-mCherry where all or part of the synaptic SEP was photobleached. (D) (Top) SEP-TM-StgCtail or SEP-GluA2 fluorescence recovery in synapses targeted for full or partial synapse photobleaching, mean \pm s.e.m. Experiments were interleaved in neurons co-expressing either SEP-TM-StgCtail or SEP-GluA2. (E) SEP-TM-StgCtail or SEP-GluA2 fluorescence recovery at 5 sec and 11 min after photobleaching. $n_{\text{StgCtail, full}} = 27 \text{ PSDs}/9 \text{ neurons}/2 \text{ cultures}$, $n_{\text{StgCtail, partial}} = 18/9/2$, $n_{\text{GluA2, full}} = 15/7/2$, $n_{\text{GluA2, partial}} = 13/6/2$. Two-way ANOVA with Bonferroni's multiple comparisons tests was performed $**p = 0.0012$, $*p = 0.037$ for 5 sec; $*p = 0.032$, ns not significant $p > 0.999$ for 11 min. (F) (Left) The PSD area and recovered fraction 11 minutes after partially or fully bleaching SEP-GluA2 in each synapse (ns $p = 0.14$ for partial, $p = 0.81$ full); (Right) after partially or fully bleaching SEP-TM-Bind in each synapse (ns $p = 0.33$ for partial, $*p = 0.026$ full).

To test this in living synapses, I performed partial synaptic photobleaching in neurons expressing either SEP-GluA2 or SEP-TM-Bind (Fig. 2.5C). Following full synapse photobleaching, I detected little fluorescence recovery after 5 seconds ($3.2 \pm 0.7\%$ SEP-GluA2, $2.3 \pm 0.4\%$ SEP-TM-Bind; $n = 15$ synapses in 7 neurons SEP-GluA2, 27 synapses in 9 neurons SEP-TM-Bind; Fig. 2.5D), suggesting that the rapidly exchanging populations of both large and small membrane proteins were very small in these synapses. After 11 min, $35.6 \pm 4.6\%$ of synaptic AMPAR fluorescence was recovered, consistent with previous reports (Ashby et al., 2006; Sharma et al., 2006; Frischknecht et al., 2009; Arendt et al., 2010; Kerr and Blanpied, 2012), whereas $58.7 \pm 3.8\%$ of synaptic membrane probe was recovered. These relative recovery fractions were as expected based on full-spine photobleaching (Fig. 2.2).

Following partial synapse photobleaching (performed during the same time series on neighboring synapses), recovery of AMPAR within the bleached subregion of the synapse was slightly higher after 5 seconds but not different after 11 min compared to fully bleached synapses ($6.7 \pm 1.6\%$ and $34.0 \pm 6.2\%$ for partial; $n = 13$ synapses in 6 neurons; $p = 0.037$ and 0.98 compared with fully bleached synapses; Fig. 2.5E). However, recovery of the small probe SEP-TM-Bind was higher after 5 seconds than in fully bleached synapses ($6.5 \pm 1.1\%$ for partial; $n = 18$ synapses in 9 neurons; $p = 0.0012$ compared to fully bleached synapses; Fig. 2.5E left). Importantly, it remained higher after 11 min ($77.5 \pm 1.7\%$ for partial; $p = 0.031$ compared to fully bleached synapses; Fig. 2.5E right).

Image acquisition itself caused minimal photobleaching, as fluorescence intensity in neighboring unbleached synapses remained nearly constant ($94.5 \pm 4.3\%$ of baseline for SEP-GluA2, $99.2 \pm 1.8\%$ for SEP-TM-Bind after 11 min). I assessed the bleached fraction

in the synaptic subregion not targeted for photobleaching. It was determined first by outlining the entire synapse excluding the half targeted for bleaching and then calculating the fluorescence lost immediately after photobleaching. I calculated this because the confocal laser spot inevitably affects part of the synapse unintended for bleaching, and I reasoned that the fraction of unbleached proteins could influence the recovery within the bleached region. However, I found that the bleached fractions in regions unintended for photobleaching were not different for both proteins (mean \pm s.e.m.: $40 \pm 4\%$ for SEP-GluA2, $36 \pm 4\%$ for SEP-TM-Bind; unpaired t-test $p = 0.17$). Bleached fractions in the synaptic subregion targeted for photobleaching were also not different (mean \pm s.e.m.: $67 \pm 2\%$ for SEP-GluA2, $67 \pm 2\%$ for SEP-TM-Bind; unpaired t-test $p = 0.88$). It is possible that this modest difference in bleached fractions between two subregions of the synapse resulted in a dynamic range that was insensitive to a significant subpopulation of AMPARs that exchanged laterally on the order of minutes within the synapse. Nonetheless, the difference in recovery between the two proteins was robust on a minute timescale (Fig. 2.5D,E).

It is possible that AMPARs were overall less mobile within the larger-than-average PSDs required to perform partial synaptic FRAP reliably. However, the synaptic areas were not different for the two proteins (Homer1c-mCherry area median [interquartile range] μm^2 : 0.18 [0.14-0.31] SEP-GluA2, 0.21 [0.14-0.28] SEP-TM-Bind, Mann-Whitney U test $p = 0.63$). Furthermore, the recovery fraction of SEP-GluA2 was uncorrelated with PSD area in both partial and full synapse bleaching schemes ($r^2 = 0.19$, $p = 0.14$, $n = 13$ PSDs for partial; $r^2 = 0.005$, $p = 0.81$, $n = 15$ full; Fig. 2.5F left). Moreover, the recovery fraction of the small binding probe was uncorrelated with PSD area in the partial synapse bleaching

case, and negatively but weakly correlated with PSD area in the full synapse bleaching case ($r^2 = 0.061$, $p = 0.33$, $n = 18$ PSDs for partial; $r^2 = 0.19$, $p = 0.026$, $n = 27$ full; Fig. 2.5F right). Thus, the difference in recovery between the two proteins as measured by partial synapse photobleaching was likely not caused by the selective use of large synapses.

In the partial bleaching assay, this difference in recovery between probes of two sizes could arise from a difference in the ratio of their diffusion coefficients in versus out of the synapse, or from their differential interactions with the PSD interior milieu that slow overall mobility (e.g. differential access to percolation routes within the synapse). I cannot disentangle these possibilities based on experimental data. However, our modeling suggests that at least some of the difference may be due to steric effects.

Mobility of small and large membrane proteins within the living synapse

To obtain higher resolution of protein mobility within the synapse, I turned to single-molecule tracking PALM (smtPALM). I replaced the SEP in each probe with mEos3.1 (Zhang et al., 2012), a green fluorescent protein that can be converted to red fluorescence with UV exposure. After co-transfection with Homer1c-GFP, weak UV irradiation prompted appearance of sparse, well-isolated, red molecules that could be tracked over time either within or outside the border of the synapse (Schneider et al., 2015). The average trajectory persisted for 6 frames before disappearing ($n = 28320$ tracks for all conditions in Fig. 2.6). Given the relative short length of tracks, I obtained the instantaneous, effective diffusion coefficient (D_{eff}) as the best weighted linear fit of the MSD curve for every track that persisted for at least 4 frames (see Materials and Methods) as this method optimally

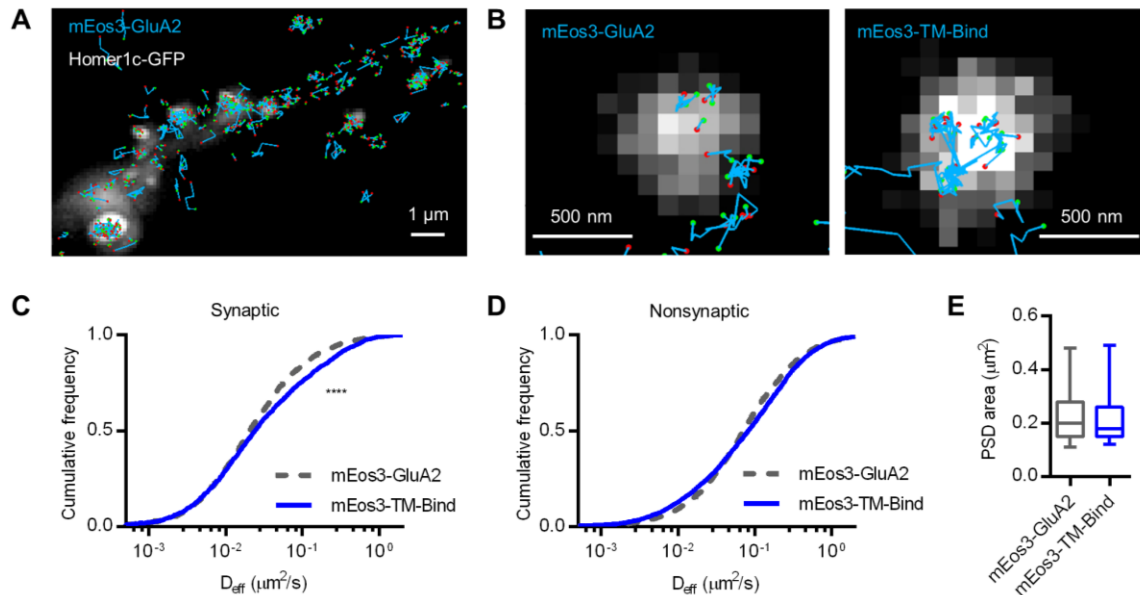


Figure 2.6. Diffusion of small membrane protein and AMPAR within and near the excitatory synapse. (A) Tracked motion of mEos3-GluA2 (blue tracks) on PSDs marked by Homer1c-GFP. Green and red circles indicate start and end of individual tracks. (B) Tracks of receptor (B, left panel) or smaller probe (B, right panel) on representative single PSDs marked by Homer1c-GFP. (C) Cumulative frequency plot of synaptic diffusion coefficients ($n_{\text{mEos3-GluA2}} = 2065$ tracks/239 PSDs/13 neurons/2 cultures, $n_{\text{mEos3-TM-Bind}} = 2403/284/12/2$). (D) Cumulative frequency plot of nonsynaptic diffusion coefficients ($n_{\text{mEos3-GluA2}} = 3177$ tracks/13 neurons/2 cultures, $n_{\text{mEos3-TM-Bind}} = 4044/12/2$) (E) Areas of Homer1c-GFP puncta that contained tracks ($n_{\text{mEos3-GluA2}} = 239$ PSDs, $n_{\text{mEos3-TM-Bind}} = 284$). Statistics for C-E: Mann-Whiney U test (**** $p < 0.0001$ for C, $p = 0.058$ D, $p = 0.055$ E), K-S test ($p < 0.0001$ for C, D).

separated distributions of nearly immobile molecules from more mobile ones (Lu et al., 2014).

To determine whether the small transmembrane probe and the large receptor diffuse differently within the synapse, I segregated the tracks into two groups. Tracks that were within the full-width at half maximum border of Homer1c-GFP puncta were considered synaptic; the remaining tracks were classified as nonsynaptic only if they were within the neuronal border and outside of dendritic clusters of unknown origin defined by a robust, automatic segmentation program, SR-Tesseler (Levet et al., 2015) (see Materials and Methods). A typical reconstruction of the individual moving mEos3-GluA2-containing AMPARs or mEos3-tagged membrane probe (Fig. 2.6A,B) showed that the displacements were heterogeneous inside individual synapses. The synaptic mEos3-GluA2 and mEos3-TM-Bind had identical distributions of D_{eff} below $0.015 \mu\text{m}^2/\text{s}$ (Fig. 2.6C), which suggests that a fraction of synaptic membrane proteins, could be so tightly bound to scaffolds or tightly packed such that they could not diffuse distinguishably regardless of protein size. On the faster end of the diffusion spectrum ($>0.15 \mu\text{m}^2/\text{s}$), the small transmembrane probe diffused on average faster than the large receptor (Fig. 2.6C), which suggests the existence of a subpopulation that can traverse the PSD more readily, consistent with partial synapse photobleaching results. The distribution of nonsynaptic D was in general shifted towards larger mobility compared to that of synaptic D for both proteins (Fig. 2.6C,D). The nonsynaptic D_{eff} of the AMPARs and the small binding probe had nearly identical distributions and their medians were not different (Fig. 2.6D). The synaptic areas as estimated by taking the full-width half-maximum of the Homer1c-GFP puncta that contained tracks were not different on average for the two membrane proteins (Fig. 2.6E),

suggesting that the difference in mobility is independent of the difference in synaptic size. Indeed, the averaged D_{eff} within each PSD was not correlated with PSD size ($r^2 \ll 0.001$, $p = 0.91$, $n = 239$ PSDs for mEos3-GluA2; $r^2 = 0.006$, $p = 0.24$, $n = 284$ mEos3-TM-Bind). Altogether, results of simulation, partial bleaching, and single-molecule tracking show that the small transmembrane probe moves more freely than the AMPAR within the PSD. These observations provide support for the hypothesis that steric hindrance within the PSD can be a prominent factor that impedes the movement of transmembrane proteins, and suggests that the synapse selectively restricts protein distribution based on protein size.

PDZ-mediated binding was only partially responsible for stabilizing the synaptic mobility of the small membrane probe

To test directly the influence of binding to synaptic scaffold on the mobility of the membrane probe, I made a nonbinding variant of the transmembrane probe (TM-Nonbind) by mutating threonine in the -2 position of the Stargazin C-tail to glutamate (T321E), a point mutation that has been shown by previous studies to abolish the binding between Stargazin and PSD-95 (Chetkovich et al., 2002; Choi et al., 2002). I examined fluorescence recovery 140 seconds after photobleaching (Fig. 2.7A,B), and also measured the near-equilibrium recovery within 52 min of photobleaching (Fig. 2.7C). The early recovery kinetics of nonbinding probe (SEP-TM-Nonbind) lay intermediate between the binding probe (SEP-TM-Bind) and the probe that lacked intracellular residues (SEP-TM) (Fig. 2.7B,C). At 30 seconds after bleaching the whole spine, the fluorescence of SEP-TM-Nonbind recovered less than that of SEP-TM and more than that of SEP-TM-Bind (mean \pm s.e.m.: 50.1 \pm 2.4% TM, 33.0 \pm 3.1% TM-Nonbind, 20.0 \pm 1.8% TM-Bind; $n = 28$ synapses/10 neurons TM, 27/3 TM-Nonbind, 42/11 TM-Bind; $p < 0.0001$ ANOVA; Fig.

2.7D), suggesting that binding to PSD-95 is required for maximally stabilizing the mobility of fast exchanging receptors. At 140 seconds, the spine fluorescence recovery extents of SEP-TM and SEP-TM-Nonbind were not different (mean \pm s.e.m.: $73.8 \pm 3.5\%$ TM, $67.8 \pm 3.1\%$ TM-Nonbind; $p = 0.23$), but they were both higher than that of SEP-TM-Bind ($38.5 \pm 3.0\%$; $p < 0.0001$ compared with TM or TM-Nonbind; Fig. 2.7E). At 52 min, the recovered spine fractions of all three probes were not statistically different (Fig. 2.7F), indicating that a single PDZ binding motif is not sufficient to regulate the relative proportions of mobile and immobile TM proteins in the spine. The fluorescence recovery of all three probes were not different following photobleaching the dendritic shaft (mean \pm s.e.m.: $67.1 \pm 2.1\%$ TM, $73.5 \pm 3.8\%$ TM-Nonbind, $75.2 \pm 3.4\%$ TM-Bind; $n = 21$ dendritic shaft segments/9 neurons TM, 18/3 TM-Nonbind, 27/9 TM-Bind; $p = 0.18$; Fig. 2.7G).

The spine enrichment of SEP-TM-Bind was the highest of the three probes, essentially identical to Homer 1C, whereas SEP-TM or SEP-TM-Nonbind were strikingly less enriched and not different from one another (Fig. 2.7I). Thus, the PDZ-binding motif was necessary and sufficient for accumulating the TM probe in the spine. The PSD areas of the photobleached spines were not different for all three probes (Fig. 2.7H). The recovered fraction of SEP-TM-Bind in individual spines was negatively correlated with the size of the synapse at 30 and 140 seconds, although the correlation was weak as the variation in synapse size could only explain 15-17% of the variation in recovery; there was no correlation at 52 min after bleaching (Table 2.2). There was no correlation between the recovered fraction and synapse size for SEP-TM and SEP-TM-Nonbind at any time after bleaching (Table 2.2). In addition, there was no correlation between the recovered fraction and spine enrichment for any of the three probes (Table 2.2). Altogether, these results

indicate that the reduction TM probe mobility by the addition of the non-binding Stg C-tail did not arise due to a difference in synapse sizes or in concentration gradients of molecules between the spine head and dendrite, but instead reflects the effect of the added intracellular bulk.

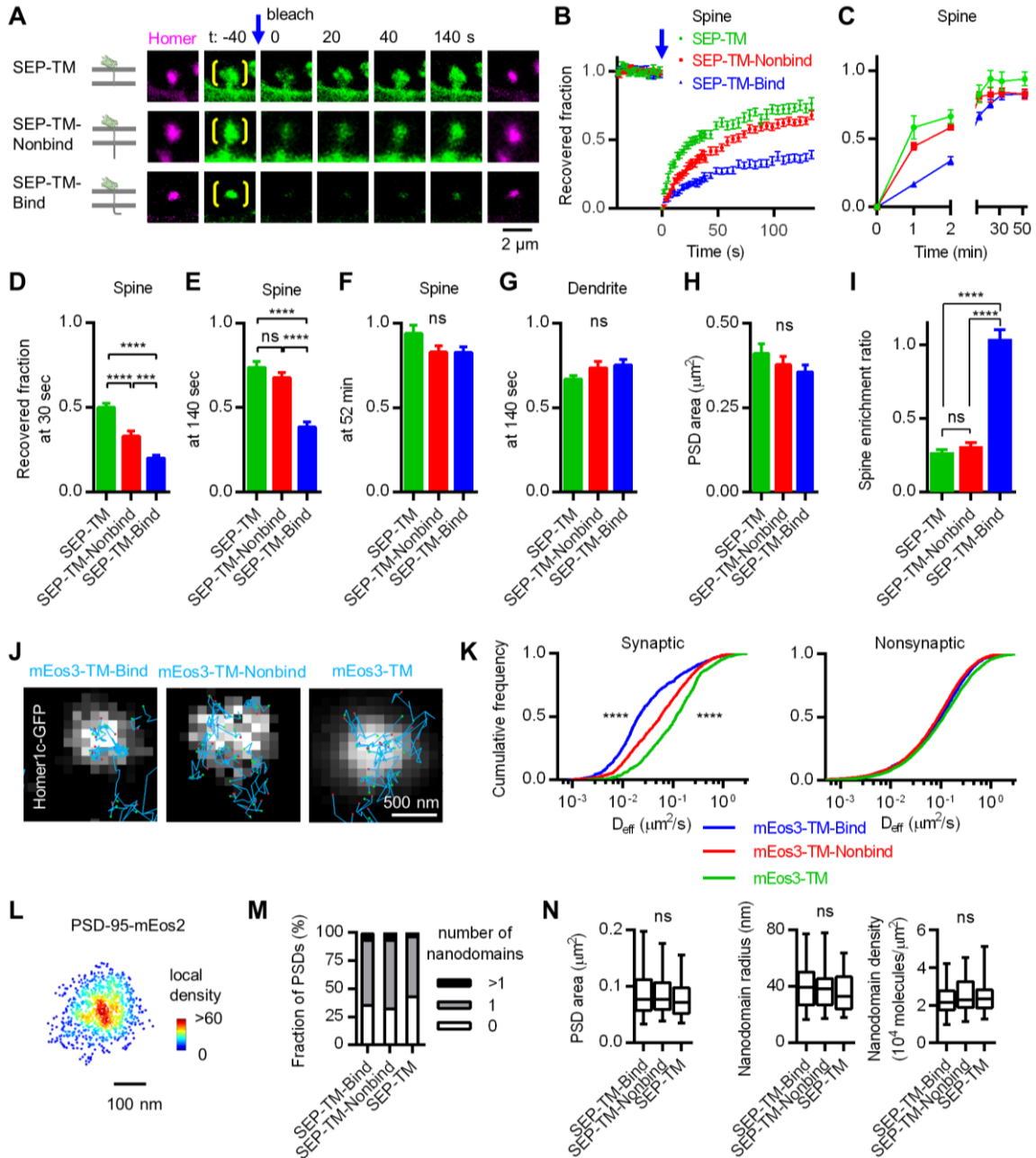
Kinetics of recovery after photobleaching an entire spine are influenced not only by diffusion within the synapse but also by mobility on the spine head and dynamics of transit across the spine neck to the dendritic shaft. To measure directly the diffusion of TM probes in the synapse, I applied smtPALM (Fig. 2.7J). Outside the synapse, the three TM probes showed nearly identical diffusion distributions (Fig. 2.7K right), consistent with the notion that TM protein diffusion is only weakly dependent on protein size in the relative absence of obstacles. However, within the synapse, mEos3-TM-Nonbind diffused faster than mEos3-TM-Bind but more slowly than mEos3-TM (Fig. 2.7K left). This indicates that while PDZ-mediated binding can limit protein motion in the synapse, it is not the only factor in stabilizing the synaptic diffusion of the membrane probe.

As it could be the case that introducing exogenous PSD-95-binding motifs could alter the interior landscape of the PSD and thus indirectly influence diffusion of the expressed probe, I examined PSD-95 distribution using PALM (MacGillavry et al., 2013). I knocked down endogenous PSD-95, rescued expression with a knock-down resistant PSD-95-mEos2 (MacGillavry et al., 2013) (Fig. 2.7L), and co-expressed in the same neurons one of the three SEP-tagged probes. After 3-4 days of co-expression, the nano-organization of PSD-95 (i.e. PSD area, nanodomain size, and molecular density within nanodomain) was on average not different for cells expressing any of the three probes (Fig.

2.7M, N). Taken together, these results support a model in which protein-protein binding is not the only factor in stabilizing the synaptic diffusion of transmembrane proteins.

Figure 2.7. PDZ-mediated binding is partly responsible for stabilizing the synaptic mobility of a small membrane probe.

(A) Representative examples of FRAP in spines of neurons co-expressing *Homer1c*-mCherry and one of the SEP-tagged transmembrane probes: TM, TM-Nonbind, or TM-Bind. (B) Recovery curves of 140-sec FRAP on spines (SEP-TM $n = 28$ ROIs/10 neurons/2 cultures, SEP-TM-Nonbind 27/7/2, SEP-TM-Bind 42/11/2). (C) Recovery curves of 52-min FRAP on spines (SEP-TM $n = 12$ ROIs/3 neurons/3 cultures, SEP-TM-Nonbind 14/3/3, SEP-TM-Bind 19/3/3). (D) Recovered fractions in the spine at 30 sec, (E) at 140 sec, and (F) at 52 min. (G) Recovered fractions in the dendrite at 140 sec (SEP-TM $n = 25$ ROIs/10 neurons/2 cultures, SEP-TM-Nonbind 23/7/2, SEP-TM-Bind 27/11/2). (H) The PSD areas and (I) spine enrichment in spines that were targeted for bleaching in B and C. (J) Representative smtPALM tracks (cyan segments, green and red dots indicate where localizations appeared and disappeared) superimposed on individual synapses marked by *Homer1c*-GFP. (K) Cumulative frequency plots of instantaneous diffusion coefficients (D_{eff}) inside *Homer1c*-GFP-marked synapses (left, *mEos3*-TM-Bind $n = 918$ tracks/132 PSDs/10 neurons/2 cultures, *mEos3*-TM-Nonbind 1269/178/10/2, *mEos3*-TM 686/180/13/2) and outside synapses (right, *mEos3*-TM-Bind $n = 3553$ tracks, *mEos3*-TM-Nonbind 6247, *mEos3*-TM 6156). Statistics on synaptic D_{eff} : K-S test and Mann-Whitney U test **** $p < 0.0001$ (*mEos3*-TM-Bind vs. *mEos3*-TM-Nonbind, or *mEos3*-TM-Nonbind vs. *mEos3*-TM). (L) Representative nanoscale map of *mEos2*-tagged *shrPSD-95* co-expressed with one of the three probes: SEP-TM-Bind, SEP-TM-Nonbind, and SEP-TM. Local density calculated as in (MacGillavry et al., 2013). (M) Relative proportion of PSDs with 0, 1, or more PSD-95 nanodomains in cells expressing SEP-TM-Bind, SEP-TM-Nonbind, or SEP-TM (SEP-TM-Bind $n = 110$ PSDs/8 neurons/2 cultures, SEP-TM-Nonbind 59/7/2, SEP-TM 128/5/2). (N) PSD area, PSD-95 nanodomain radius, and PSD-95 molecular density in nanodomain (SEP-TM-Bind $n = 110$ PSDs/79 nanodomains, SEP-TM-Nonbind 59/44, SEP-TM-Bind 128/79) with statistics: Kruskal-Wallis ANOVA ns ($p = 0.23$ for PSD area, $p = 0.35$ nanodomain radius, and $p = 0.24$ nanodomain density). Statistics for D-I: one-way ANOVA ($p < 0.0001$ for D, E, and I, ns not significant $p = 0.10$ F, $p = 0.18$ G, $p = 0.27$ H) with Bonferroni-corrected post hoc pairwise comparisons (**** $p < 0.0001$, *** $p = 0.0004$, ns $p = 0.68$ for E, ns $p > 0.99$ I).



Intracellular protein bulk can influence the synaptic mobility of the small transmembrane probe

The PSD consists of a large number of high molecular weight proteins (Husi et al., 2000; Sheng and Hoogenraad, 2007; Burette et al., 2012), which include submembranous scaffold proteins typified by PSD-95. The dense assembly of these scaffolding proteins could sterically interact with transmembrane proteins like receptors through their

cytoplasmic domains. However, it is unclear whether and how steric hindrance proximal to the inner face of the postsynaptic membrane influences protein diffusion. To examine the effect of intracellular protein bulk on the mobility of the membrane probe, I fused the GFP variant Cerulean3 to the cytoplasmic terminus of the TM probe (SEP-TM-Cerulean), and examined recovery after photobleaching spines. SEP-TM-Cerulean and SEP-TM-Nonbind recovered similarly slower than SEP-TM at 30 seconds after bleaching (Fig. 2.8A,B,D), indicating that intracellular protein bulk can influence the lateral mobility of a TM protein on the spine surface membrane. Near the equilibrium state, the recovered fractions of the three probes were not different in the spine (Fig. 2.8C,E,F) or dendrite (Fig. 2.8G), indicating as expected that the reduced mobility was not associated with lower fractional exchange, but an increased retention time in the synapse. The PSD areas and the spine enrichment of the three probes in the photobleached spines were not different (Fig. 2.8H,I) and importantly there was no correlation between the recovered spine fraction and either the synapse size or spine enrichment for any of the three probes (Table 2.2) . Altogether, these results indicate TM protein mobility is reduced by added intracellular bulk. This is not due to a difference in synapse size or an altered concentration gradient

Table 2.2. Correlation between FRAP and either PSD area or spine enrichment of various TM probes.

Probe	Recovered fraction (t) vs. PSD area			Recovered fraction (t) vs. spine enrichment		
	30 s	140 s	52 min	30 s	140 s	52 min
SEP-TM	ns, $p = 0.10$ $n = 62/15/5$	ns, $p = 0.14$ $n = 62/15/5$	ns, $p = 0.27$ $n = 12/3/3$	ns, $p = 0.92$ $n = 62/15/5$	ns, $p = 0.19$ $n = 62/15/5$	ns, $p = 0.095$ $n = 12/3/3$
SEP-TM-Nonbind	ns, $p = 0.46$ $n = 46/11/5$	ns, $p = 0.76$ $n = 46/11/5$	ns, $p = 0.38$ $n = 14/3/3$	ns, $p = 0.24$ $n = 46/11/5$	ns, $p = 0.44$ $n = 46/11/5$	ns, $p = 0.12$ $n = 14/3/3$
SEP-TM-Bind	$p = 0.011$ $r = - 0.39$ $n = 42/11/2$	$p = 0.0064$ $r = - 0.41$ $n = 42/11/2$	ns, $p = 0.66$ $n = 19/3/3$	ns, $p = 0.16$ $n = 42/11/2$	ns, $p = 0.92$ $n = 42/11/2$	ns, $p = 0.66$ $n = 19/3/3$
SEP-TM-Cerulean	ns, $p = 0.074$ $n = 43/6/3$	ns, $p = 0.11$ $n = 43/6/3$	ns, $p = 0.58$ $n = 17/3/3$	ns, $p = 0.17$ $n = 43/6/3$	ns, $p = 0.25$ $n = 43/6/3$	ns, $p = 0.57$ $n = 17/3/3$

Statistics of linear regression analyses for recovered fraction at various time points and either PSD area or spine enrichment ratio of various TM probes. ns: not significant. Sample number n is shown in number of spines / neurons / cultures.

between the spine head and its parent dendrite, but most likely arises from reduced diffusibility in the crowded environment of the synapse.

To examine this directly, I applied smtPALM on cells expressing each of the mEos3-tagged probes while co-expressing a PSD-marking protein Homer1c-GFP (Fig. 2.8J). Within the synapse, both mEos3-TM-Nonbind and mEos3-TM-Cerulean diffused slower than mEos3-TM (Fig. 2.8K left). Interestingly, the effect of added Cerulean was not as great as that of the non-binding Stg C-tail, which suggests that factors other than total bulk can influence mobility within the synapse, perhaps tertiary structure. Outside of the synapse, the three probes exhibited nearly identical distributions of D_{eff} (Fig. 2.8K right). Altogether, these results indicate that the bulk of the intracellular domain alone can influence the mobility of a transmembrane protein within the synapse, consistent with the

notion that dense and irregular environment of the PSD provides substantial steric hindrance to the movement of receptors and other synaptic TM proteins.

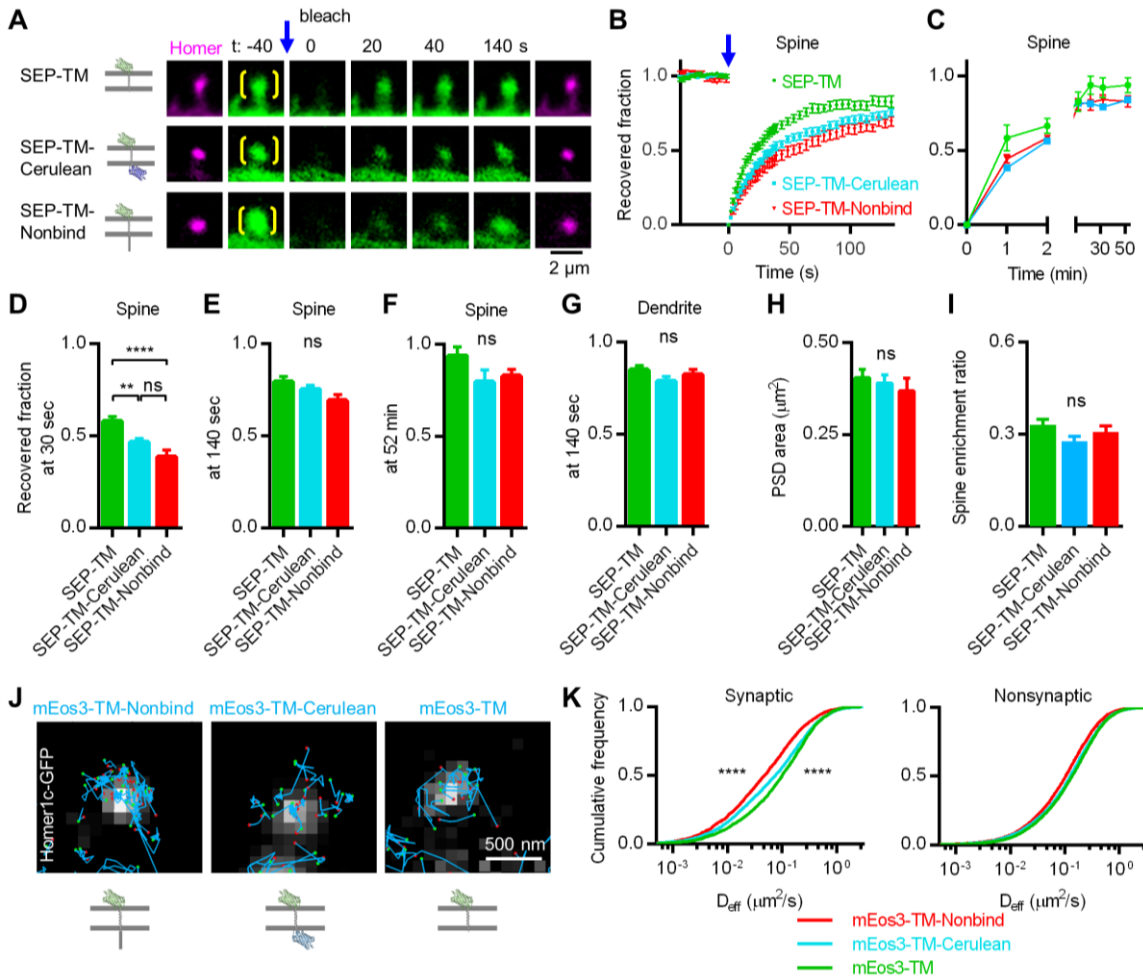


Figure 2.8. Intracellular protein bulk can influence the mobility of small membrane protein.

(A) Representative examples of FRAP in spines of neurons co-expressing *Homer1c*-mCherry and one of the SEP-tagged transmembrane probes: TM, TM-Cerulean, or TM-Nonbind. (B) Recovery curves of 140-second FRAP on spines (SEP-TM $n = 34$ ROIs/5 neurons/3 cultures, SEP-TM-Cerulean 43/6/3, SEP-TM-Nonbind 19/4/3). (C) Recovery curves of 52-min FRAP on spines (SEP-TM $n = 12$ ROIs/3 neurons/3 cultures, SEP-TM-Cerulean 17/3/3, SEP-TM-Nonbind 14/3/3). (D) Recovered fractions in the spine at 30 sec, (E) at 130 sec, and (F) at 52 min. (G) Recovered fractions in the dendrite at 140 sec (SEP-TM $n = 34$ ROIs/5 neurons/3 cultures, SEP-TM-Cerulean 34/6/3, SEP-TM-Nonbind 15/4/3). (H) Areas of *Homer1c*-mCherry puncta and (I) spine enrichment in spines that were targeted for bleaching. (J) Representative smtPALM tracks (cyan segments, green and red dots indicate where localizations appeared and disappeared) superimposed on individual synapses marked by *Homer1c*-GFP. (K) Cumulative frequency plots of instantaneous diffusion coefficients (left, mEos3-TM-Nonbind $n = 3283$ tracks/423 PSDs/14 neurons/3 cultures, mEos3-TM-Cerulean 3645/602/20/3, mEos3-TM 2500/265/10/3) and outside synapses (right, mEos3-TM-Nonbind $n = 8024$ tracks, mEos3-TM-Cerulean 10439, mEos3-TM 5816). Statistics on synaptic D : K-S test and Mann-Whitney U test **** $p < 0.0001$ (mEos3-TM-Nonbind vs. mEos3-TM-Cerulean, or mEos3-TM-Cerulean vs. mEos3-TM). Statistics for D-I: one-way ANOVA ($p < 0.0001$ for D, ns not significant $p = 0.054$ E, $p = 0.24$ F, $p = 0.92$ G, $p = 0.53$ H, $p = 0.26$ I) with Bonferroni-corrected post hoc pairwise comparisons (**** $p < 0.0001$, ** $p = 0.0028$, ns $p = 0.16$ for D).

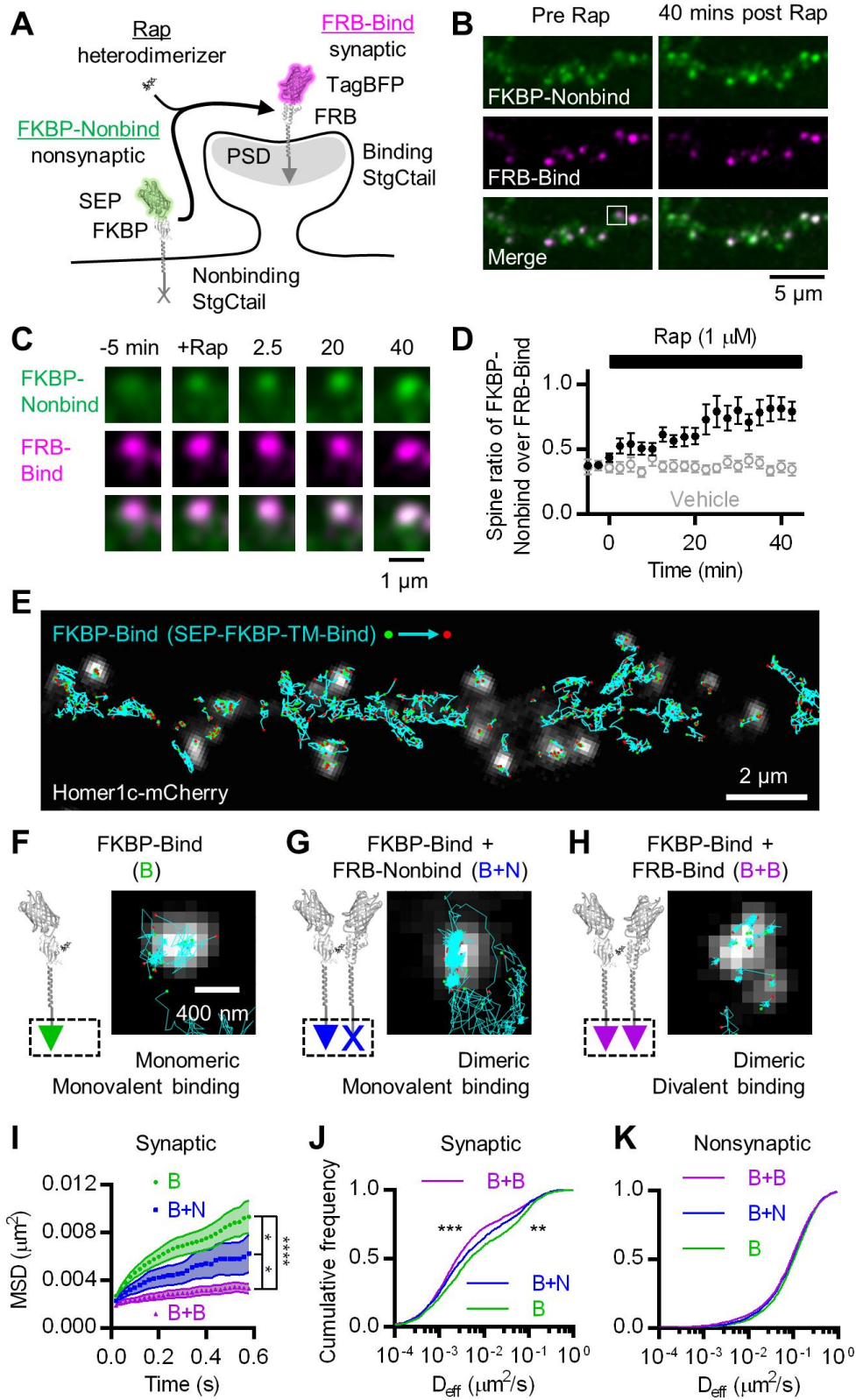
Divalent PDZ-binding interactions within the synapse can stabilize the mobility of transmembrane proteins more than monovalent interactions can

AMPA receptors could bear multiple TARPs capable of binding PSD scaffold molecules (Hastie et al., 2013). To test the role of divalent receptor-scaffold interactions on receptor mobility in the synapse, I developed a chemically inducible heterodimerization strategy that would permit us to acutely convert our typical monovalent binding probe to one with divalent PDZ-binding capacity. To do this, I added to our TM probes either FKBP or FRB, protein domains which can be crosslinked via the small molecule rapalog (Fig. 2.9A). By crosslinking one binding probe to a second probe either carrying a second binding motif or not, the additional effect of divalent binding could be assessed as well as distinguished from the effect of added bulk. To avoid potential off-target effects of lengthening the binding C-tail via insertion in the cytoplasmic domain, I inserted the dimerization motifs in the extracellular domain, and created four fusion proteins: SEP-FKBP-TM-Bind (FKBP-Bind), SEP-FKBP-TM-Nonbind (FKBP-Nonbind), TagBFP-FRB-TM-Bind (FRB-Bind), and TagBFP-FRB-TM-Nonbind (FRB-Nonbind).

I tested the dimerization assay in neurons co-expressing FKBP-Nonbind and FRB-Bind. In the absence of rapalog, FKBP-Nonbind was on average 37% as enriched as FRB-Bind in spines; incubation with 1 μ M rapalog resulted in an increase in the spine enrichment of FKBP-Nonbind which plateaued on average to 79% after 40 min, whereas incubation with the vehicle resulted in no change (Fig. 2.9B-D). Thus, rapalog can induce dimerization between TM probes containing extracellular FKBP and FRB domains.

Figure 2.9. Divalent PDZ-binding motifs can stabilize TM proteins within the synapse more than monovalent binding can.

(A) Cartoon illustrating the strategy to induce dimerization and translocation of TM probes into dendritic spines using Rapalog (Rap). (B) A DIV 16 hippocampal neuron expressing SEP-FKBP-TM-Nonbind (FKBP-Nonbind) and TagBFP-FRB-TM-bind (FRB-Bind) for 2 days, before (Pre) and 40 min after (Post) bath incubation with 1 μ M Rap. (C) Time-lapse of the highlighted region drawn in B. (D) Enrichment of FKBP-Nonbind (mean \pm s.e.m.) at dendritic spines containing FRB-Bind ($n = 34$ spines/3 fields/3 cultures for Rapalog, 28/3/3 vehicle) before and after Rapalog or vehicle (0.2% ethanol) application. (E) The first (green) and last (red) localized positions of FKBP-Bind (SEP-FKBP-TM-Bind) molecules tracked for ≥ 8 frames, superimposed on a typical dendritic segment co-expressing Homer1c-mCherry as a synaptic marker. (F) Cartoon representing the FKBP-Bind the monomeric binding probe (left), and typical tracks in synapses co-expressing this probe (B) and Homer1c-mCherry (right). (G) Cartoon representing the FKBP-Bind and FRB-Nonbind (TagBFP-FRB-TM-Nonbind) dimerized into a monovalent binding probe in the presence of Rapalog (left), and typical synaptic tracks in cells co-expressing these two probes (B+N) and Homer1c-mCherry (right). (H) Cartoon representing the FKBP-Bind and FRB-Bind (TagBFP-FRB-TM-Bind) dimerized into a divalent binding probe in the presence of Rapalog (left), and typical synaptic tracks in cells co-expressing these two probes (B+B) and Homer1c-mCherry (right). (I) Mean squared displacement over time within synapses ($n = 352$ tracks/3 cultures for B, 174/3 B+N, 251/3 B+B). Kruskal-Wallis ANOVA ($p < 0.0001$) post hoc comparisons by Mann-Whitney U test, $*p = 0.0194$ (B vs. B+N), 0.0395 (B+N vs. B+B), $***p < 0.0001$ (B vs. B+B). (J) Cumulative frequency distributions of D_{eff} within synapses (left; $n = 1982$ tracks/231 PSDs/7 cells/3 cultures for B+B, 868/201/9/3 B+N, 1415/273/7/3 B). Kruskal-Wallis ANOVA ($p < 0.0001$) post hoc comparisons by K-S test $***p = 0.0004$ (B+B vs. B+N), $**p = 0.0021$ (B+N vs. B), and by Mann-Whitney U test $p = 0.0053$ (B+B vs. B+N), $p = 0.0003$ (B+N vs. B). (K) Cumulative frequency distributions of D_{eff} outside of synapses (right; $n = 3621$ tracks for B+B, 3465 B+N, 5750 B).



I then co-transfected three groups of cultured neurons, obtaining distinct

populations expressing only FKBP-Bind (a monomeric binding probe) (Fig. 2.9F cartoon), FKBP-Bind and FRB-Nonbind (which can dimerize to form a monovalent binding probe) (Fig. 2.9G cartoon), or FKBP-Bind and FRB-Bind (which can dimerize to form a divalent binding probe) (Fig. 2.9H cartoon). To measure the surface mobility of the probes, I employed uPAINT single-molecule tracking of fluorescently conjugated nanobodies recognizing SEP but not TagBFP (Fig. 2.9E). I measured the mean squared displacement and effective diffusion coefficients of FKBP-Bind in these groups of neurons after a 1- to 2-hour pre-incubation with 1 μ M rapalog (Fig. 2.9F-H right). The D_{eff} distributions of these three probes outside of the synapse were nearly identical (Fig. 2.9K), consistent with the notion that diffusion coefficient is only weakly dependent on particle size in membrane regions with few obstacles. Within the crowded environment of the synapse, however, they behaved differently. The monomeric probe explored a larger area (Fig. 2.9I) and diffused faster (Fig. 2.9J) in synapses than both dimeric probes, indicating that dimerization even without adding an extra receptor-scaffold binding motif can reduce TM protein mobility within the synapse. As expected, the divalent binding probe explored even less area (Fig. 2.9I) and more slowly (Fig. 2.9J) than the dimeric but monovalent binding probe, indicating that polyvalent receptor-scaffold binding interactions can confine TM proteins more effectively than monovalent binding can within the synapse. Altogether, these results support the hypothesis that both steric and binding interactions can stabilize the mobility of TM proteins within the synapse.

Discussion

Combining simulations and live-cell imaging methods, we examined the influence of protein-protein binding and of protein steric hindrance within the postsynaptic density on

the mobility of synaptic membrane proteins. Measurements of molecular mobility across the lateral extent of the synapse and dendritic spines revealed that the dynamics of a receptor-like TM probe strongly depended on two features of the intracellular domain: the presence of protein bulk and the capacity for protein-protein binding. By simulating receptor diffusion within a model incorporating the measured positions of the critical postsynaptic scaffold macromolecule PSD-95, our simulations suggest that the nanoscale heterogeneous organization of PSD-95 alone can alter the dwell time of synaptic receptors or any other intracellularly bulky membrane protein. We propose that the nanoscale organization of scaffold proteins in the PSD shapes the mobility and distribution of synaptic membrane proteins through two mechanisms: steric effects and establishing the position and density of binding partners in the synapse. These steric effects will depend on the size of the diffusing protein. Overall, the interplay between these mechanisms will likely regulate the spatial distribution and dynamics not just of neurotransmitter receptors, but of numerous critical transmembrane proteins such as ion channels and adhesion molecules.

A previous study has suggested that the PSD could act as a size-exclusion environment akin to the synaptic cleft, demonstrated by using lipids tagged by differently sized bulks in the extracellular domain (Renner et al., 2009). Our results extend this picture of the sieve-like synapse in several key ways. First, they demonstrate that this idea applies to transmembrane proteins. Second, they indicate that the larger the intracellular bulk of the membrane protein, the smaller the synaptic area it could explore. This was demonstrated by simulations and deduced from photobleaching within individual synapses that showed a size-dependence in protein mobility. Finally, they suggest that the dense

crowding of synaptic scaffolding proteins limits the escape of mobile membrane proteins from the PSD (and consequently their incorporation as well). This was demonstrated in simulations which showed that PSDs modeled with the measured distributions of scaffolding proteins retained receptors longer than those with randomized distributions. More support of this notion comes from the experimental results that added intracellular bulk slowed down the exchange of the small TM probe.

It is well known that the PDZ-mediated binding motif of Stargazin plays a prominent role in stabilizing the mobility of AMPARs (Chen et al., 2000; Bats et al., 2007; Sainlos et al., 2011), and here we showed that it could also stabilize even minimal synthetic transmembrane proteins. However, our results further demonstrated that intracellular bulk could have substantial influence on the lateral mobility of transmembrane proteins, as well as their positioning within subdomains of the synapse. This influence may have significant impact on excitatory synaptic transmission in diverse situations. In particular, the physical bulk of an AMPAR complex is ultimately determined by multiple classes of proteins (Tomita et al., 2003; Cho et al., 2007; Milstein et al., 2007; Schwenk et al., 2009; Soto et al., 2009; Kalashnikova et al., 2010; von Engelhardt et al., 2010) that additionally associate with the GluA tetramer. In fact, biochemically isolated, native AMPAR complexes are 20% to 120% larger than the GluA tetrameric core (Schwenk et al., 2012). We speculate that differently sized AMPAR subcomplexes can have dramatic impact on function not only due to their diverse binding motifs and channel gating kinetics, but also because of their differences in protein bulk.

Given this, it is possible that a significant fraction of synaptic receptors which remain following disruption to receptor-scaffold binding (Bats et al., 2007; Sainlos et al.,

2011) are retained in the synapse by steric effects. In an interesting further example, desensitization-driven dissociation of AMPARs from Stargazin (Tomita et al., 2004; Constals et al., 2015) not only alters binding to PSD-95 but also reduces their size. Each of these effects may contribute to the observed increase in mobility of desensitized receptors (Constals et al., 2015). Together, these considerations suggest that protein-size dependent regulation of protein mobility and dwell times could be a mechanism regulating the synaptic distribution of AMPARs.

A notable aspect of steric interactions is that they are agnostic to molecular identity, and so will influence synaptic distribution of ion channels, adhesion proteins, or any transmembrane protein. A recent study showed that synaptic accumulation of receptors can occur regardless of the type of receptor (Granger et al., 2013). It is tempting to speculate that macromolecular crowding offers a mechanism to explain how the synapse can retain TM proteins, regardless of specific protein-protein binding motifs. Note that molecular crowding alone cannot account for the synaptic enrichment of receptors, but in combination with binding presents an efficient way to accumulate and retain membrane proteins at the synapse (Holcman and Triller, 2006; Haselwandter et al., 2011; Masson et al., 2014). Thus, we suggest a two-step process that can distribute receptors throughout the synapse interior. TM proteins first need binding partners to accumulate at the periphery of the PSD (Bats et al., 2007; Opazo and Choquet, 2011). Indeed, we found that a PDZ-binding motif was necessary and sufficient to drive spine enrichment of the TM probes. Secondly, even proteins that have unbound from scaffolds can be non-selectively incorporated to the interior by the minute-scale morphing of the PSD (Blanpied et al., 2008; Kerr and Blanpied,

2012) as well as molecular positional dynamics and exchange of synaptic scaffolding proteins (Gray et al., 2006; MacGillavry et al., 2013; Chazeau et al., 2014).

Our simulations assumed that, other than the mobile probe molecules, PSD-resident proteins were held in stable positions. Consistent with this assumption, the turnover of endogenous PSD-95 at the synapse is extremely slow, as FRAP of PSD-95 bearing a Venus tag in a knock-in mouse exchanges only about 10% in 60 min (Fortin et al., 2014). Exchange of overexpressed PSD-95 is elevated compared to this but still slow, with time constants of 30 to 100 minutes in hippocampus (Gray et al., 2006; Sharma et al., 2006; Blanpied et al., 2008), depending on age (Gray et al., 2006). These observations suggest that within the short time frame of our simulations, such exchange will be of minimal impact and PSD-95 can be considered immobile. However, ongoing spine actin polymerization alters PSD morphology over minutes (Kuriu et al., 2006; Kerr and Blanpied, 2012; Ziv and Fisher-Lavie, 2014), the nanoscale organization of the PSD is temporally dynamic (Nair et al., 2013) and activity-dependent (MacGillavry et al., 2013), and single-molecule tracking has revealed that a substantial proportion of PSD-95 molecules (at least when overexpressed) is mobile within the synapse (Chazeau et al., 2014). As a preliminary attempt to investigate the role of a dynamic PSD, we explored in several models the potential effects of these various forms of PSD molecular dynamics. As expected, if PSD-95 scaffold molecules were permitted to diffuse, a larger subset of receptors could escape compared to the static case because the pattern of PSD-95 drifted towards randomized (data not shown). Other models incorporating less diffusion or other forms of motion that recapitulated the observed maintenance of PSD-95 density patterns could produce large, moderate, or negligible effects. Thus, dynamics within the PSD can

alter the relative contribution of steric effects on receptor retention. However, detailed effects of this morphological plasticity depend very strongly on parameters that have not yet been deduced experimentally. Therefore, it will be important to gain more quantitative understanding of PSD molecular dynamics in order to gauge the time course over which these dynamics permit escape of sterically trapped receptors, or the trapping of proteins newly incorporated to the PSD.

It is tempting to speculate that such synaptic scaffold protein dynamics may play an important role in functional synaptic plasticity. Supporting this notion, molecular destabilization of the PSD is prominent during induction of LTP and LTD (Steiner et al., 2008; Xu et al., 2008), suggesting that periods of plasticity involve enhanced reorganization or disassembly of internal scaffold distribution. These observations are consistent with the model that synaptic potentiation could result from reorganization and restabilization of scaffolds to favor retention of bulky membrane proteins. On the other hand, synaptic depression could arise from homogenization and mobilization of scaffold positions, favoring dispersion of receptors. Thus, identifying mechanisms that govern the positional dynamics of synaptic scaffolding proteins themselves will be crucial to understanding the synaptic modifications that underlie learning, memory, and neuropsychiatric disorder.

Chapter 3: Control of transmembrane protein diffusion within the postsynaptic density assessed by simultaneous single-molecule tracking and localization microscopy²

Abstract

Postsynaptic transmembrane proteins are critical elements of synapses, mediating trans-cellular contact, sensitivity to neurotransmitters and other signaling molecules, and flux of Ca and other ions. Positioning and mobility of each member of this large class of proteins is critical to their individual function at the synapse. One critical example is that the position of glutamate receptors within the postsynaptic density (PSD) strongly modulates their function by aligning or misaligning them with sites of presynaptic vesicle fusion. In addition, the regulated ability of receptors to move in or out of the synapse is critical for activity-dependent plasticity. However, factors that control receptor mobility within the boundaries of the synapse are not well understood. Notably, PSD scaffold molecules accumulate in domains much smaller than the synapse. Within these nanodomains, the density of proteins is considerably higher than that of the synapse as a whole, so high that steric hindrance is expected to reduce receptor mobility substantially. However, while numerical modeling has demonstrated several features of how the varying protein density across the face of a single PSD may modulate receptor motion, there is little experimental information about the extent of this influence. To address this critical aspect of synaptic organizational dynamics, we performed single-molecule tracking of transmembrane proteins using uPAINT over PSDs whose internal structure was simultaneously resolved using PALM. The results provide important experimental confirmation that PSD scaffold density protein strongly influences the mobility of transmembrane proteins. Tracking a

² Li TP, Blanpied TA (2016) Control of Transmembrane Protein Diffusion within the Postsynaptic Density Assessed by Simultaneous Single-Molecule Tracking and Localization Microscopy. *Frontiers in Synaptic Neuroscience*.

protein with a cytosolic domain that does not bind PSD-95 still was slowed in regions of high PSD-95 density, suggesting that crowding by scaffold molecules and perhaps other proteins is sufficient to stabilize receptors even in the absence of binding. Because numerous proteins thought to be involved in establishing PSD structure are linked to disorders including autism and depression, this motivates further exploration of how PSD nanostructure is created. The combined application PALM and uPAINT should be invaluable for distinguishing the interactions of mobile proteins with their nano-environment both in synapses and other cellular compartments.

Introduction

Transmembrane proteins such as receptors diffuse on the cell surface to reach their sites of action. In doing so, they must make their way through complex environments typified by varying densities of obstacles and potential binding partners. The average behavior of proteins moving through such environments has been well characterized (Frick et al., 2007). However, on small spatial scales or within small compartments, the local organization of potential interactors will dominate the influence on receptor motion paths (Kusumi et al., 2014). For instance, locally high concentrations of steric obstacles create a phenomenon called macromolecular crowding (Ryan et al., 1988) that can slow mobility and result in anomalous diffusion (Saxton, 1994; Santamaria et al., 2010). Thus, high resolution information about the distribution of even non-binding obstacles is necessary to understand motion trajectories of transmembrane proteins on small scales.

Perhaps the most complex compartment of the plasma membrane in neurons is the postsynaptic density (PSD). The PSD of glutamatergic synapses concentrates numerous receptor types aligned to the presynaptic active zone. Despite the small size of the average

PSD ($\sim 0.08 \mu\text{m}^2 \times 50 \text{ nm}$) (Harris and Weinberg, 2012), roughly 500 species of proteins can be found in this compartment (Husi et al., 2000; Sheng and Hoogenraad, 2007). Because of the high local density of transmembrane proteins, receptor-binding proteins such as PSD-95, and juxtamembrane cytosolic molecules, protein motion within the membrane at the synapse is likely extremely obstructed (Santamaria et al., 2010). This complicated environment is critical to understand, because protein organization in the PSD directly regulates synaptic transmission in many ways. The number of glutamate receptors present in the PSD sets an upper limit on the strength of the synapse (Huganir and Nicoll, 2013), and receptors exchange continuously by diffusion between the PSD and the perisynaptic plasma membrane (Opazo and Choquet, 2011; Choquet and Triller, 2013). Further, alterations to the PSD are a critical component of activity-driven plasticity mechanisms regulating receptor number (Inoue and Okabe, 2003; Bosch et al., 2014). Thus, understanding mechanisms within the PSD that control motion of glutamate receptors is critical for determining how receptor number is modulated during plasticity.

Even beyond the clear importance of the number of receptors, however, their distribution within the synapse in the plane of the membrane is a vital regulator of synaptic strength (MacGillavry et al., 2011). This is because when glutamatergic vesicles fuse with the presynaptic plasma membrane, the result is a highly concentrated but narrow spike of released neurotransmitter. The rapid dissipation of this spike by glutamate diffusion means that receptors laterally displaced from the site of fusion even by less than 100 nm often fail to activate (Xie et al., 1997; Raghavachari and Lisman, 2004; Santucci and Raghavachari, 2008; Freche et al., 2011). Amplifying this effect, receptors in the PSD are concentrated in $\sim 80 \text{ nm}$ subdomains (MacGillavry et al., 2013; Nair et al., 2013) where the principle

receptor-binding scaffold PSD-95 is also concentrated (Fukata et al., 2013; MacGillavry et al., 2013). In previous work, we modeled diffusion within PSDs where the heterogeneous distribution of PSD-95 was measured, and found that the clustered nature of this scaffold had the capability of strongly limiting the ability of transmembrane proteins to enter (or escape) the crowded regions of the PSD (Li et al., 2016). Thus, nanoscale regional variation in protein composition within a single PSD may have strong impact on synaptic transmission by controlling the subsynaptic distribution of receptors.

A major impediment to further understanding of this issue is the technical challenge of simultaneously measuring the nanoscale distribution of the protein environment while simultaneously measuring protein motion through it. To address this, I developed a combined single-molecule imaging approach that uses smtPALM (Manley et al., 2008) to map the positions of PSD-95 molecules within the synapse (MacGillavry et al., 2013), while simultaneously tracking the motion of proteins in the plasma membrane by uPAINT (Giannone et al., 2010). Using this strategy, I could directly investigate the influence of both obstacle density and protein binding on motion through the PSD. The results provide direct experimental confirmation that macromolecular crowding within the PSD can strongly limit the motion of even small transmembrane proteins, likely helping to establish the distribution and dynamic exchange characteristics of glutamate receptors and other molecules.

Materials and Methods

Neuronal culture and transfection. Dissociated hippocampal neuron cultures were prepared from E18 rat embryos as described previously (Frost et al., 2010). Prior to plating the cells on coverslips, the coverslips were first cleaned as reported previously

(MacGillavry et al., 2013), subsequently coated with lateral-drift tracking, yellow-green fluorescent 100-nm beads (F8803; Thermo Fischer Scientific) diluted 1:25,000 in 100% ethanol (dried within 25 minutes in the hood), and then coated overnight with poly-L-lysine (Sigma). Cells were transfected at DIV10-13 using Lipofectamine 2000 (Thermo Fischer Scientific) and imaged 72-96 hours later (unless stated otherwise). Individual coverslips were transfected with 0.5-0.75 μ g of cDNA for each expression construct.

Expression constructs. Plasmid cDNAs were obtained as follows (with original sources): the binding and nonbinding probes, SEP-TM-Bind and SEP-TM-Nonbind (Li et al., 2016), the PSD-95-mEos2 replacement plasmid shrPSD-95-mEos2 (MacGillavry et al., 2013).

Two-color single-molecule imaging. PALM-PAINT, a combination of uPAINT (Giannone et al., 2010) and PALM (Betzig et al., 2006; Hess et al., 2006), was performed simultaneously through a Photometrics DV2 on an Olympus IX81 ZDC2 inverted microscope that was described by MacGillavry et al. (2013). Cells expressing the indicated constructs were imaged in a previously described extracellular buffer (Li et al., 2016). Super ecliptic phluorin (SEP)-containing probes were labeled with ATTO647N-conjugated anti-GFP nanobodies (GFPBooster-647N, Chromotek), bath applied to a final concentration of 0.5 to 2 nM once the first stretch of synapses was identified for each coverslip. Cells remained at 25 °C for no more than 30 minutes per imaging session.

I imaged the red and far red bands by interleaving excitation at 561 and 640 nm. Imaging was conducted at 29 Hz, with 10-ms duration excitation per frame for 5,000 to 20,000 frames. The two channels were overlaid based on calibration images of TetraSpeck beads (100 nm; Thermo Fischer Scientific) deposited on an acellular coverslip as described

by MacGillavry et al. (2013). 100-nm yellow-green beads ethanol-diluted and dried onto the coverslips prior to plating the cells (F8803; Thermo Fischer Scientific) were excited and captured once every 1000 frames to monitor lateral drift. To correct lateral drift, I localized fiducials *post hoc* from images of the yellow-green beads. I screened for spurious localizations by the duration of fluorescence and mobility. Namely, the bead ought to be present on the first frame, persist for as long as each imaging session, and displace < 100 nm (1 pixel) per 1,000 frames. Such a filtering process provided a list of localizations that correspond to fiducials. From this list I calculated the sample lateral drift as the weighted average of the displacements of all fiduciary localizations between each set of 1000 frames. For weights, I used the inverse of the estimated localization uncertainty (Thompson et al., 2002) of each fiducial. The single linear correction in drift I applied to each subset of 1000 frames was the average correction obtained from the estimates of 2-10 fiducials in the field of view.

Single-molecule localization, tracking analysis, and PSD nanostructure analysis.

All data analysis was performed offline using custom routines in MATLAB (The MathWorks). The algorithms for determining molecule location and criteria for filtering molecules to be considered for further analysis were applied as previously described (MacGillavry et al., 2013). In addition to filtering by localization precision, elliptical form, and brightness, I also utilized a Voronoi-based segmentation program SR-Tesseler (Levet et al., 2015) to filter out spurious localizations outside of putative neuronal border. Criteria for defining a track were described by Li et al. (2016). Instantaneous effective diffusion coefficients (D_{eff}) at individual track time points were calculated for tracks that persisted at least 8 frames (the duration in which the mean MSD was linear; a more detailed

description can be found in Lu et al. (2014)). For comparing diffusion inside and outside of PSDs, tracks that entered or exited the PSD were divided into two portions, a synaptic and an extrasynaptic subtrack, the D_{eff} of which were calculated by averaging the instantaneous D_{eff} for the tracked localizations therein. For the rare tracks that entered and exited PSDs multiple times, synaptic D_{eff} was determined by averaging the instantaneous D_{eff} of all the tracked locations inside the PSD border; vice versa to calculate the extrasynaptic D_{eff} . To calculate the D_{eff} of subtracks in other cases (i.e. particular range of PSD-95 regional density, or below the detection limit of D_{eff}), I calculated the average of instantaneous D_{eff} of localizations therein. The lower detection limit of D_{eff} was determined conservatively by calculating the D_{eff} of a theoretical immobile particle displaced as much as the average trajectory error ~ 30 nm (Savin and Doyle, 2005; Lu et al., 2014) per time frame, which amounted to $0.003 \mu\text{m}^2/\text{s}$.

Briefly, the PSD-95 localizations appearing in consecutive frames separated by no more than 200 nm were considered one molecule, and their positions were taken from the first frame they appeared. To estimate the density of PSD-95 molecules surrounding each position of a tracked probe molecule, I counted the number of PSD-95 molecules within a 30 nm radius (the average trajectory error) per position; to calculate the regional density of PSD-95 surrounding the probe at each position, I calculated the forward running average of regional densities for 8 frames (as long as the number of frames used to estimate instantaneous diffusion coefficient), which reduced the noisy fluctuations particularly for fast moving probes. The PALM PSD border was determined by taking the convex hull of the PSD-95 molecular positions. To determine the Gaussian-blurred border of each PSD, I first constructed a 2-dimensional molecular density map of 25×25 nm subpixels from PSD-

95 molecules for each PSD. I then convolved it with a constant-amplitude Gaussian image profile ($\sigma = 125$ nm, image width = 900 nm) that is similar to an ideal microscope point-spread function with a full-width at half max (FWHM) of ~ 250 nm. To determine the FWHM border of the blurred PSD, I thresholded the convolved image at half-maximum intensity. To determine the 95%-border, I thresholded it at 5% of the maximum intensity.

Statistics. Where means are presented, the accompanying errors are the standard error of the mean; additionally, these data were normally distributed according to the Shapiro-Wilk normality test. Where box-and-whisker plots are presented, the middle bar represents the median, the upper and lower limit of the boxes denote the interquartile range, and the whiskers extend to 5% and 95% of the distribution; additionally, these data were not normally distributed according to the Shapiro-Wilk normality test. Different sets of statistical tests were used for normally and non-normally distributed data. Pairwise statistical tests were performed using unpaired t test with Welch's correction for normally distributed data; they were performed using Mann-Whitney U test for non-normally distributed data. Where two-way ANOVA was used, a Bonferroni correction was used for post-hoc pairwise comparisons. Kolmogorov-Smirnov tests were applied for cumulative frequency distributions. In all cases, means (or medians) were considered significantly different if the test reported $p < 0.05$. Most statistical tests and all graphing were done using Prism (GraphPad Software). Two-way ANOVA was done in MATLAB (The MathWorks).

Results

To perform single-molecule tracking during superresolution imaging of the PSD, I co-transfected 13-17 DIV hippocampal neurons with two cDNA constructs. The first encoded a single-pass transmembrane (TM) protein composed of an extracellular SEP, the TM

domain, and the intracellular carboxy terminus of stargazin, which enables this protein to bind PSD-95. Thus, I refer to it as SEP-TM-Bind (Li et al., 2016). This was co-transfected with shrPSD-95-mEos2, which expresses shRNA targeting PSD-95 along with an RNAi-resistant, mEos2-tagged PSD-95 (MacGillavry et al., 2013). To track motion of SEP-TM-Bind at the cell surface, I used uPAINT (Giannone et al., 2010) and applied anti-GFP nanobodies carrying Atto647N in the chamber to a final concentration of 0.5 to 2 nM. Concurrently, I localized the positions of PSD-95-mEos2 using conventional smtPALM methods (Fig. 3.1A).

The SEP-TM-Bind probe exhibited clearly different mobility inside and outside of the PSD (Fig 1A right), as expected based on the behavior of AMPA-type glutamate

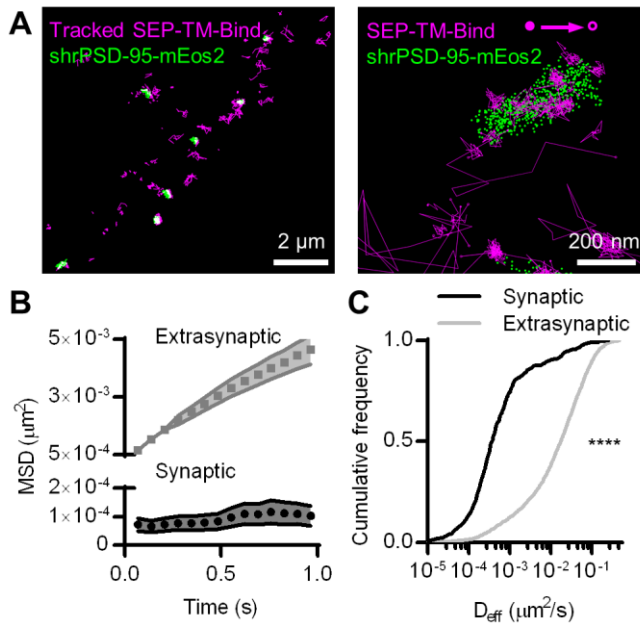


Figure 3.1. PALM-PAINT, single-molecule tracking during PALM imaging.

(A) (Left) SEP-TM-Bind molecules tracked for at least 8 frames super-imposed on molecules of shrPSD-95, accumulated from 5,000-20,000 frames. (Right) A typical example of tracked probes superimposed on positions of shrPSD-95 molecules. The first and last localized positions are indicated as filled and open circles, respectively. (B) Mean squared displacement over time of connected subsegments of tracks (subtracks) that are lasted at least 15 frames ($n = 156$ synaptic and 2907 extrasynaptic tracks/113 PSDs/13 fields/11 cells/3 cultures). (C) Cumulative frequency distributions of D_{eff} for subtracks that are at least 8 frames long ($n = 654$ synaptic and 3349 extrasynaptic tracks/113/13/11/3).

receptors (Bats et al., 2007; Hoze et al., 2012), neuroligin (Chamma et al., 2016), and NMDA-type glutamate receptors (Dupuis et al., 2014). I compared the diffusion patterns of molecules inside and outside of the PSD, when the PSD border was defined by the convex-hull border of PSD-95 positions. Probes outside of the PSD displayed near-free

diffusion as evidenced by an almost linear MSD plot (Fig. 3.1B). However, probes within the PSD showed a much slower mobility and appeared highly confined in their motion, as evidenced by saturation of the relationship between mean-squared displacement and time. This curve approached a plateau of $104 \pm 35 \text{ nm}^2$, suggesting confinement within $<60 \text{ nm}$ diameter regions of the PSD (Ehlers et al., 2007). The effective diffusion coefficients (D_{eff}) of the synaptic subtracks were ~ 2 orders of magnitude slower than those of the extrasynaptic subtracks (Fig. 3.1C).

The improved resolution of the PSD border obtained by imaging the positions of individual PSD-95 molecules as opposed to using widefield or confocal microscopy should improve discrimination of which molecules are within the synapse. The average PSD area

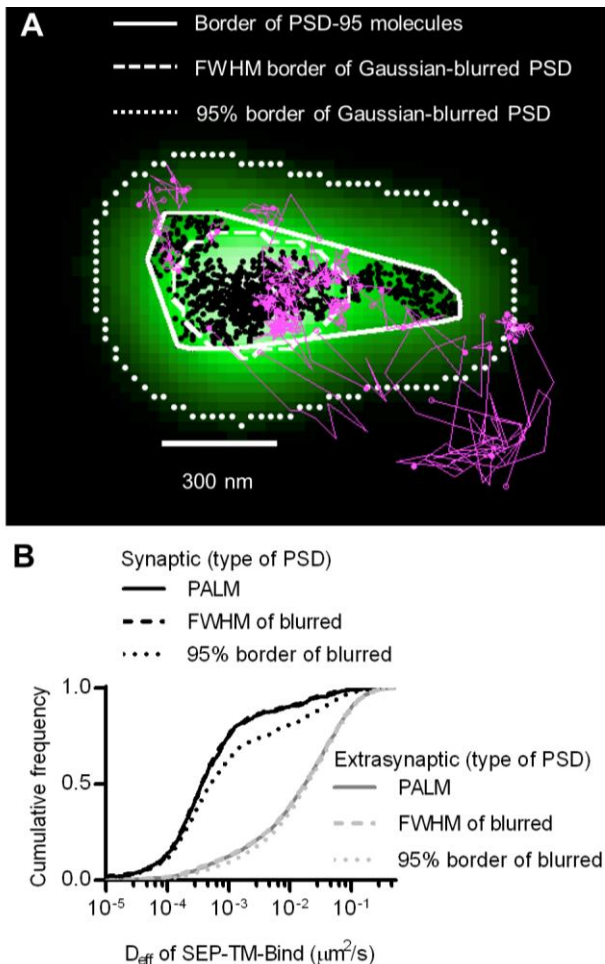


Figure 3.2. Better discrimination of PSD border reveals strong reduction of mobility within synapses.

(A) Typical tracks of the binding probe (magenta) and positions of *shrPSD-95* (black circles) super-imposed. Convex hull border of PSD-95 positions (solid line), full-width half max (FWHM) border of Gaussian-blurred *shrPSD-95* positions (dashed line), and full-width 5% max (95%) border (dotted lines). (B) Cumulative frequency distribution of synaptic (black lines) and extrasynaptic (gray lines) tracks segregated using the synaptic borders of PSDs determined using PALM'ed *shrPSD-95* (solid lines), FWHM of Gaussian-blurred *shrPSD-95* positions (dashed lines), or full-width 5% max (95% border) of the Gaussian-blurred *shrPSD-95* positions (dotted lines) ($n = 654$ synaptic/3349 extrasynaptic tracks for PALM'ed PSDs, 658/3345 FWHM, 1197/3125 95% border; 113 PSDs, 11 cells, 3 cultures).

($0.085 \pm 0.006 \mu\text{m}^2$, $n = 263$ PSDs/21 neurons) was within the ranges as previously detected by PALM (MacGillavry et al., 2013; Nair et al., 2013) and by electron microscopy (Harris and Stevens, 1989; Schikorski and Stevens, 1997; Shinohara et al., 2008). To test whether diffraction-limited PSD borders could perform as well as PALM of PSDs at segregating synaptic and extrasynaptic probes, I simulated diffraction by blurring the PSD-95 molecular density maps with a Gaussian point-spread function. Taking the full-width half maximum of this intensity distribution as the border of the diffraction-blurred PSDs, as was done by Li et al. (2016) (or see Chapter 2), performed nearly as well as the PALM'ed PSD border in segregating synaptic and extrasynaptic probe movements. Taking the 95% border of the blurred PSDs diminished the difference between synaptic and extrasynaptic D_{eff} (Fig. 3.2). Thus, how the PSD border is defined in diffraction-limited approaches can influence the accuracy of segregating diffusing molecules in different sub-compartments of the cell.

Synaptic TM protein diffusion is not influenced by PSD size or whole-synapse PSD-95 density

Interestingly, the D_{eff} distribution within different synapses varied widely, and individual molecules exhibited D_{eff} spanning more than 5 orders of magnitude. We reasoned that this broad range may arise because the diffusion environment within the PSD might vary based on synaptic size or geometry, or because the density of binding sites could influence how

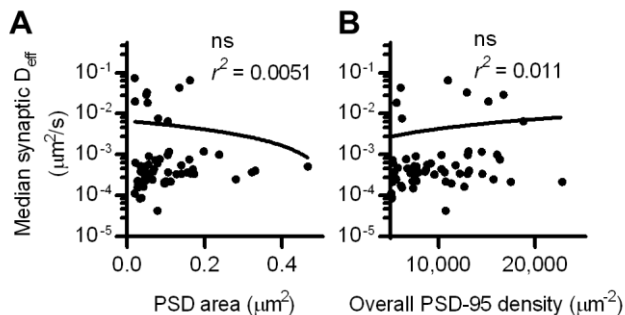


Figure 3.3. PSD size and density do not correlate with intrasynaptic mobility. (A) PSD area and median D_{eff} within each of the PSDs; linear regression test ($n = 113$ PSDs/11 cells/3 cultures). (B) PSD-95 density and median D_{eff} within each of the PSDs; linear regression test ($n = \text{same as in A}$).

likely a probe is able to be bound at any given time. To test this, I first examined the relationship between the area of the PSD and the median D_{eff} of probes found within it. Based on linear regression analysis, I found no statistically significant correlation (Fig. 3.3A). However, our previous study found that the fluorescence recovery of these probes after photobleaching spines was negatively correlated with PSD area (Li et al., 2016). Combined with this finding, this suggests that the size of the synapse correlates with the rate with which these probes enter and exit the spine, but does not influence their diffusion within the synapse. To determine whether overall PSD-95 density within the synapse can determine the diffusion of the binding probes, I examined the relationship between the density of PSD-95-mEos2 localizations and the synaptic median D_{eff} of probes in each PSD. The absolute density of localizations in all calculations was adjusted by the average expected number of blinks (one) of mEos2 in our experimental conditions (Annibale et al., 2011; MacGillavry et al., 2013). It should be noted that this measure of density does not incorporate the unknown fraction of total PSD-95 molecules that were mapped, and also ignores the numerous other binding partners of SEP-TM-Bind that may not correlate with the measured density of PSD-95-mEos2 as well as the likelihood of slight overexpression compared to endogenous protein level (~1.6x, see MacGillavry et al. (2013)). Nevertheless, I found no statistically significant correlation (Fig. 3.3B), suggesting that, given these caveats, the overall density of PSD-95 within the PSD does not influence the median diffusion of binding TM proteins in the synapse.

The control of TM protein diffusion by binding and steric hindrance within the PSD

Though the overall measured density of PSD-95 did not correlate with the diffusion coefficient of SEP-TM-Bind, it would be surprising if this key scaffolding protein did not

affect the mobility of its binding partners at all. We thus considered that the distribution of PSD-95 molecules is highly heterogeneous within single synapses (Fukata et al., 2013; MacGillavry et al., 2013; Nair et al., 2013; Broadhead et al., 2016) and can display multiple regions of high density within the synapse. Namely, two synapses of the same PSD-95 density can have very different arrangement of PSD-95 molecules, an organization that could obscure the effect that PSD-95 molecular density can have on the diffusion of probes when measured at the level of the entire synapse. Consistent with this notion, computer modeling has demonstrated that measured arrangements of PSD-95 molecules can prevent a larger fraction of TM proteins from escaping the synapse than homogeneously distributed PSD-95 molecules, without changing the overall density of PSD-95 (Li et al., 2016).

To test whether the density of PSD-95 immediately surrounding the probe can influence its diffusion within the synapse, I defined a subsynaptic metric, termed regional PSD-95 density, to be the number of PSD-95 molecules surrounding a tracked probe position. I measured the regional density using a fixed radius based on the average positional error of the tracked molecules (30 nm, see methods). However, the results of the following analyses depended only very weakly on the radius over the range of 15 to 80 nm

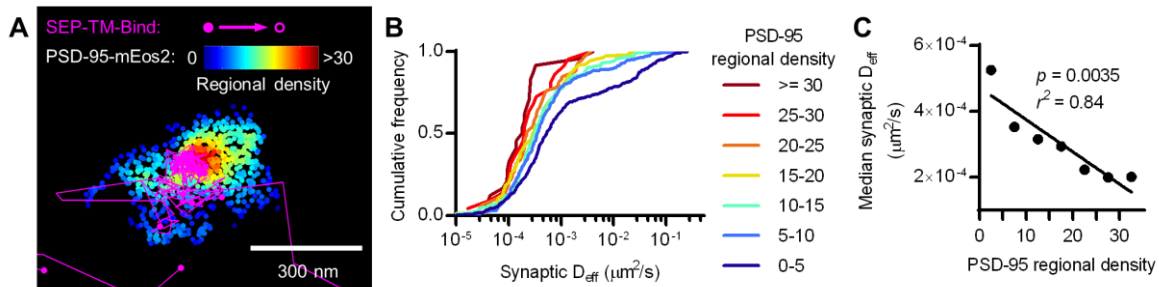


Figure 3.4. Nanoscale regional density of PSD-95 within the synapse correlates with probe diffusion coefficient.

(A) Typical example of tracks and PSD-95 positions. Inter-frame segments of tracks pseudo-colored by D_{eff} , PSD-95 positions pseudo-colored by regional density. (B) Cumulative frequency distributions of probe D_{eff} binned in increasing regional densities of PSD-95 surrounding the subtracks ($n = 448$ subtracks in 0-5 PSD-95, 281 in 5-10, 159 in 10-15, 106 in 15-20, 59 in 20-25, 22 in 25-30, 24 in 30+). (C) PSD-95 regional density and the median D_{eff} of the binding probe; relationship tested by linear regression.

(data not shown). I subdivided tracks into subsegments (subtracks) based on the regional PSD-95 density at each of their positions, and plotted the D_{eff} for subtracks based on their regional density. This analysis revealed that the higher the regional PSD-95 density, the slower the diffusion coefficients of the subtracks in that area of the PSD (Fig. 3.4A, B). In fact, the median probe D_{eff} with the synapse was strongly correlated with the regional density of PSD-95 (Fig. 3.4C).

The control of TM protein diffusion by steric hindrance alone within the PSD

At a first glance, this result may not be surprising, as it supports the idea that the more scaffold binding partners there are in the synapse, the more likely the probe will be bound and thus immobilized before diffusing further. However, this effect is more difficult to interpret as PSD-95 not only binds this probe, but can serve as a steric obstacle. In fact, PSD-95 is a hub for binding many other proteins that can serve as additional obstacles which can, without binding the probe, hinder its diffusion. To isolate the effect of steric hindrance from the combined effect of steric hindrance and probe-scaffold binding, I performed PALM-PAINT on a probe variant which cannot bind to PSD-95 (SEP-TM-

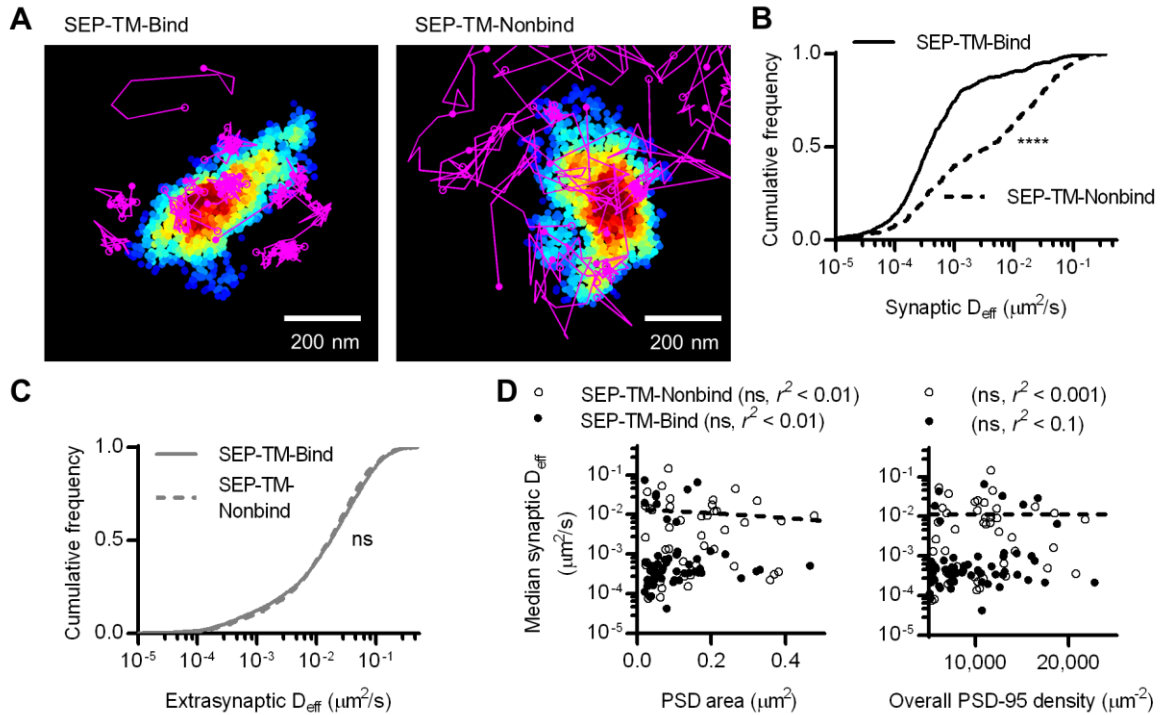


Figure 3.5. A non-binding transmembrane protein enters and slows within the synapse, but not as much as if it can bind PSD-95.

(A) Typical examples of tracked probes (purple) superimposed on *shrPSD-95* positions (pseudo-colored on a scale of regional density same as Fig. 4A; binding probe SEP-TM-Bind (left), nonbinding probe SEP-TM-Nonbind (right). (B) Cumulative frequency distributions of the binding probe and nonbinding probe D_{eff} within PSDs ($n = 654$ tracks/113 PSDs/11 cells/3 cultures for SEP-TM-Bind, 519/91/10/3 SEP-TM-Nonbind). (C) Cumulative frequency distributions of the binding probe and nonbinding probe D_{eff} outside of PSDs ($n = 3349$ tracks for SEP-TM-Bind, 4470 SEP-TM-Nonbind). (D) (Left) PSD area and median D_{eff} within each of the PSDs; linear regression test ($n = 91$ PSDs/10 cells/3 cultures of SEP-TM-Nonbind, same as in Fig. 3 for SEP-TM-Bind). (Right) Overall synaptic PSD-95 density and median D_{eff} within each of the PSDs; linear regression test ($n =$ as in left panel).

Nonbind from Li et al. (2016)). Interestingly, SEP-TM-Nonbind still entered synapses and diffused within them, but did not enrich within the PSD nearly as greatly as SEP-TM-Bind (Fig 3.5A and see also Li et al. 2016). Importantly, diffusion of this nonbinding probe within the synapse was dramatically faster than that of the binding probe (Fig. 3.5B). Importantly, the extrasynaptic diffusion of the nonbinding probe was not different from that of the binding probe (Fig. 3.5C). Intriguingly, the shoulder-like shape of the cumulative D_{eff} distribution suggests that probes undergo multiple influences on their

diffusion within the synapse. However, neither PSD area nor whole-synapse PSD-95 density correlated with probe diffusion within the PSD (Fig. 3.5D).

I considered whether the regional density of PSD-95 immediately surrounding the nonbinding probe can sterically control the probe diffusion. To test this, I first subdivided the tracks into subtracks and binned them into increasing regional densities of PSD-95 molecules, as in Fig 4B. This revealed that despite the lack of a PSD-95-binding motif, the probe still diffused more slowly within higher density regions of the PSD (Fig. 3.6A). The effect appeared to saturate at low D_{eff} since the mobility of these slowly moving molecules is below our detection limit ($0.003 \mu\text{m}^2/\text{s}$).

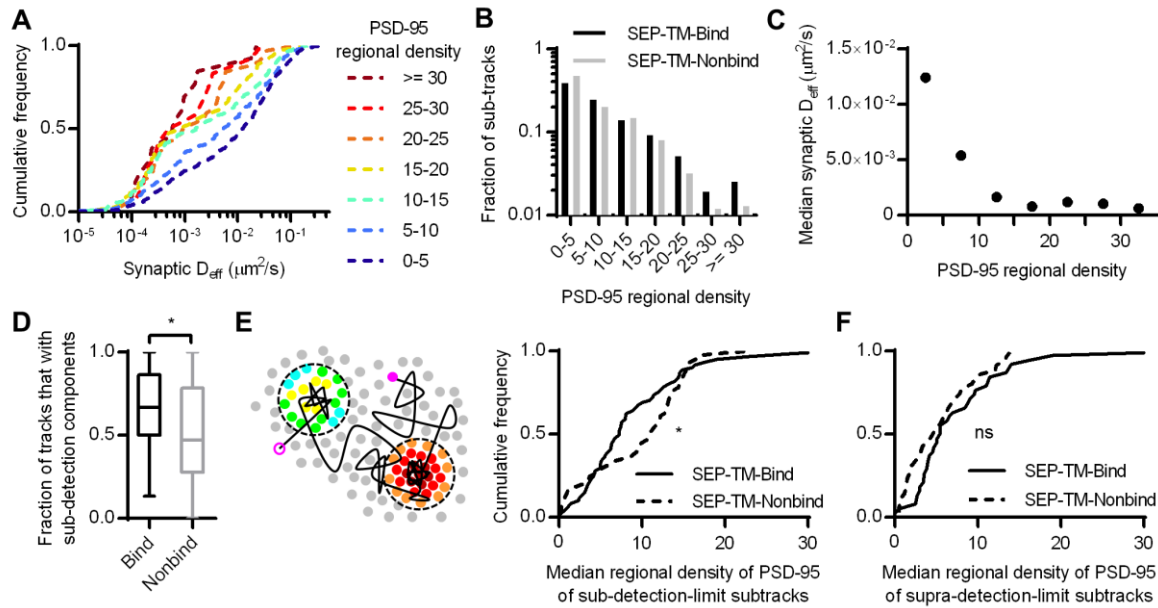


Figure 3.6. Subsynaptic regional density of PSD-95 influences the mobility of a probe that does not bind PSD-95.

(A) Cumulative frequency distributions of the nonbinding probe D_{eff} binned in increasing regional densities of PSD-95 surrounding the subtracks ($n = 480$ subtracks in 0-5 PSD-95, 204 in 5-10, 148 in 10-15, 81 in 15-20, 32 in 20-25, 12 in 25-30, 13 in 30+). (B) Fraction of subtracks in different regional densities of PSD-95. (C) PSD-95 regional density and the median D_{eff} of the nonbinding probe. (D) Fraction of tracks with subsegments that were slowed below the detection limit per PSD ($n = 113$ PSDs for SEP-TM-Bind, 91 SEP-TM-Nonbind; $*p = 0.0123$ Mann-Whitney U test). (E) (Left) Cartoon highlighting the PSD-95 molecules surrounding subtrack durations that diffused below the detection limit. The open and closed purple circles indicate the beginning and end of a track, the circles pseudo-colored by regional density were within 30 nm of sub-detection limit subtracks. We calculated the median regional density of PSD-95 of all subtrack durations that diffused below the detection limit with every PSD. (Right) Median regional density of PSD-95 surrounding subtracks that were below the detection limit (n same as in panel D; $*p = 0.0325$ K-S test). (F) Median regional density of PSD-95 surrounding subtracks that above the detection limit (n same as in panel D; ns Not significant $p = 0.158$ K-S test).

If steric obstruction influences probe mobility, it may influence the overall pattern of probe position within the synapse. I thus compared the fraction of subtracks found in different regional PSD-95 densities (Fig. 3.6B). Interestingly, though the binding and the nonbinding probes were distributed similarly through most density values, the nonbinding probes appeared to be preferentially excluded from the highly dense subregions (i.e. >25 regional molecules) of the synapse. Because of the small number of subtracks in these bins, however, this difference was not significant. Note also that the distribution of tracked molecules may not completely faithfully represent the total steady-state distribution of probe molecules, since molecules immobilized in the synapse for long periods are less likely to be recognized by a nanobody and be tracked by UPaint.

It appeared that regional densities of PSD-95 higher than 10 had minimal effect on diffusion of the nonbinding probe in the D_{eff} range below our detection limit (Fig. 3.6C); whereas the regional density of PSD-95 linearly correlated with the diffusion of the binding probe (Fig. 3.4B, C). Thus I wondered whether the two probes required different degrees of steric hindrance in order to be stabilized. To test this, I first considered only the subtracks with D_{eff} below the detection limit within the synapse. A higher fraction of these sub-detection-limit trajectory portions were found for SEP-TM-bind than SEP-TM-Nonbind (Fig. 3.6D), indicating that the binding probes were more often slowed down in the synapse than were the non-binding probes. If steric hindrance slows mobility of the both the binding and non-binding probes, but only binding is able to slow SEP-TM-bind, then SEP-TM-Bind would be expected to show a greater tendency to slow its mobility in relatively less dense PSD subregions; that is, even sparse binding partners can capture and immobilize SEP-TM-Bind whereas higher concentrations of molecules would be required to sterically

obstruct SEP-TM-Nonbind. Consistent with this, when I analyzed the sub-detection-limit portion of the nonbinding probe subtracks, I found that these were found in locales of higher regional density of PSD-95 compared those of the binding probes (Fig. 3.6E). Interestingly, the fraction of the subtracks above the detection limit did not show any difference in regional PSD-95 density (Fig. 3.6F), with a trend to the opposite relationship.

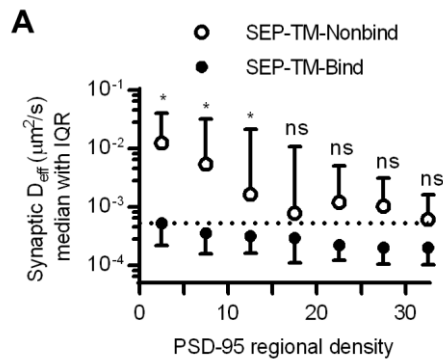


Figure 3.7. Estimating how dense PSD-95 is when protein mobility is slowed sterically.

(A) D_{eff} of SEP-TM-Nonbind and of SEP-TM-Bind within synaptic subregions of different PSD-95 densities (n of SEP-TM-Nonbind same as in Fig. 6 B; that of SEP-TM-Bind same as in Fig. 4B; two-way ANOVA, effect of binding $F_{1,6} = 15.27$ $p < 0.001$, effect of regional PSD-95 density $F_{1,6} = 13.53$ $p < 0.0001$, post hoc Bonferroni multiple comparisons tests between probes in increasing regional densities * $p < 0.05$, ns Not significant).

Altogether, these results suggest that crowding by scaffold molecules and perhaps other proteins is sufficient to stabilize TM proteins in the absence of binding. How dense does the molecular environment have to be in order to slow the TM probes sterically as much as the combined influence of steric hindrance and probe-scaffold binding? To estimate an answer to this question, I compared the diffusion coefficients of the binding and nonbinding probes within increasing regional densities of PSD-95 (Fig. 3.7). As expected based on Figs 4 and 6, the synaptic D_{eff} of both probes

decreased gradually with increasing PSD-95 regional density. However, the D_{eff} of SEP-TM-Nonbind decreased precipitously over the range of 0 to 15 yet did not decrease further at higher densities. Further, the D_{eff} of SEP-TM-Nonbind plateaued at the D_{eff} value displayed by SEP-TM-Bind at very low PSD-95 densities. Thus, by this analysis, ~15 PSD-95 molecules per region of 30-nm radius (~5,000 molecules/ μm^2) is the threshold beyond which the steric hindrance is as strong as both steric and binding influences combined.

Discussion

Using simultaneous single-molecule tracking and localization microscopy enabled by uPAINT and PALM, we demonstrated that the subsynaptic regional density of a scaffold protein PSD-95 can stabilize the surface membrane diffusion and positional organization of a single-pass transmembrane protein probe. The denser the regional density of PSD-95, the slower was the diffusion of the TM probe. This influence was apparent even in the absence of probe-scaffold binding, indicating steric hindrance by macromolecular crowding can complement protein-protein binding interactions in organizing TM proteins within the synapse.

The roles of receptor-scaffold binding and macromolecular crowding in subsynaptic organization.

The mobility of AMPARs in the synapse is increased when the binding of their accessory subunit Stargazin to PSD-95 is disrupted (Bats et al., 2007; Sainlos et al., 2011), providing strong evidence that receptors are acutely stabilized by PSD-95 binding. However, even in these conditions some stabilization of receptors in the synapse occurs, and our results indicate specifically that even small probes carrying a cytosolic tail unable to bind PSD-95 is still slowed substantially in the synapse. What controls this stabilized fraction even in the absence of binding has been a mystery. Mechanisms such as additional binding interactions have been proposed, which is not unlikely considering that AMPARs have numerous auxiliary subunits (Tomita et al., 2003; Cho et al., 2007; Soto et al., 2009; Kalashnikova et al., 2010; von Engelhardt et al., 2010; Erlenhardt et al., 2016) that can bind to various scaffolding proteins. However, even a cytosolic domain composed of just a GFP-type molecule is slowed within the synapse (Li et al., 2016). Thus, we propose a

more general mechanism that likely applies not only to glutamate receptors but also to other TM proteins critically important for synaptic function. In this model, receptor-scaffold binding is a ticket to entry and exit; PSD morphing redistributes even bound receptors within the synapse; and macromolecular crowding in combination with binding stabilizes the receptors at subsynaptic domains highly packed with other proteins important for synaptic transmission.

A density of 5,000 proteins/ μm^2 translates to an average ~ 14 nm inter-PSD-95 distance, very similar to the mean nearest-neighbor distance of ~ 13 nm between the “vertical filaments” corresponding to PSD-95 as measured in EM tomography (Chen et al., 2008). The similarity between these values suggests that rather subtle variations in scaffold density could change TM protein mobility substantially. This high density packing is similar to what has been measured for AMPA receptors (e.g. 2000 to 4000/ μm^2 , see Levet et al. (2015)). Indeed, receptor-scaffold binding may facilitate the assembly of this tight packing. Though the fractional time synaptic AMPARs spend bound to PSD-95 is not known, macromolecular crowding is likely to augment maintenance of this architecture once assembled, because receptors in crowded areas that dissociate from scaffolds will face a longer escape time from the region and thus are more likely to rebind PSD-95.

Advantages and disadvantages of PALM-PAINT

PALM of the PSD border improves discrimination of those molecules definitively within the synapse proper. However, we suspect that the effect of crowding may have been underestimated in our analysis because spatial and temporal alignment of the uPAINT and PALM data was subject to residual errors that may have diminished a larger underlying effect. The two color channels faced an alignment error of ~ 6 nm, which would somewhat

blur our measurement of regional PSD-95 density around individual tracked locations. In addition, the uPAINT data is subject to error stemming from the finite precision of individual localizations. The Atto647N we used for tracking is a relatively bright organic dye and helps to maximize this precision and thus minimize error in the estimate of D_{eff} . However, brighter, longer-lasting fluorophores could be advantageous. Nanobody-labeled small quantum dots (Wang et al., 2014) have been used to track AMPARs in and around synapses, and have the additional advantage of being so bright as to facilitate tracking in 3D (Cai et al., 2014). However, 3D mapping of the PSD would require high localization numbers and longer imaging durations (Legant et al., 2016) (and see below), and the z resolution normally obtainable without 4pi detection is usually worse than 100 nm for fluorescent proteins, making this difficult to implement.

In our application of PALM-PAINT, there was only limited temporal relationship between individual tracks (generally lasting <1 sec) and the PALM map (aggregated over the imaging session of generally 4 to 6 min). Though lateral drift was corrected during this time (to an error we estimated as <10 nm), ongoing morphing and internal reorganization of the PSD (Kerr and Blanpied, 2012; MacGillavry et al., 2013) presumably degraded many details of the PSD-95 distribution in our final images. The reduced precision in capturing the true regional density of PSD-95 molecules would diminish the difference we saw between probes in different regional densities, and also reduce the difference between binding and nonbinding probe. Further, probes in a similar subsynaptic space but tracked early vs late in the mapping might have not truly experienced the same degree of steric hindrance. However, the differences we observed were robust even in the face of these errors. Ideally, to capture the true effect size, one would need to monitor lateral drift

continuously (Bon et al., 2015) and achieve more rapid mapping (Huang et al., 2013). However, in structures with low protein copy number, a large fraction of the proteins must be mapped to achieve statistical reliability (MacGillavry et al., 2013; Legant et al., 2016), which may precludes time-lapse imaging except if the protein exchange rate is high compared to the photobleaching rate induced by imaging.

We hope the combined approach of PALM-PAINT will help answer many key questions regarding synapse architecture and plasticity. One key issue is what mechanisms assemble the particular organization of PSD-95, a pattern that appears to dictate receptor number and position (Opazo et al., 2012). One possibility is that the more deeply positioned multi-domain proteins in the PSD, such as the Shank and GKAP families (Valtschanoff and Weinberg, 2001; Dani et al., 2010), may establish a platform of loose spacing with which the more superficial proteins such as PSD-95 may interact (Chen et al., 2008). Interestingly, in this case, a close interaction of the deeper PSD with cytoskeleton (Frost et al., 2010; MacGillavry et al., 2016) may thus provide a link between activity-dependent plasticity of spine and PSD structure. Alternatively, cleft-resident adhesion molecules have distinct organizational patterns (Perez de Arce et al., 2015; Chamma et al., 2016), that may guide intracellular protein organization in both the presynaptic and postsynaptic cells. Dissecting these possibilities, which require nanoscale resolution of position and mobility of multiple proteins, may be aided by future PALM-PAINT applications.

Chapter 4: Quantifying the effect of sub-synaptically aligned neurotransmitter release and receptors on synaptic strength³

Abstract

The spatial alignment between the site of neurotransmitter release and the enriched postsynaptic region of receptors is a key determinant of synaptic strength. However, the precise architecture of this type of alignment and how it can influence synaptic transmission is poorly understood. By using localization microscopy we found that key proteins mediating vesicle priming and fusion are co-enriched in regions smaller than the presynaptic active zone. Using a newly developed method to map positions of vesicle fusion within individual synapses, we found that fusion preferentially occurred in these subsynaptic regions of enhanced local density of RIM proteins. By using two-color 3D localization microscopy, we found that these presynaptic RIM nanoclusters are frequently aligned with concentrated regions of postsynaptic receptors and scaffolding proteins. Using computer modeling, I found that this type of preferential alignment of release sites and receptors can boost the synaptic strength by 20-30%. Importantly, the nano-columnar alignment is mutable in various forms of induced synaptic plasticity. Together with results shown in Chapter 2 and 3, these data suggests that a simple and efficiently mutable architectural organization within the synapse—supported in part by postsynaptic macromolecular crowding—can modulate the strength of synaptic transmission.

Introduction

Synaptic transmission is maintained by a delicate, subsynaptic molecular architecture, and even mild alterations in synapse structure drive functional changes during experience-

³ Part of a bigger manuscript (Tang A-H, Chen H, Li TP, Metzbower SR, MacGillavry HD, Blanpied TA (2016) A transsynaptic nanocolumn aligns neurotransmitter release to receptors. Nature.)

dependent plasticity and pathological disorder (Zoghbi and Bear, 2012; Fromer et al., 2014; Volk et al., 2015). Key to this architecture is how the distribution of presynaptic vesicle fusion sites corresponds to the position of receptors in the postsynaptic density (Xie et al., 1997; Lisman et al., 2007). The notion that this spatial relationship modulates synaptic strength has been suggested long ago by numerical modeling incorporating AMPAR channel kinetics, glutamate diffusion and reuptake, and known spatial and temporal distribution of glutamate concentration per vesicular fusion event (Franks et al., 2003; Raghavachari and Lisman, 2004). However, a major limitation to these modeling studies was that they assumed that the release event always occurred centrally and that the postsynaptic receptors are uniformly distributed on the lateral face of the synapse. Thus, it was unclear whether the nonuniform organization of postsynaptic receptors or the location of release event within individual synapse could influence synaptic strength. The recent discovery that AMPARs are distributed heterogeneously within the synapse (Fukata et al., 2013; Nair et al., 2013) motivated additional numerical modeling to predict the influence of such an organization on synaptic function. The results demonstrate that glutamate releases directly and near dense local regions of AMPARs produce stronger synaptic response than release occurring elsewhere in the synapse (MacGillavry et al., 2013; Nair et al., 2013). However, it remained unclear whether the location of glutamate release could change over the lifetime of a synapse, and how the possible variation in release locations could influence synaptic function.

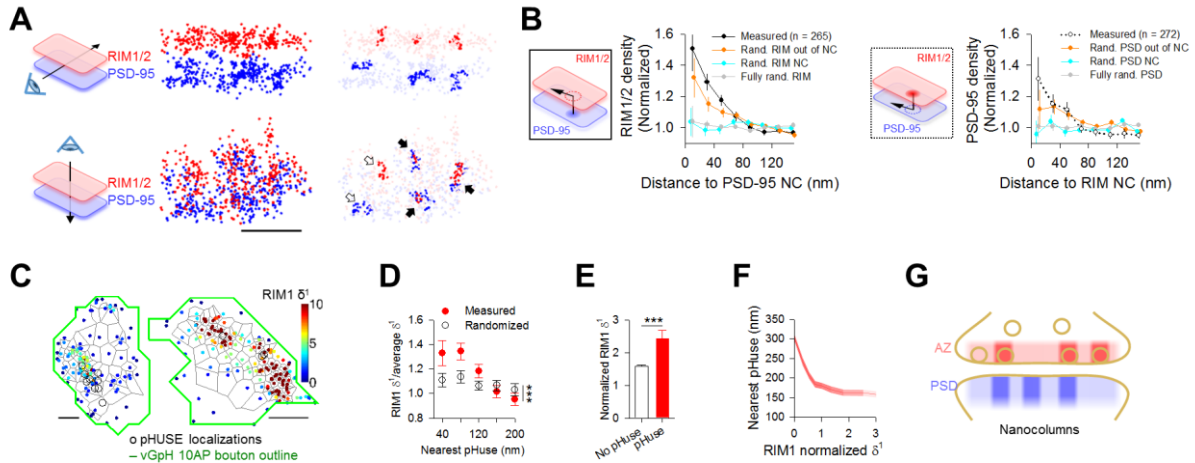


Figure 4.1. Sites of glutamate release preferentially align with regions of high PSD-95 density
(A) Side and en-face views of a synaptic RIM1/2 and PSD-95 pair as the distribution of localizations (left) and with identified nanoclusters (NC) highlighted (right), scale 200 nm. Filled arrows indicate aligned NCs, open arrows non-aligned NCs.
(B) RIM1/2 protein enrichment as a function of distance from translated PSD-95 NC centers (left, filled points) and PSD-95 enrichment relative to RIM1/2 NCs (right, open points).
(C) Tessellated RIM1-mEos and pHuse (phluorin-vGlut uncovering sites of exocytosis) localizations over the same boutons, scale 200 nm. See Tang et al., 2016 (in press) for more details.
(D) Tesseler first-rank density (δ^1) for RIM1 measured vs randomized distributions as a function of distance from pHuse localizations.
(E) Comparison within boutons of average δ^1 for RIM1 localizations within 40 nm to a pHuse localization vs not.
(F) Average nearest pHuse distance as a function of RIM1 δ^1 .
(G) Cartoon summarizing the organization of docked vesicles of glutamate (gold) with respect to dense regions of RIM1/2 (red) and PSD-95 (blue). AZ = active zone; PSD = postsynaptic density.
D-E, $n = 26/13$ * $p < 0.05$, ** $p < 0.01$, *** $p < 0.001$. n given in synapses/experiments.

Using localization microscopy, we have demonstrated that evoked glutamate release preferentially occurs near regions of high PSD-95 density and AMPARs (Tang et al., 2016). Briefly, we used localization microscopy to show that immunostained endogenous proteins critical for mediating vesicle priming (RIM1/2) are frequently co-enriched with postsynaptic scaffold protein PSD-95 important accumulating and retaining (Fig. 4.1A,B). Importantly, we determined locations of presynaptic release determined by localizing the vesicular glutamate transport 1 fused to a pH-sensitive GFP that only fluoresces upon vesicular release evoked by field stimulation, in relation to an expressed RIM1 protein localization PALM (Fig. 4.1C). Interestingly, regions surrounding release

sites are denser in RIM1 than regions without detected release (Fig. 4.1D-F). In other words, releasable vesicles of glutamate tended to be situated in regions co-enriched in pre- and post-synaptic scaffolding proteins (Fig. 4.1G), which we defined as transsynaptic molecular nanocolumn. This architecture suggests a simple organizational principle of CNS synapses to maintain and modulate synaptic efficiency.

To study the effects of the nanocolumnar synaptic organization on synaptic function, I used a deterministic computer modeling approach to determine the average fraction of AMPARs activated due to all possible release events from maps of release sites and receptor location estimated from measured locations of pre- and post-synaptic scaffolding proteins. I found that synapses in which release sites and receptors are aligned—even in the presence of other possible release sites outside the alignment—produced on average stronger synaptic response compared to other configurations. This result suggests that the internal structure can be efficiently re-organized to tune synaptic potency without the need to change the number of any synaptic protein.

Materials and Methods

See Tang et al. (2016) for details on cell preparation, immunostaining, 3D STORM imaging, single molecule localization processing and analysis, synaptic cluster and nanocluster analysis, vesicular exocytosis imaging and analysis, simultaneous imaging of RIM1 and glutamate exocytosis, Voronoi- or Tesseler-based local density metrics, and protein enrichment analysis

Synaptic modeling. I used an experimentally constrained deterministic approach to study the dependence of synaptic strength on the spatial distribution of release sites and

AMPARs. Central to this approach is the relationship between channel opening probability and its distance from a release site, determined previously by stochastic modeling approaches (Franks et al., 2003; Raghavachari and Lisman, 2004):

$$P_o(r) = 0.42 e^{-r/88 \text{ nm}}, \quad (1)$$

where r is the lateral distance between an AMPAR and a release site. In brief, the distribution of RIM1/2 proteins and GluA2/3-containing AMPA receptors measured by STORM were used to determine the spatial coordinates of release sites and AMPARs on a model synapse. Since the precise photophysics and blink distribution of dyes are complicated and the exact efficiency of antibody labeling is unknown, I calculated gradient maps of spatial coordinates to determine putative RIM1/2 protein and AMPAR locations from the single-molecule images. First, the 3D spatial coordinates were projected onto 2D planes orthogonal to the manually determined axodendritic axis. Each projected point was assigned a Gaussian function, the amplitude and width of which were determined by the normalized local density and the lateral STORM localization precision (20 nm). Overlapping Gaussian functions within the AZ or PSD convex hull were integrated to create the pre- and post-synaptic gradient maps. The sampling pixel size was 2.5 nm (the calculated synaptic response was independent of pixilation level for sampling size from 1 to 20 nm, data not shown). The pre- and post-synaptic gradient maps were separated by 20 nm, the cleft distance used to determine Equation 1 (Franks et al., 2003).

The model synaptic response for a single synapse was computed as the expected fraction of receptors that would open given a single release, averaged over all possible release locations in the AZ. For any single release event, the expected open fraction of channels at the peak of the response was calculated as follows:

$$O(i) = \sum_j \left[P_o(r_{ij}) \frac{LD_j}{\sum_j LD_j} \right], \quad (2)$$

where r_{ij} is the lateral distance between the i^{th} pixel in the presynaptic gradient map and the j^{th} pixel in the postsynaptic gradient map; the expected fraction of open channels $O(i)$ from the i^{th} release site is sum of channel opening probabilities at all pixels in the postsynaptic gradient map, where each j^{th} pixel is weighted by its normalized local density LD_j (i.e. the channel fraction is assumed to be directly proportional to the channel local density). To constrain the location of release events in the AZ, I utilized the live-cell pHuse-PALM data (Tang et al., 2016), which showed that release events preferentially occurred in regions with normalized RIM local density greater than 1.5, and these events occurred over 20-60% of the AZ area (spontaneous pHuse area / PALM'ed RIM area, and evoked pHuse area / spontaneous pHuse area). To account for these measured features, I modeled the spatial likelihood of release as a piecewise sigmoidal function dependent on the normalized local RIM density:

$$Pr(i | \text{release}) = \begin{cases} 0.5 \left[\frac{(1-s) \frac{LD_i}{LD_{inflect}}}{2-s - \frac{LD_i}{LD_{inflect}}} \right] & \text{if } LD_i \in [0, LD_{inflect}) \\ 0.5 + 0.5 \left[\frac{(1-s) \frac{LD_i - LD_{inflect}}{LD_{max} - LD_{inflect}}}{2-s - \frac{LD_i - LD_{inflect}}{LD_{max} - LD_{inflect}}} \right] & \text{if } LD_i \in [LD_{inflect}, LD_{max}] \end{cases} \quad (3)$$

where s is the steepness of the sigmoid transition, LD_i is the normalized local density of RIM at the i^{th} pixel of the presynaptic gradient map, $LD_{inflect}$ is the point of inflection in the sigmoidal function, and LD_{max} is the maximum normalized local density of RIM in a

STORM-measured example (Tang et al., 2016). LD_{inflex} and s were fitted to be 1.5 and 0.959 in order to yield a fractional release area of 40%. To calculate the average peak synaptic response per release, I calculated the expected open channel fraction averaged over all possible release sites weighted by the spatial probabilities of release:

$$Open\ channels\ at\ peak\ response\ (\%) = \sum_i \left[o(i) \frac{Pr(i | release)}{\sum_i Pr(i | release)} \right] \quad (4)$$

Statistical analysis. Statistical tests were performed with Graphpad. Data are presented as mean \pm s.e.m. unless otherwise specified.

Results

Given that the probability of AMPAR activation declines ~50% within ~60 nm from sites of glutamate release (Fig. 4.2A) as previously determined by stochastic modeling which incorporated measured channel kinetics, astroglial glutamate transporter kinetics, and glutamate diffusion (Xie et al., 1997; Franks et al., 2003; Raghavachari and Lisman, 2004), we can estimate the synaptic potency by using the observed RIM1/2, glutamate release locations, and receptor distributions (Tang et al., 2016).

I hypothesized that synapses can be potentiated by synaptic configurations if which there is preferential alignment between release and receptors. If this were true, I would predict that the response in a synapses where some release sites are preferentially occur over dense clusters of receptors would be stronger than other synaptic configurations where release occurs randomly in the active zone, or where releases preferentially occur away from the highly dense local regions of receptors. To test this, we selected a measured synapse, in which there was a single nanocolumn where dense RIM molecules and

receptors, estimated its synaptic efficacy using deterministic computer modeling, and compared it to the efficacy estimated from other simulated configurations in the same synaptic boundary.

Estimating synaptic efficacy required incorporating the spatial arrangement of RIM proteins, release sites, and receptors in a single model synapse. However, this was not straightforward, because we were technically limited from measuring all three pieces of information simultaneously. The spatial relationship between RIM proteins and release sites and the relationship between RIM proteins and receptors were determined from two independent experiments observing two different sets of synapses. To overcome the technical limitation, I reasoned that a map of probable release locations can be estimated by considering two additional findings: 1) vesicle fusion is more likely to occur in regions with RIM density greater than 1.5 times the overall RIM density in the synapse, and 2) detectable release sites covered 20-60% of the active zone area (Tang et al., 2016). To account for these metrics in the model, I made a reasonable assumption that the probability of release at any given location is sigmoidally dependent on the local density of RIM molecules at that location. The rationale for using a sigmoidal function was partly technical, as the inflection point and the steepness of the sigmoid could be adjusted independently to fit both measured metrics (see Discussion for structural and functional implications). Thus, I transformed a map of measured RIM localizations into a map of glutamate release likelihood within a single active zone (Fig. 4.2B-D), consistent with the measured results that glutamate release preferentially occurs in presynaptic regions of high RIM density.

To simulate synaptic strength, I combined map of release likelihoods with the corresponding map of immunostained GluA2/3 localizations within the same synapse (Fig.

4.2E left). A single release site can cause only a fraction of AMPAR channels to open. I modeled this phenomenon deterministically by first determining the radial distance between the release site and every postsynaptic channel position, and then incorporated the previously modeled spatial distribution of channel opening probability as a function of this distance to calculate number of channels opened by a single release (see Methods and Franks et al. (2003)). The fraction of opened channels per release then is this number divided by the total number of channels.

As shown by Tang et al. (2016), release can occur in multiple different locations over even a few minutes in the lifetime of a synapse. We predicted that the aligned nanocolumn configuration is likely to produce on average a stronger synaptic response over many events compared to a uniformly distributed distribution or to an offset configuration in which release events are more likely to occur away from enriched nanoclusters of receptor channels. To test this, I calculated the postsynaptic response or the fraction of open channels due to a single release on average weighted by the spatial likelihood of release, and compared among different configurations of release site and receptor channel positions (Fig. 4.2F). The average modeled synaptic response was ~21% in the case measured structure, in which the channels positions and release sites were estimated from measured localizations of RIM and GluA2/3 (Fig. 4.2G). To investigate the influence of the nanocolumn arrangement, we also simulated the synaptic strength in 4 different randomized configurations. Without altering the channel distribution, randomizing RIM positions and nearly homogenizing the spatial distribution of release sites notably weakened the synaptic response on average; randomizing the RIM positions outside of the nanocluster slightly weakened the response; and randomizing the position of the RIM

nanocluster reduced the response as well. Randomizing pre- and post-synaptic scaffold proteins reduced the synaptic response the most ($21.83 \pm 0.54\%$). Altogether, these results suggest that the nanocolumnar synaptic architecture can be relevant in regulation of synaptic physiology and likely facilitates higher single vesicle response potency.

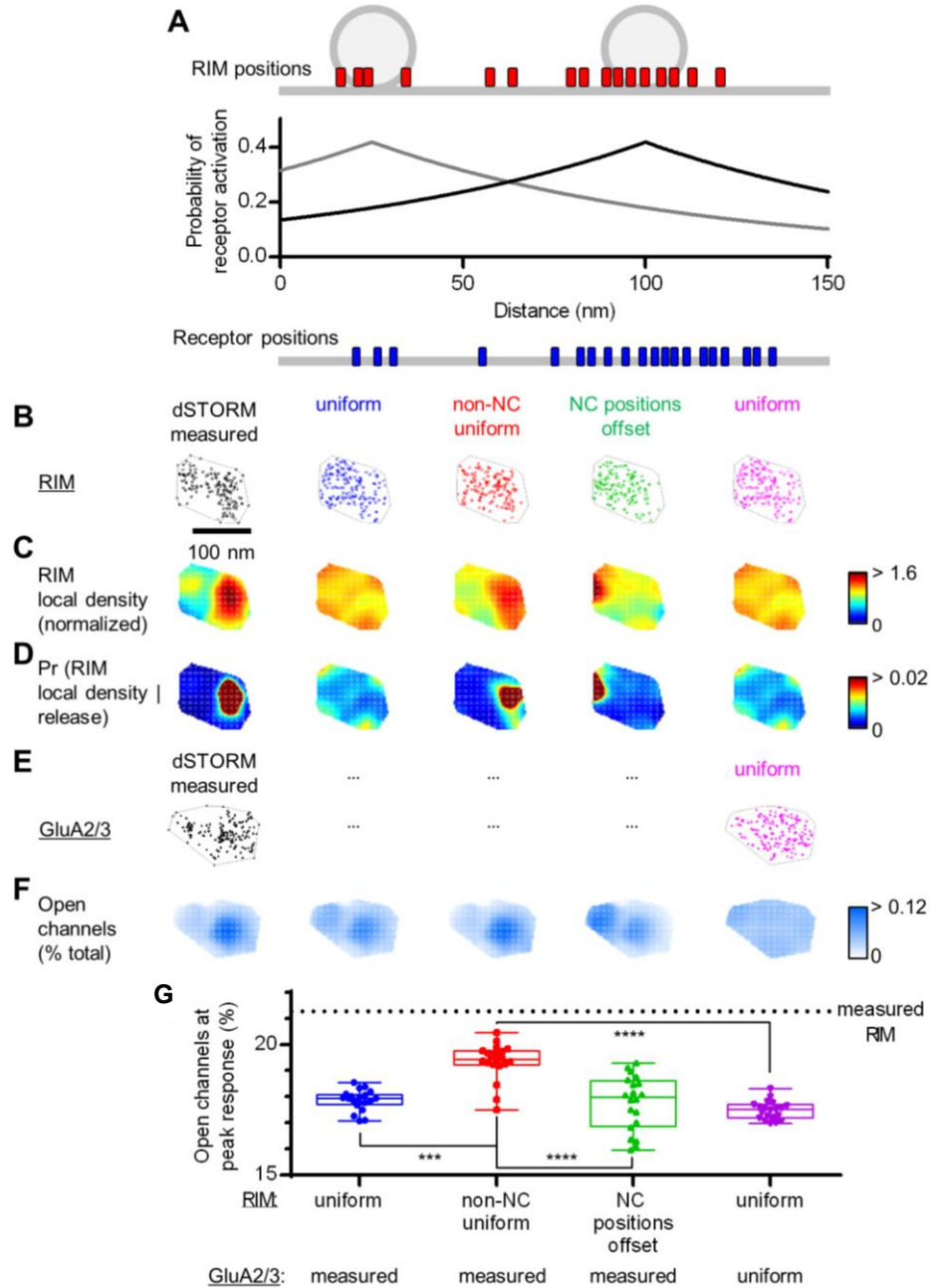


Figure 4.2. Preferential release in nanocolumns can increase synaptic strength.

(A) The spatial distributions of channel opening at the peak of response determined from previous stochastic numerical modeling studies (Franks et al., 2003; Raghavachari and Lisman, 2004) in an illustrated side-view of release sites, RIM positions, and PSD-95 positions determined from single molecule imaging (Tang et al., 2016). (B) Distributions of measured RIM localizations (black open circles) within a single active zone (AZ) boundary (grey), and the same number of localizations with other simulated configurations: all randomly distributed (blue and magenta), only the localizations outside of nanoclusters randomized (red), only the positions of nanoclusters were randomized (green). (C) Maps of RIM local density normalized to the overall densities within the AZs. (D) Probability density maps of possible release sites given that a release occurs. (E) Distributions of GluA2/3 locations (black filled circles) within the PSD boundary (grey) of the same measured synapse (ellipses refer to this distribution) and randomized (magenta). (F) Maps of fraction of open channels at peak response per average release from the respective AZs directly above them in D. (G) Expected open channels at peak response. Dotted line indicates fraction of open channels estimated from modeling releases in a synapse of measured RIM and GluA2/3 positions. Other configurations randomized in multiple times ($n = 20$ randomly generated molecular distributions).

Discussion

Because there is a substantial fraction of proteins outside nanodomains of scaffolding proteins and receptors, it has been unclear quantitatively how strong a role the clustering effect plays in modulating the amplitude of the synaptic response. By using a computer model incorporating the spatial likelihood of release events estimated from measured positions of RIM, previously published data the spatial distribution of channel opening probability, and the measured positions of AMPARs, we found that the nanocolumnar alignment of release sites and AMPARs can boost synaptic strength compare to other simulated unaligned configurations. Thus, modulating the alignment of release site and AMPARs can be additional point of control in the regulation of synaptic efficacy.

The strengths of deterministic computer modeling are that it is simple and computationally fast. However, they can also be its downfall. The major weakness of this approach as employed here is in the use of the spatial distribution of channel opening probability determined in another stochastic model (Franks et al., 2003), which had its own inherent assumptions, namely the stochastic model determined the relationship from a single circularly shaped PSD of a fixed diameter (500 nm) and cleft gap (20 nm). It is unclear whether this relationship would hold the same in synapses of different sizes, shapes, and cleft gaps. Remarkably, the fraction of open channels per release on average is similar to the median degree of receptor nonsaturation determined through ratio between evoked/miniature EPSC and the maximal iontophoretically evoked EPSC measured previously (Liu et al., 1999; McAllister and Stevens, 2000). Nonetheless, it would be important to perform careful stochastic numerical modeling on the same empirical data presented here to further confirm the validity of the finding, and enable the investigation

of how other morphological and structural parameters of the synapse and can contribute to the regulation of synaptic function.

Another weakness of this modeling approach lies in the assumption of how RIM molecular density dictates the location of vesicular release. We assumed a sigmoidal relationship, suggesting that release probability is low in areas where vesicle priming machinery is scarce or incomplete, high in areas of dense RIM, and semi-linearly variable in between. While this assumption is not nonsensical, it would need experimental support. Tang et al. (2016) could not directly accurately determine the spatial map of release likelihoods as we could detect only a handful of events per synapse before the primary hippocampal culture no longer responds to field stimulation, likely due to photobleaching of pHluorin in unreleased vesicles. We would need novel approaches to image 100's or at least 10's of release events per synapse in order to determine more directly and accurately the relationship between release likelihood at any given location in the active zone and the surrounding density of RIM proteins.

The physiologic effects predicted here are consistent with effect sizes posited by previous models (Tarusawa et al., 2009; MacGillavry et al., 2013; Nair et al., 2013), lending further support for the idea that the architectural structure within the synapse can contribute to the regulation of synaptic function. However, further scrutiny of past modeling studies and my own revealed an interesting discrepancy. Nair et al. (2013) proposed that the maximum AMPAR channel activation occurs exactly between two nanoclusters of receptors, and the closer the clusters in space the stronger the response. The maximum response remained in clusters separated by as much as 200 nm. We simulated the channel activation in a measured synapse expressing two nanoclusters separated by

~200 nm, and found, on the contrary, that the maximum channel activation occurred on one of the two nanoclusters (data not shown). The difference in our results could be explained by the difference in the distribution of channels between the two modeling studies. Notably, the simulation by Nair study Nair et al. (2013) assumed that the density of channels within the two nanoclusters are identical; however, we used a measured distribution of channel locations where the nanoclusters could express variable densities of channels. Taken together, I am tempted to speculate that multiple metrics in the channel distribution can contribute to modulating synaptic strength. These factors include the number of channel nanoclusters, distance of separation between nanoclusters, and the differential channel densities in nanoclusters. It is possible that similar factors in the presynaptic scaffolding protein organization can contribute to this regulation as well. To test this idea in the future, I would group all measured synapses into different categories based on their differences in organization and systematically examine the relationship between different metrics of nano-organization and synaptic physiology.

To minimize complexity and isolate as few informative variables as possible, we completed the modeling on a single measured synapse containing a single nanocolumn. However, the nanostructure is much more variable across different synapses; different plasticity induction protocols amplified this variability (Tang et al., 2016). It is conceivable that the role of nanocolumnar structure can be amplified or diminished in different types of synapses or in similarly organized synapses of larger or smaller size. For example, the nanocolumnar structure could have a smaller effect in a larger synapse containing a single nanocolumn, in which the larger fraction of proteins unassociated with the nanocolumn would dominate the synaptic response. For another example, having multiple nanocolumns

that cover almost the entirety of a small synapse could saturate the response and diminish the variability within a single synapse. On the other hand, the increased enrichment of PSD-95 aligned with RIM in chemically LTP'ed synapses (Tang et al., 2016) could boost synaptic strength, but the magnitude of this enhancement could be different synapses containing variable number of nanoclusters. It would be important in the future to determine how other subtle variations in nanostructure can dictate synaptic response.

Overall, the gradients of protein density we observed suggest a nanocolumn model, in which AZ regions with the highest likelihood of release are aligned to the densest receptor areas, optimizing the potency of neurotransmission. This provides a simple organizational principle that may hold for many small, CNS synapses, and will have the largest influence at synapses that typically release only one vesicle following an AP (Bolshakov and Siegelbaum, 1995). The compartmentalized AZ architecture is reminiscent of protein organization in *Drosophila* neuromuscular junction (Liu et al., 2011) and vertebrate ribbon synapses (Frank et al., 2010), where vesicles and priming proteins are arrayed around tight clusters of Ca^{2+} channels. However, observations in small CNS synapses of both clustered (Holderith et al., 2012; Ermolyuk et al., 2013; Nakamura et al., 2015) and random distribution of Ca^{2+} channels (Scimemi and Diamond, 2012), and emerging evidence for channel mobility as an equalizer of *Pr* for vesicles independent of channel positioning (Schneider et al., 2015) suggest that their precise distribution may not be the sole determinant of the AZ release likelihood landscape.

The alignment of pre and postsynaptic nanoscale subdomains (Fukata et al., 2013; MacGillavry et al., 2013; Nair et al., 2013) suggests that even small synapses may be composed of dynamic functional modules (Lisman and Raghavachari, 2006; Tarr et al.,

2013). We hypothesize that the nanocolumn represents an especially sensitive point whereby disease-associated pathways, frequently known to alter synaptic plasticity (Zoghbi and Bear, 2012; Fromer et al., 2014; Volk et al., 2015), may disrupt synapse function. It will be important to identify which, if any, of the numerous cleft-spanning adhesion systems (Siddiqui and Craig, 2011; Missler et al., 2012) or retrograde signaling mechanisms (Alger, 2002; Henry et al., 2012) mediate release-receptor alignment and permit dynamic transsynaptic realignment.

Chapter 5

Limitations

Abstract

Single molecule tracking and mapping methods are powerful, and they have revealed novel information about individual synapses at unprecedented detail. However, the requirements and execution of these techniques are not without their limitations. This chapter considers the methodological weaknesses and the modifications used or potential alternative methods to overcome them.

Overexpression of chimeric proteins

Ideally, the marker for the PSD must not interfere with the steric or binding environment of the synapse. To ensure that this was the case, we used two different approaches.

To mark the PSD in Chapter 2 for confocal and single molecule tracking approaches, I overexpressed a fluorescently tagged Homer1c. Homer1c has no known interaction motifs for binding to the stargazin tail of chimeric transmembrane probes or AMPARs. Moreover, Homer1c overexpression has been demonstrated previously by immunostaining not to alter the synaptic targeting or level of PSD-95 (Usui et al., 2003). Thus, the overexpression of Homer1c likely does not interfere with the binding or steric environment for the diffusing proteins of interest.

To mark the PSD in Chapter 3 and 4, where experiments required an assay to monitor the architectural organization of PSD-95, I used a replacement construct of PSD-95 that was fused to a GFP or mEos2 (MacGillavry et al., 2013). This replacement construct knocks down endogenous PSD-95 by a short hairpin RNA and expresses a knock-

down resistant variant of PSD-95. Comparing PSDs in transfected cells and neighboring untransfected cells, immunostaining for PSD-95 showed that this construct produced a mild 1.4x overexpression. Interpretations of the results from the PALM-PAINT assay require control experiments to ensure that the expressed protein is organized similarly to its endogenous counterpart. By immunostaining and single-molecule mapping, we compared the PSD-95 nanostructure of untransfected cells with those expressing the replacement construct PSD-95-mEos2 (MacGillavry et al., 2013;Tang et al., in press). These were not different in terms of PSD area, number of subsynaptic nanoclusters, and the size of those nanoclusters. Thus, we believe the mEos2 tag does not affect PSD nanostructure, at least in the absence of severe PSD-95 overexpression. Furthermore, mEos2 is fused at the c-terminal end of the PSD-95, not altering the positions of the various protein-protein interaction motifs. Thus, we believe tagging itself and a mild overexpression have minimal, if any, effect on the PSD-95 organization and its interaction with other proteins.

Several alternative approaches have emerged in the recent years to circumvent overexpressing PSD-95. One such approach utilizes an expressible piece of antibody that recognizes PSD-95, known as intrabody (Gross et al., 2013). Though small, it would still be necessary to carry out control experiments to ensure that it does not interfere with PSD-95 organization within the synapse and binding to its partners. Another approach would be to knock in the fluorescently tagged PSD-95 avoiding transient gene delivery approaches altogether. However, standard knock-in strategies lead to the global expression of the fluorescently-tagged protein of interest, resulting in poor imaging contrast and lacking in cell-type specificity (Herzog et al., 2011). The ideal approach would to use a conditional

mouse genetic strategy termed endogenous labeling via exon duplication, which can be used to fluorescently label endogenous proteins in sparse subset of neurons, maintaining imaging contrast and cell-specific labeling (Fortin et al., 2014).

Automatic identification of PSDs and extrasynaptic tracks

The raw single-molecule data collected from Chapter 2 and 3 consist of tens of thousands individual location coordinates or localizations. To increase the throughput of data acquisition and analysis, all analysis was performed using custom-made routines in a programming language MATLAB (Mathworks). The localizations were filtered by their shape and photon brightness as described previously (MacGillavry et al., 2013), in order to increase the specificity of molecule detection. The filtering process resulted in molecules with a maximal precision of 25 nm (defined as in Thompson et al. (2002)).

To identify PSDs in Chapter 3 for each field of imaging, I constructed a 2-dimensional molecular density map of 25x25 nm subpixels for the mEos emission. The intensity of each subpixel is determined by the number of molecules found therein. This map was thresholded resulting in a binary map of subpixels that contained at least two molecules. Objects containing more than 30 contiguous subpixels and a density of more than 5,000 molecules/ μm^2 were analyzed as PSDs. These thresholds are determined based on the smallest PSD area detectable by electron microscopy (Schikorski and Stevens, 1997) and the minimum number of PSD-95 detectable by a fluorescence-based technique (Sugiyama et al., 2005).

The PSD filtering algorithm increases my confidence that the identified PSDs are real PSDs in synapses, but inevitably leaves a fraction of PSDs undetected, especially those with low copy number of PSD-95, which are considered to be outside of the defined

“synaptic region”. These undetected PSDs can produce a paradoxical difference in diffusion between binding and nonbinding probes or between the small binding probe and the large AMPAR in the extrasynaptic space. As tracks moving in through PSDs (detectable or not) are likely to be clustered, I used an additional filtering step avoid tracks that are clustered outside of the PSDs, and applied it without bias to every experiment.

By using a convenient software package SR-Tesseler (Levet et al., 2015). I segregated the extrasynaptic localizations into two groups: localizations within the nonsynaptic clusters (on-cluster) and those outside (off-cluster) (Fig. 5.1) (see Chapter 2 Methods for details). The on-cluster localizations outside of PSDs were reminiscent of clustered receptors in the dendrite reported by other groups using smtPALM (Hoze et al., 2012; Levet et al., 2015), dSTORM (Levet et al., 2015), and immunogold EM (Nair et al., 2013). This analysis revealed that on-cluster tracks diffused slower than off-cluster tracks for neurons expressing mEos3-GluA2 and neurons expressing mEos3-TM-Bind (Fig. 5.1C,D).

The origins of these clusters may well be multifaceted; interpreting them is outside the scope of this study, but potential contributions include synapses with low synaptic scaffold protein expression, regions with a high density of endocytic adaptor molecules,

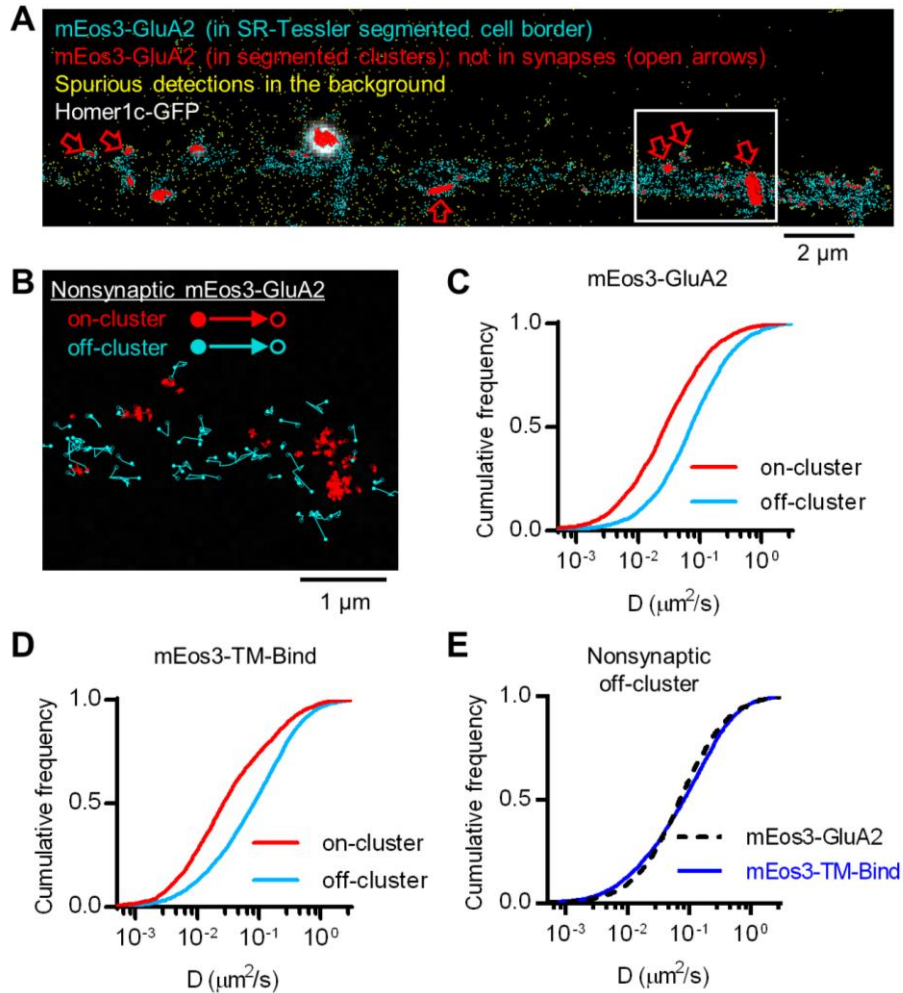


Figure 5.1. The AMPARs and small membrane probes diffuse similarly in unenriched nonsynaptic regions. (A) PALM detections of mEos3-GluA2 superimposed on PSDs marked by Homer1c-GFP: inside SR-Tesseler-segmented cell border (cyan), inside segmented clusters of high enrichment (red), inside segmented clusters but not PSDs (red arrows), outside cell border (yellow). (B) Nonsynaptic mEos3-GluA2 tracks inside (red) and outside (cyan) highly enriched clusters. (C) Nonsynaptic mEos3-GluA2 diffusion coefficients on and off clusters ($n_{\text{on-cluster}} = 2983$ tracks, $n_{\text{off-cluster}} = 3177$, in 13 neurons/2 cultures), derived from localizations in white box of (A). (D) Nonsynaptic mEos3-TM-Bind diffusion coefficients on and off clusters ($n_{\text{on-cluster}} = 3123$ tracks, $n_{\text{off-cluster}} = 4044$, in 12 neurons/2 cultures). (E) Nonsynaptic mEos3-GluA2 and mEos3-TM-Bind diffusion coefficients off clusters. Their medians were not different (Mann-Whitney U test, $p = 0.058$).

sites of plasma membrane-ER apposition, or zones of dense cortical cytoskeleton. Regardless, mobility within these regions is not easily interpretable, and we therefore excluded on-cluster nonsynaptic tracks from further analysis.

Agents other than PSD-95 which can contribute to postsynaptic crowding

It should be noted that the regional density of PSD-95—used in Chapter 3 to assess the crowding environment surrounding diffusing TM proteins—does not incorporate unknown fraction of total PSD-95 molecules, and ignores numerous other binding partners of SEP-TM-Bind that may not correlate with the measured density of PSD-95-mEos2. Of the many types of scaffold proteins in the synapse, we considered PSD-95 first because it is the closest to the postsynaptic membrane as it associates directly with the inner leaflet membrane through N-terminal palmitoylation. Though PSD-95 is not the only one of the MAGUK family, it is the most studied and the most abundant of the MAGUKs. PSD fraction mass spectroscopy determined that PSD-95 is 300% more abundant than the other MAGUKs combined (Cheng et al., 2006), suggesting that receptors and other TM proteins are predominantly influenced by PSD-95 in the PSD. Other MAGUK family members likely play a smaller contributing role in crowding. Nonetheless, it would be informative to determine whether their distributions are identical or different from that of PSD-95.

An ideal approach to assess the relative importance of different subtypes of MAGUKs would be to knock down simultaneously the major forms of MAGUKs as recently demonstrated (Levy et al., 2015), and re-express MAGUK members individually or in combination to determine their relative roles in steric effects on receptor diffusion.

Receptors as crowding agents

Receptors, unlike PSD-95, may contribute as obstacles in the extracellular, transmembrane, and intracellular domains. My data so far suggests that receptor density would have to be near 5,000 molecules/ μm^2 in order to alter the diffusion of other diffusion TM proteins sterically. However, its known density in various microdomains of the plasma

membrane suggests that it likely plays a contributing crowding role in some but not all places. Immunogold electron microscopy demonstrate that the density of AMPARs outside of the synapse is 10 ± 17 per μm^2 (Masugi-Tokita et al., 2007). There are 15-50 AMPARs per exocytic vesicle (Yudowski et al., 2007; Tao-Cheng et al., 2011); given the average vesicle diameter of $0.15 \mu\text{m}$, the density of receptors in exocytic vesicle likely has minimal crowding effect on diffusion. In fact, majority of the exocytic events dissipate quickly within seconds (Jullie et al., 2014). Some persist for at least 30 seconds due to kiss-and-run events. Endocytic zones label intensely for transferrin receptors but sparsely for AMPARs (Tao-Cheng et al., 2011), suggesting crowding could contribute to trapping diffusing TM proteins for endocytosis. The number of glutamate receptors within the synapse, though less than PSD scaffold proteins, ranges from 5-200 as determined by various techniques of measurements such as electrophysiology, mass spectrometry, and immunogold EM (Nusser et al., 1998; Matsuzaki et al., 2001; Smith et al., 2003; Peng et al., 2004; Tanaka et al., 2005; Cheng et al., 2006; Masugi-Tokita et al., 2007). Interestingly, AMPARs co-enrich with high-density regions of PSD-95 as shown by single molecule imaging (MacGillavry et al., 2013). Thus, subtle changes in the regional density of receptors can contribute to crowding.

The TM probes were overexpressed and likely influence the crowding environment. Assessing this influence would require post-hoc immune-staining and protein counting after each single molecule tracking session. Though certainly feasible to do, inevitable alterations in PSD morphology during steps of fixation and multiple hours of antibody incorporation preclude accurate estimates of TM probe density in the synapse. Alternatively, one could correlate TM diffusion with the relative expression level of TM probe per PSD

(as estimated by either the photon count or relative fluorescent intensity). However, the brightness of fluorescence strongly correlates with the subtle variations in the displacement between the fluorescent source and the source of excitation, which would be nearly impossible to assess for every individual PSD. However, these subtle variations likely does not bias the measured effects one way or another, because the random nature of transfection rate and expression level ensures that no single group of PSDs have a systematically higher expression level than another.

Disadvantages of PALM-PAINT

In the application of PALM-PAINT in Chapter 3, there was only limited temporal relationship between individual tracks (generally lasting <1 sec) and the PALM map (aggregated over the imaging session of generally 4 to 6 min). Though lateral drift was corrected during this time (to an error we estimated as <10 nm), ongoing morphing and internal reorganization of the PSD (Kerr and Blanpied, 2012; MacGillavry et al., 2013) presumably degraded many details of the PSD-95 distribution in our final images. The reduced precision in capturing the true regional density of PSD-95 molecules would diminish the difference we saw between probes in different regional densities, and also reduce the difference between binding and nonbinding probe. Further, probes in a similar subsynaptic space but tracked early vs late in the mapping might have not truly experienced the same degree of steric hindrance. However, the differences we observed were robust even in the face of these errors. Ideally, to capture the true effect size, one would need to monitor lateral drift continuously (Bon et al., 2015) and achieve more rapid mapping (Huang et al., 2013). However, in structures with low protein copy number, a large fraction of the proteins must be mapped to achieve statistical reliability (MacGillavry et al.,

2013;Legant et al., 2016), which may precludes time-lapse imaging except if the protein exchange rate is high compared to the photobleaching rate induced by imaging.

Chapter 6

General discussion

In these studies, I tested the predictions from simulated diffusion of TM proteins by measuring the diffusion of a TM protein probe within the synapse, specifically in the context of the heterogeneous organization of the scaffold protein PSD-95. Both the TM probe bulk and scaffold protein organization are predicted to prevent the escape of TM probe from the synapse. Empirical data support these notions in showing that even a small cytoplasmic protein bulk contributes to regulating the diffusion of TM probes within the synapse. In addition, probe-scaffold binding slowed the diffusion of TM protein in a scaffold-density-dependent manner, the denser the scaffolds, the slower the diffusion. Surprisingly, this density-dependent effect remained even in the absence of probe-scaffold binding. Thus, I conclude that both steric effects and protein-protein binding contribute to stabilizing the positioning of AMPAR and other functionally important TM proteins within the synapse, which can have substantial influence on synaptic transmission and neural circuit performance.

The role of probe-scaffold binding interaction

FRAP and single molecular tracking demonstrate that binding to scaffold protein is not the only force that keeps TM proteins in the synapse, consistent with previous studies (Frischknecht et al., 2009; Sainlos et al., 2011). Without binding, however, the distribution of TM proteins across the dendrite appears more uniform, suggesting that proteins are dispersed from the synapse, consistent with previous findings (Bats et al., 2007). However, it was difficult to tease apart the influence of binding and bulk other studies as they either removed the entire cytoplasmic tail or removed the entire binding ligand for PDZ domains,

thus changing both the binding and protein bulk. Here we abolished binding without changing bulk of the cytoplasmic domain, and find that the effect on the net rate of entry and exit was not as large as that of removing the entire cytoplasmic domain altogether, challenging the notion that binding interaction is the only factor that can stabilize protein diffusion.

It is noteworthy, however, that TM proteins could not be enriched in the synapse in the absence of binding. In fact, PDZ-mediated binding was necessary and sufficient to drive the synaptic enrichment of TM proteins. Consistent with this idea, another group found that fusing a single TM domain with a ligand that can bind inhibitory scaffold protein targets it to the inhibitory synapses (Masson et al., 2014). Thus, I conclude that receptor-scaffold binding facilitates entry to the synapse, but long-term retention within the synapse requires more than binding.

The role of TM protein size in the mobility and distribution of synaptic TM proteins

Considering that the steric effects from macromolecular crowding are agnostic to the identity of the diffusing molecule, the expressible single-pass TM protein probe is a suitable proxy to study how crowding would affect TM proteins in general. The simplicity of this probe enabled us to investigate independently the effect of protein bulk and of binding. The dimerized version of this probe via chemical induction is representative of dimerizable adhesion molecules such as Neuroligin (Shipman and Nicoll, 2012). However, this experimental paradigm need not be limited to only dimer probes, as the constructs can be modified further to become inducible multi-pass transmembrane proteins by fusing multiple dimerizable motif on one probe.

The bigger the size the slower the diffusion in the synapse. This finding supports the notion that the synapse is like a sieve as previously proposed, but effects of crowding shown here are likely not only valid for synapses but also for other structured and crowded environments like the axonal initial segment (Winckler et al., 1999), and the neck of a membrane protrusion in a heterologous cell (Lin et al., 2013). Surprisingly, though the GFP-sized bulk was larger than the StgCtail by more than 200 residues in absolute number of amino acids, the GFP was not as slow and stabilized as the non-binding version of the StgCtail, suggesting that other features of the cytoplasmic domains such as protein morphology, charge, and orientation (Hafner et al., 2015) could play a role in the regulation of protein diffusion.

The finding that the dimeric TM probe with a single functional binding motif diffused slower within the synapse than the less bulky monomeric TM probe with a single binding motif further supports the notion that additional protein bulk can influence diffusion. However, it would be more informative to determine the role of extracellular and TM domain bulk, separated from the intracellular influence.

The role of TM domain bulk is also worthwhile to consider. AMPARs carry a multitude of auxiliary proteins that modulate its trafficking, channel kinetics, binding capacity for scaffolding proteins, and, importantly, width of the TM domain (Schwenk et al., 2012). It has been shown through single-molecule tracking of constitutively desensitized AMPAR subunits and AMPAR subunits covalently linked to stargazin that the association between GluA2 and stargazin modulates the stability of AMPAR diffusion (Constals et al., 2015), suggesting that a change in binding capacity for PSD-95 via Stargazin can influence the organization of AMPARs within the synapse. The results of

our dimerized TM probe with increasing binding capacity for PSD-95 support this notion, but also suggest TM domain could play a substantial role in regulating the stability of TM protein within the synapse. It is tempting to speculate that the change in diffusion of AMPARs with or without TARPs could be due to a difference in TM and cytoplasmic bulk in addition to the change in binding capacity.

The role of PSD architectural organization in the arrangement and stability of synaptic TM proteins

A small fraction of the large receptors underwent exchange in seconds and no detectable fraction traversed through the synapse for at least ten minutes (Fig. 2.5), which at face value appeared at odds with smtPALM showing that 50% of AMPARs within the synapse diffuse at $> 0.2 \mu\text{m}^2/\text{s}$ (Fig. 2.6). However, a more detailed consideration reveals that these results are compatible for at least two reasons.

First, we emphasize that the complementary approaches of partial synapse FRAP and smtPALM revealed qualitatively similar effects, that the smaller TM probe was less stabilized than the larger AMPARs within the synapse. However, it is true that the sometimes very slow time course of recovery in FRAP experiments through the years (Ashby et al., 2006; Frischknecht et al., 2009; Makino and Malinow, 2009; Kerr and Blanpied, 2012) appears difficult to reconcile with the fast diffusion consistently measured with single-molecule tracking (Heine et al., 2008; Hoze et al., 2012; Nair et al., 2013). In our modeled synapse, the apparent median diffusion of the receptors were $0.038 \mu\text{m}^2/\text{s}$ with interquartile range (IQR) 0.02-0.06 for the small tracer, and $0.03 \mu\text{m}^2/\text{s}$ IQR 0.01-0.04 for the AMPAR-sized tracers—faster than the measured median synaptic diffusion.

Nonetheless, FRAP curves simulated in the model incorporating these apparent diffusion rates matched the measured FRAP curves very well (Fig. 2.3G).

Second, we considered the question of how such fast-diffusing receptors can exchange so slowly between two halves of the synapse. The simulations in this work and experimental results shown by other groups indicate that receptors, even with fast diffusion, do not necessarily have the capability to move through entire expanse of the synapse. We showed that AMPAR-sized tracers can move through only a small fraction of the synapse (Fig. 2.2E). In addition, single-molecule imaging by other groups have shown that there are multiple small subregions (80-100 nm in diameter) in the synapse which can confine receptor movement (Ehlers et al., 2007; MacGillavry et al., 2013; Nair et al., 2013; Levet et al., 2015). Thus, it is possible that fast diffusing receptors could be confined to subsynaptic regions and not move appreciably between two halves (~200 nm) of the synapse.

Using both FRAP and SMT in the same study is informative in more ways than what has been mentioned. First, partial synapse photobleaching does not require that synaptic TM protein be labeled with bulky fluorescently conjugated targeting ligand such as Q-dot tagged antibodies. An important limitation is that the bulky ligand limits access of targeted TM proteins into small and crowded environment of the synapse (Groc et al., 2007; Triller and Choquet, 2008). Consequently, the labeling process preferentially targets extra synaptic and perisynaptic TM proteins, precluding the study of their mobility within the synapse proper, particularly within the most interior portions of the PSD where the architectural organization is most complex. The use of a leaner combination of fluorescent moiety and targeting ligand such as dye-conjugated nanobodies in uPAINT (see Chapter

4) provides a powerful alternative for studying mobility within the synapse. However, the most stable organic fluorescent dyes to-date provide significantly shorter tracking lengths precluding the comparison of steady-state kinetics as TM proteins travel to or become release from the synapse. The use of expressed SEP-tagged TM proteins with FRAP is a powerful complementary approach for studying mobility on a short and long time-scale, while retaining confidence that the same synaptic population of proteins is being observed.

Partial synapse FRAP reveals that AMPARs were confined within subregions of the synapse not just for seconds, but minutes, whereas the smaller TM protein was not as confined. This argues against a corral model of the PSD structure and indicates that TM proteins are embedded in a crowded sieve-like environment which could dictate their subsynaptic position based on their bulk. PALM-PAINT indicates that TM proteins can be positioned in dense subregions even in the absence of binding. The dense packing of PSD molecules (Chen et al., 2008; Dani et al., 2010) creates an environment so crowded that diffusion of receptors is limited even if they do not remain bound to scaffold partners. Indeed modeling of TM protein diffusion suggests that elastic collisions between TM proteins and obstacle proteins that do not bind them can promote retention and heterogeneous subsynaptic organization. A regulated interplay of binding and crowding can modulate the positioning of TM proteins.

What kind of proteins can participate in crowding?

A diverse class of molecules could participate in crowding: transmembrane proteins (other receptors, ion channels, adhesion molecules, presynaptic transmembrane proteins with significant extracellular extensions), intracellular proteins near the postsynaptic membrane (other scaffolds, and cytoplasmic signaling proteins that can bind to scaffolds).

AMPARs have a very bulky extracellular domain (Sobolevsky et al.) which extends 75% of an average cleft gap. It is possible that non-specific extracellular interactions will substantially obstruct diffusion. For example, ECM impedes AMPAR diffusion indicated by the finding that degrading the ECM accelerated AMPAR exchange in and out of the synapse (Frischknecht et al., 2009), although immobilized fraction did not change in the synapse. Thus, the ECM might not play a substantial organizing role within the synapse proper. However, even though the synaptic cleft is rich with protein elements as shown by tomographic electron-microscopy (Lucic et al., 2005; High et al., 2015), it is only half as dense as the PSD (Burette et al., 2012), so the overall contribution to crowding by cleft proteins might not be more important than TM and postsynaptic molecules. In fact, computer-simulations suggest that the reduced crowding in the cleft would fail to slow and retain receptors in the synapse as well as the amount of crowding observed in the PSD (Santamaria et al., 2010). Whether this is indeed the case in living synapses is unclear and requires further investigation.

Contribution to transmembrane steric obstruction could come from different kinds of adhesion molecules. For example, Neuroligin binds to PSD-95 positioned close proximity with AMPARs, and it bridges across the cleft to bind neuroxin presynaptically (Mondin et al., 2011) making them ideal candidate transmembrane barriers to AMPAR lateral diffusion. The dense packing of these adhesion molecules, which are themselves possibly regulated by the steric influence of PSD-95 and other synaptic proteins, could facilitate the dense packing of AMPARs and thus the strength within nano-columns where synaptic release preferentially occurs. In addition to Neuroligin, there are multitude of other adhesion molecules in the synapse such as N-cadherin (Saglietti et al., 2007),

LRRTM (de Wit et al., 2013), and several other types of transmembrane protein elements which are arranged heterogeneously within the PSD (High et al., 2015). The combined effect of these adhesion molecules on the organization and stability of receptors requires further investigation.

On the intracellular side, multiple macromolecular species can contribute to crowding. Besides PSD-95, other MAGUKs such as PSD-95 and SAP102 (Chen et al., 2015; Levy et al., 2015) can serve as additional obstacles and contribute to the steric influence on receptor diffusion. It would be informative study the mobility of non-binding TM probes in synapses that are devoid of these three major MAGUKs. In addition to submembranous scaffold proteins, close positioning of GKAP to the membrane (Valtschanoff and Weinberg, 2001; Dani et al., 2010), and SynGAP (Araki et al., 2015)—only to name a few—by interaction with PSD-95 can further amplify the dense packing of the PSD. Thus, it will be important for future experiments to develop approaches to manipulate the crowding within the synapse without changing the protein composition or number.

CaMKII can be juxtamembranous, studded over the cytosolic face of the PSD shown in EM images of immunogold-labeled biochemically isolated PSDs (Petersen et al., 2003; Gaertner et al., 2004), well positioned to enhance macromolecular crowding. Interestingly, CaMKII undergoes translocation into spines following stimulation (Shen and Meyer, 1999); another relatively abundant synaptic protein within the PSD translocates away from spines following stimulation (Araki et al., 2015). Is tempting to speculate that these cytosolic proteins can serve as the gates close and opening diffusion channels to control TM protein entry and stabilization. To test whether filling the PSD with

additionally bulky proteins can indeed change the crowding environment and its influence on receptor organization or diffusion, one could take advantage of the expressible antibody-like proteins or intrabodies that can bind to synaptic scaffolding proteins (Gross et al., 2013)

The role of PSD architectural dynamics

We found using computer modeling that the heterogeneous organization of PSD-95 and the bulk of the diffusing TM protein molecules can dictate where in the synapse a TM protein can or cannot access, suggesting that steric influence alone can determine the positioning and distribution of TM proteins, all in the absence of changing binding affinity or absolute number of proteins. It is tempting to speculate that this can serve as an energetically efficient and rapid mechanism to arrange and re-arrange the positions of AMPARs relative to where neurotransmitter release occurs and modulate the strength of synaptic response.

Note that we made a critical assumption in the computer models due to a lack of experimentally determined constraints: the PSD-95 scaffolds are immobile relative to the rapid movement of TM proteins. Prior studies have shown that PSD-95 can be dynamic in at least two ways, 1) the exchange in and out of the synapse and 2) the arrangement within the synapse. The exchange in and out of the synapse can be considered nearly immobile on the timescale of minutes. As has been established from a number of studies, endogenous turnover of PSD-95 at the synapse is extremely slow. FRAP of PSD-95 bearing a Venus tag in a knock-in mouse exchanges only about 10% in 60 min (Fortin et al., 2014). Exchange of overexpressed PSD-95 is elevated compared to this but still slow, with time constants of 30 to 100 minutes in hippocampus, (Gray et al., 2006; Sharma et al., 2006; Blanpied et al., 2008), depending on age (Gray et al., 2006). These observations suggest

that within the short time frame of our simulations, such exchange will be of minimal impact and PSD-95 can be considered immobile.

However, ongoing spine actin polymerization alters PSD morphology over minutes (Kuriu et al., 2006; Kerr and Blanpied, 2012; Ziv and Fisher-Lavie, 2014), and single-molecule tracking has revealed that a substantial proportion of PSD-95 molecules (at least when overexpressed) is mobile within the synapse (Chazeau et al., 2014). As the internal dynamics of individual PSD-95 molecules remains poorly understood, we explored the potential effects of PSD molecular dynamics by considering a few presumptive models (Chapter 2 Discussion). PSD-95 molecular dynamics can certainly alter the contribution of steric effects on TM protein retention, but detailed effects depend very strongly on parameters that have not yet been deduced empirically. Clarifying these will require new approaches to determine how the individual PSD-95 molecules re-arrange during PSD morphing, whether they move in concerted motion as in a matrix-like mesh, or re-arrange haphazardly as the PSD morphs.

Implications for synapse function

The strength of synaptic transmission at individual excitatory synapses is ultimately determined by the number of postsynaptic AMPARs activated by presynaptic glutamate release. Since not all receptors open at once in response to release (Silver et al., 1996; McAllister and Stevens, 2000), two key parameters dictate the strength of response: 1) the density of receptors, 2) positioning of receptors relative to release. Indeed, local diffusion can replace desensitized AMPARs and fine-tune the fidelity of synaptic transmission under high frequency stimulation (Heine et al., 2008). Moreover, this regulation is mediated by

the uncoupling of desensitized AMPARs from stargazin (Constals et al., 2015), which not only alters the binding capacity but also the overall bulk of AMPARs. Considered together with results shown in Chapter 2 and 3, this further supports the notion that both binding interactions and protein-bulk-dependent steric effects can influence receptor lateral diffusion and hence its highly dense assembly of receptors. The interplay between binding and crowding likely play important roles in modulating the density of TM proteins such as AMPARs relative to release sites, potentially regulating the strength and reliability of synaptic transmission. Indeed, computational modeling in Chapter 5 showed that preferential release over dense locale of AMPARs produce between 20-30% larger responses compared to randomly located release. The long-term retention, depletion, or reorganization of ensembles of synaptic receptors may provide a basis for enduring yet flexible information storage at the level of individual synapses. It would be important to develop new approaches to measure release locations, synapse ultrastructure, and synaptic transmission within the same neuron to test this prediction.

In theory, macromolecular crowding can help achieve synaptic stability for much longer time than binding can. Non-covalent binding interactions have a definite probability of unbinding (Saro et al., 2007; Hafner et al., 2015). As estimated from the highest binding energy among PSD-resident proteins, the expected time to unbind is < 1 msec (Santamaria et al., 2010). Thus, the bound time of AMPAR to any PSD-resident protein or even a handful of binding partners is much smaller than the characteristic time scale of LTP or LTD expression, on the order of hours. Sans steric obstruction, AMPARs even if bound to several other PSD-resident proteins would escape the PSD within seconds. On the other hand, uniformly distributed scaffolds in the PSD could prevent an receptor from escaping

for up to hours as simulated previously (Santamaria et al.). As was shown in Chapter 2, the heterogeneous arrangement of scaffolds and the bulk of the diffusion protein can enhance this retention even longer. Notably, this type of sterically enhanced stability can be achieved without any change in the phosphorylation state, transcription rate, or translation rate—essentially energy-free. Interestingly, though the PSD-95 turnover can be considered nil on the order of minutes (noted previously), the spatial organization can rearrange on the order of minutes (Kerr and Blanpied, 2012; MacGillavry et al., 2013), potentially opening and restricting channels of diffusion in the process. It would be important to investigate whether this type of PSD dynamics is suppressed or enhanced during the induction or maintenance of LTP and LTD.

The implication of the nanocolumnar structure for synaptic transmission could be dramatic or negligible depending the synapse type. I showed that rearranging the alignment between the release sites and the receptors increased the spread of possible synaptic strengths (Fig. 4.2G). This wide range of response amplitudes could contribute to a dynamic range of the synaptic strength that might be even wider than what was proposed (Bartol et al., 2015), resulting in higher capacity for information storage per synapse. This could enable any given neural circuit to maintain a large repertoire of connected patterns. An additional advantage of the nanocolumnar structure is that it could allow neural networks to change connected pattern without the need to eliminate or generate new dendritic spines, and hence support fast, efficient, and flexible learning capability. These benefits are likely not greatly influential in synapses where receptors are saturated by glutamate release, such as climbing fiber synapses on the Purkinje cells of the cerebellum (Poncer et al., 1996; Foster et al., 2002; Harrison and Jahr, 2003). However, they could be

critically important for the function in, for example, the hippocampal synapses (Mainen et al., 1999; McAllister and Stevens), calyces of Held (Yamashita et al., 2003), and even inhibitory synapses of retinal amacrine cells (Frerking et al., 1995) in which receptors are not saturated by single glutamate release events.

That macromolecular crowding can alter the diffusion of TM proteins in a size-dependent could partly explain the variations in diffusion, number, and distribution among the different types of glutamate receptors and adhesion molecules. AMPAR numbers in the range of 5-200 demonstrated by mass spectrometry, immunogold EM, and electrophysiological experiments (Nusser et al., 1998; Matsuzaki et al., 2001; Smith et al., 2003; Peng et al., 2004; Masugi-Tokita et al., 2007). On the other hand, calcium imaging studies estimate 1-5 NMDARs in CA1 hippocampal synapses (Nimchinsky et al., 2004). In addition, these two types glutamate receptors display different spatial distributions within the PSD. AMPARs are either peripherally distributed or homogeneous distributed throughout the PSD (Masugi-Tokita et al., 2007). However, NMDARs are more compactly concentrated at the center of the PSD (Kharazia and Weinberg, 1997). These differences likely occur independent of the constraints on receptor diffusion, as single particle tracking showed that GluA2 and NR1 showing that the two receptors exhibited similar effective diffusion coefficients within the synapse (Groc et al., 2004). It is possible that distinct binding partners of their cytosolic tails dictate where the receptors are positioned, and steric obstruction of diffusion ensure the stability of receptors in their respective clusters of binding partners. Though nearly identical in their extracellular and transmembrane bulk and structure, NMDARs are larger than AMPARs in the cytosolic tails by >500 amino acids in length. Bulkier cytosolic domains could contribute to multiple protein-protein

interactions and more severe steric obstruction. In addition, the diverse binding partners of the extracellular domains can additionally contribute to controlling their spatial distribution within the synapse. In fact, extracellular domains of AMPARs associated with N-Cadherin (Nuriya and Huganir, 2006; Silverman et al., 2007) and LRRTM2 (de Wit et al., 2009), which may localize to diverse locations of the PSD (Uchida et al., 1996; Saglietti et al., 2007; Chamma et al., 2016), contributing to the diverse distribution of AMPARs in the PSD (MacGillavry et al.; Nair et al.). Surprisingly, LRRTM2, though smaller in both extracellular and intracellular length than Neuroligin1, in fact diffuses slower than Neuroligin1 (Chamma et al., 2016). Moreover, LRRTM2 is more compactly distributed in the center than the larger Neuroligin1, which suggests that the arrangement of TM proteins cannot be predicted by their bulk alone. However, the association of LRRTM2 with AMPARs directly could increase the effective bulk of LRRTM2, and thus the distribution of both proteins could be controlled as one complex instead of individual separate entities.

Potential regulators of crowding within the synapse.

Synaptic scaffold proteins are particularly well-suited for the organizing role in PSD architecture as they possess multiple protein-protein interaction motifs and are the most abundant proteins within the synapse (Sheng and Hoogenraad, 2007) altering them can influence multiple levels of interacting proteins and organization. Some central members of the scaffolding protein class besides PSD-95 are Shank and GKAP. Shank3 genetic mutations and deletions are linked to ASD and other neurodevelopment disorders (Bonaglia et al., 2001; Durand et al., 2007) as well as schizophrenia (Gauthier et al., 2010). In fact, deleting Shank3 in mice produced synaptic defects and autistic-like behaviors (Wang et al., 2011; Yang et al., 2012). Re-expression of Shank3 even in adult mice led to

improvements in synaptic protein composition, spine density, and neural function in the striatum (Mei et al., 2016), indicating that a neurodevelopment pathology can be reversed much later after initiation. Overt changes of spine loss required at least 7 days of expressing pan-Shank knockdown microRNAs to become apparent in mature dissociated hippocampal culture (MacGillavry et al., 2016); we speculate that changes in PSD organization occurs well before that.

Mutations in the GKAP family members have been linked to pathological grooming and obsessive-compulsive disorders (OCD) in human patients (Bienvenu et al., 2009); over expressing in cultured neurons a mutant family member, of which the turnover cannot be regulated by activity, impaired homeostatic synaptic scaling (Shin et al., 2012); moreover, the deletion of another GKAP family member in mice result in both a synaptic dysfunction and an OCD-like behavioral phenotype (Welch et al., 2007).

It will be important to expand our analysis of synaptic dysfunction in disease models beyond measurements of spine density and morphology and apply the imaging methods developed in this dissertation to test whether more subtle pathology in synapse organization underlies neuropsychiatric disorders.

Relation to disease mechanisms

Increasing evidence suggest that subtle disruptions of receptor positioning may be capable of altering synaptic transmission. The model we propose for crowding-mediated synaptic receptor retention and arrangement suggests that these perturbations may induce pathological disruption of synaptic function, even without an overt loss of proteins from the synapse (much less a gross loss of dendritic spines) through altered architectural organization and diffusion of TM proteins in the synapse. Indeed, there is an ever-

expanding set of evidence that TM protein diffusion could be involved in the plasticity of diverse neural circuits. Regulating AMPAR diffusion within the synapse is associated with a type of treatment for major depressive disorder, such that an antidepressant drug tianeptine favors the stabilization of AMPAR diffusion in the synapse, enhances a type of LTP in the hippocampus, and rescues this type of LTP suppressed by acute stress or corticosterone (Zhang et al., 2013). The extracellular matrix, a feature known to obstruct the diffusion to AMPARs (Frischknecht et al., 2009), has been found to be disrupted in distinct ways in different types of neuropsychiatric and neurodegenerative diseases such as autism spectrum, Fragile X syndrome, Rett syndrome, mood disorders, Alzheimer's disease, and epilepsy (reviewed by Pantazopoulos and Berretta (2016)). Antibodies purified from patients suffering from NMDAR autoimmune encephalopathy can reduce surface NMDAR diffusion in rat hippocampal neurons and also prevent LTP in these neurons (Dupuis et al., 2014), even though these antibodies do not change NMDAR activity as measured by NMDAR-mediated miniature EPSC (Moscatto et al., 2014). These results suggest that the altered receptor diffusion and organization could contribute to the symptoms of short-term memory deficits in these patients, and it is likely that altering the surface diffusion of glycine receptors could contribute to the brainstem and spinal cord symptoms in some patients with autoimmune progressive encephalitis with rigidity and myoclonus (Crisp et al., 2016). Neuromodulators such as dopamine has been implicated in directly modulating the lateral diffusion of NMDAR on the plasma membrane in and near the excitatory synapses of cultured hippocampal neurons (Dupuis et al., 2014), but how this influences brain function on a higher level remains to be tested.

It is becoming increasingly clear that the surface dynamics of TM protein such as receptors can play important roles in health and disease. However, we are only beginning to scratch the surface of a fertile field of nanostructural studies. In addition to investigating the role of receptor diffusion, it would be important to investigate the role of synaptic crowding and release-receptor alignment in the pathology that occurs during addiction, autism spectrum, chronic pain syndromes, diminished synaptic function during aging and early Alzheimer's disease, the neural damage accompanying stroke and brain injury, the altered states of mood in depression, and the positive and negative symptoms of schizophrenia. While some of these diseases often involve the loss of dendritic spines and synapses, I argue that more subtle pathologies are likely to occur in these diseases well before detectable micro- and macro-scopic morphological alterations. Discovering how these subtle changes underlie the various disease phenotype promises new insights into methods of intervention.

References

- Abraham WC, Logan B, Greenwood JM, Dragunow M (2002) Induction and experience-dependent consolidation of stable long-term potentiation lasting months in the hippocampus. *The Journal of neuroscience : the official journal of the Society for Neuroscience* 22:9626-9634.
- Alger BE (2002) Retrograde signaling in the regulation of synaptic transmission: focus on endocannabinoids. *Progress in Neurobiology* 68:247-286.
- Annibale P, Vanni S, Scarselli M, Rothlisberger U, Radenovic A (2011) Identification of clustering artifacts in photoactivated localization microscopy. *Nat Methods* 8:527-528.
- Araki Y, Zeng M, Zhang M, Huganir RL (2015) Rapid dispersion of SynGAP from synaptic spines triggers AMPA receptor insertion and spine enlargement during LTP. *Neuron* 85:173-189.
- Arendt KL, Royo M, Fernandez-Monreal M, Knafo S, Petrok CN, Martens JR, Esteban JA (2010) PIP3 controls synaptic function by maintaining AMPA receptor clustering at the postsynaptic membrane. *Nature neuroscience* 13:36-44.
- Ashby MC, Maier SR, Nishimune A, Henley JM (2006) Lateral diffusion drives constitutive exchange of AMPA receptors at dendritic spines and is regulated by spine morphology. *The Journal of neuroscience : the official journal of the Society for Neuroscience* 26:7046-7055.
- Ashby MC, De La Rue SA, Ralph GS, Uney J, Collingridge GL, Henley JM (2004) Removal of AMPA receptors (AMPA receptors) from synapses is preceded by transient endocytosis of extrasynaptic AMPARs. *The Journal of neuroscience : the official journal of the Society for Neuroscience* 24:5172-5176.
- Axelrod D, Ravdin P, Koppel DE, Schlessinger J, Webb WW, Elson EL, Podleski TR (1976) Lateral motion of fluorescently labeled acetylcholine receptors in membranes of developing muscle fibers. *Proceedings of the National Academy of Sciences of the United States of America* 73:4594-4598.
- Bagal AA, Kao JP, Tang CM, Thompson SM (2005) Long-term potentiation of exogenous glutamate responses at single dendritic spines. *Proceedings of the National Academy of Sciences of the United States of America* 102:14434-14439.

- Bartol TM, Bromer C, Kinney J, Chirillo MA, Bourne JN, Harris KM, Sejnowski TJ (2015) Nanoconnectomic upper bound on the variability of synaptic plasticity. *Elife* 4:e10778.
- Bats C, Groc L, Choquet D (2007) The interaction between Stargazin and PSD-95 regulates AMPA receptor surface trafficking. *Neuron* 53:719-734.
- Bear MF, Huber KM, Warren ST (2004) The mGluR theory of fragile X mental retardation. *Trends Neurosci* 27:370-377.
- Beique JC, Lin DT, Kang MG, Aizawa H, Takamiya K, Huganir RL (2006) Synapse-specific regulation of AMPA receptor function by PSD-95. *Proceedings of the National Academy of Sciences of the United States of America* 103:19535-19540.
- Benke TA, Luthi A, Isaac JT, Collingridge GL (1998) Modulation of AMPA receptor unitary conductance by synaptic activity. *Nature* 393:793-797.
- Bergles DE, Diamond JS, Jahr CE (1999) Clearance of glutamate inside the synapse and beyond. *Current opinion in neurobiology* 9:293-298.
- Berlucchi G, Buchtel HA (2009) Neuronal plasticity: historical roots and evolution of meaning. *Exp Brain Res* 192:307-319.
- Bernard V, Somogyi P, Bolam JP (1997) Cellular, subcellular, and subsynaptic distribution of AMPA-type glutamate receptor subunits in the neostriatum of the rat. *The Journal of neuroscience : the official journal of the Society for Neuroscience* 17:819-833.
- Betancur C, Sakurai T, Buxbaum JD (2009) The emerging role of synaptic cell-adhesion pathways in the pathogenesis of autism spectrum disorders. *Trends Neurosci* 32:402-412.
- Betzig E, Patterson GH, Sougrat R, Lindwasser OW, Olenych S, Bonifacino JS, Davidson MW, Lippincott-Schwartz J, Hess HF (2006) Imaging intracellular fluorescent proteins at nanometer resolution. *Science* 313:1642-1645.
- Bienvenu OJ et al. (2009) Sapap3 and pathological grooming in humans: Results from the OCD collaborative genetics study. *Am J Med Genet B Neuropsychiatr Genet* 150B:710-720.

- Biermann B, Sokoll S, Klueva J, Missler M, Wiegert JS, Sibarita JB, Heine M (2014) Imaging of molecular surface dynamics in brain slices using single-particle tracking. *Nat Commun* 5:3024.
- Blanpied TA, Scott DB, Ehlers MD (2002) Dynamics and regulation of clathrin coats at specialized endocytic zones of dendrites and spines. *Neuron* 36:435-449.
- Blanpied TA, Kerr JM, Ehlers MD (2008) Structural plasticity with preserved topology in the postsynaptic protein network. *Proceedings of the National Academy of Sciences of the United States of America* 105:12587-12592.
- Bliss TV, Gardner-Medwin AR (1973) Long-lasting potentiation of synaptic transmission in the dentate area of the unanaesthetized rabbit following stimulation of the perforant path. *The Journal of physiology* 232:357-374.
- Bliss TV, Lomo T (1973) Long-lasting potentiation of synaptic transmission in the dentate area of the anaesthetized rabbit following stimulation of the perforant path. *The Journal of physiology* 232:331-356.
- Bloodgood BL, Sabatini BL (2005) Neuronal activity regulates diffusion across the neck of dendritic spines. *Science* 310:866-869.
- Bolshakov VY, Siegelbaum SA (1995) Regulation of hippocampal transmitter release during development and long-term potentiation. *Science* 269:1730.
- Bon P, Bourg N, Lecart S, Monneret S, Fort E, Wenger J, Leveque-Fort S (2015) Three-dimensional nanometre localization of nanoparticles to enhance super-resolution microscopy. *Nat Commun* 6:7764.
- Bonaglia MC, Giorda R, Borgatti R, Felisari G, Gagliardi C, Selicorni A, Zuffardi O (2001) Disruption of the ProSAP2 gene in a t(12;22)(q24.1;q13.3) is associated with the 22q13.3 deletion syndrome. *Am J Hum Genet* 69:261-268.
- Borgdorff AJ, Choquet D (2002) Regulation of AMPA receptor lateral movements. *Nature* 417:649-653.
- Bosch M, Castro J, Saneyoshi T, Matsuno H, Sur M, Hayashi Y (2014) Structural and molecular remodeling of dendritic spine substructures during long-term potentiation. *Neuron* 82:444-459.

- Boyd IA, Martin AR (1956) The end-plate potential in mammalian muscle. *The Journal of physiology* 132:74-91.
- Breillat C, Thoumine O, Choquet D (2007) Characterization of SynCAM surface trafficking using a SynCAM derived ligand with high homophilic binding affinity. *Biochemical and biophysical research communications* 359:655-659.
- Broadhead MJ, Horrocks MH, Zhu F, Muresan L, Benavides-Piccione R, DeFelipe J, Fricker D, Kopanitsa MV, Duncan RR, Klenerman D, Komiyama NH, Lee SF, Grant SG (2016) PSD95 nanoclusters are postsynaptic building blocks in hippocampus circuits. *Sci Rep* 6:24626.
- Brown R (1828) A brief account of microscopical observations made in the months of June, July and August 1827, on the particles contained in the pollen of plants; and on the general existence of active molecules in organic and inorganic bodies. *Philosophical Magazine Series 2* 4:161-173.
- Burette AC, Lesperance T, Crum J, Martone M, Volkmann N, Ellisman MH, Weinberg RJ (2012) Electron tomographic analysis of synaptic ultrastructure. *J Comp Neurol* 520:2697-2711.
- Cai E, Ge P, Lee SH, Jeyifous O, Wang Y, Liu Y, Wilson KM, Lim SJ, Baird MA, Stone JE, Lee KY, Davidson MW, Chung HJ, Schulten K, Smith AM, Green WN, Selvin PR (2014) Stable small quantum dots for synaptic receptor tracking on live neurons. *Angew Chem Int Ed Engl* 53:12484-12488.
- Chamma I, Letellier M, Butler C, Tessier B, Lim KH, Gauthereau I, Choquet D, Sibarita JB, Park S, Sainlos M, Thoumine O (2016) Mapping the dynamics and nanoscale organization of synaptic adhesion proteins using monomeric streptavidin. *Nat Commun* 7:10773.
- Chazeau A, Mehidi A, Nair D, Gautier JJ, Leduc C, Chamma I, Kage F, Kechkar A, Thoumine O, Rottner K, Choquet D, Gautreau A, Sibarita JB, Giannone G (2014) Nanoscale segregation of actin nucleation and elongation factors determines dendritic spine protrusion. *EMBO J* 33:2745-2764.
- Chen L, Chetkovich DM, Petralia RS, Sweeney NT, Kawasaki Y, Wenthold RJ, Brecht DS, Nicoll RA (2000) Stargazin regulates synaptic targeting of AMPA receptors by two distinct mechanisms. *Nature* 408:936-943.

- Chen X, Winters C, Azzam R, Li X, Galbraith JA, Leapman RD, Reese TS (2008) Organization of the core structure of the postsynaptic density. *Proceedings of the National Academy of Sciences of the United States of America* 105:4453-4458.
- Chen X, Levy JM, Hou A, Winters C, Azzam R, Sousa AA, Leapman RD, Nicoll RA, Reese TS (2015) PSD-95 family MAGUKs are essential for anchoring AMPA and NMDA receptor complexes at the postsynaptic density. *Proceedings of the National Academy of Sciences of the United States of America* 112:E6983-6992.
- Chen X, Nelson CD, Li X, Winters CA, Azzam R, Sousa AA, Leapman RD, Gainer H, Sheng M, Reese TS (2011) PSD-95 is required to sustain the molecular organization of the postsynaptic density. *The Journal of neuroscience : the official journal of the Society for Neuroscience* 31:6329-6338.
- Chen Y, Lagerholm BC, Yang B, Jacobson K (2006) Methods to measure the lateral diffusion of membrane lipids and proteins. *Methods* 39:147-153.
- Cheng D, Hoogenraad CC, Rush J, Ramm E, Schlager MA, Duong DM, Xu P, Wijayawardana SR, Hanfelt J, Nakagawa T, Sheng M, Peng J (2006) Relative and absolute quantification of postsynaptic density proteome isolated from rat forebrain and cerebellum. *Mol Cell Proteomics* 5:1158-1170.
- Chetkovich DM, Chen L, Stocker TJ, Nicoll RA, Brecht DS (2002) Phosphorylation of the postsynaptic density-95 (PSD-95)/discs large/zona occludens-1 binding site of stargazin regulates binding to PSD-95 and synaptic targeting of AMPA receptors. *The Journal of neuroscience : the official journal of the Society for Neuroscience* 22:5791-5796.
- Cho CH, St-Gelais F, Zhang W, Tomita S, Howe JR (2007) Two families of TARP isoforms that have distinct effects on the kinetic properties of AMPA receptors and synaptic currents. *Neuron* 55:890-904.
- Cho KO, Hunt CA, Kennedy MB (1992) The rat brain postsynaptic density fraction contains a homolog of the Drosophila discs-large tumor suppressor protein. *Neuron* 9:929-942.
- Choi J, Ko J, Park E, Lee JR, Yoon J, Lim S, Kim E (2002) Phosphorylation of stargazin by protein kinase A regulates its interaction with PSD-95. *J Biol Chem* 277:12359-12363.

- Choquet D, Triller A (2013) The dynamic synapse. *Neuron* 80:691-703.
- Clements JD, Lester RA, Tong G, Jahr CE, Westbrook GL (1992) The time course of glutamate in the synaptic cleft. *Science* 258:1498-1501.
- Connor S, Williams PT, Armstrong B, Petit TL, Ivanco TL, Weeks AC (2006) Long-term potentiation is associated with changes in synaptic ultrastructure in the rat neocortex. *Synapse* 59:378-382.
- Constals A, Penn AC, Compans B, Toulme E, Phillipat A, Marais S, Retailleau N, Hafner AS, Coussen F, Hosy E, Choquet D (2015) Glutamate-induced AMPA receptor desensitization increases their mobility and modulates short-term plasticity through unbinding from Stargazin. *Neuron* 85:787-803.
- Crisp SJ, Kullmann DM, Vincent A (2016) Autoimmune synaptopathies. *Nature reviews Neuroscience* 17:103-117.
- Dahan M, Levi S, Luccardini C, Rostaing P, Riveau B, Triller A (2003) Diffusion dynamics of glycine receptors revealed by single-quantum dot tracking. *Science* 302:442-445.
- Dani A, Huang B, Bergan J, Dulac C, Zhuang X (2010) Superresolution imaging of chemical synapses in the brain. *Neuron* 68:843-856.
- de Wit J, O'Sullivan ML, Savas JN, Condomitti G, Caccese MC, Vennekens KM, Yates JR, 3rd, Ghosh A (2013) Unbiased discovery of glypican as a receptor for LRRTM4 in regulating excitatory synapse development. *Neuron* 79:696-711.
- de Wit J, Sylwestrak E, O'Sullivan ML, Otto S, Tiglio K, Savas JN, Yates JR, 3rd, Comoletti D, Taylor P, Ghosh A (2009) LRRTM2 interacts with Neurexin1 and regulates excitatory synapse formation. *Neuron* 64:799-806.
- Del Castillo J, Katz B (1954) Quantal components of the end-plate potential. *The Journal of physiology* 124:560-573.
- Diamond JS, Jahr CE (1997) Transporters buffer synaptically released glutamate on a submillisecond time scale. *The Journal of neuroscience : the official journal of the Society for Neuroscience* 17:4672-4687.

- Dupuis JP, Ladepeche L, Seth H, Bard L, Varela J, Mikasova L, Bouchet D, Rogemond V, Honnorat J, Hanse E, Groc L (2014) Surface dynamics of GluN2B-NMDA receptors controls plasticity of maturing glutamate synapses. *EMBO J* 33:842-861.
- Durand CM et al. (2007) Mutations in the gene encoding the synaptic scaffolding protein SHANK3 are associated with autism spectrum disorders. *Nat Genet* 39:25-27.
- Edidin M, Kuo SC, Sheetz MP (1991) Lateral movements of membrane glycoproteins restricted by dynamic cytoplasmic barriers. *Science* 254:1379-1382.
- Ehlers MD (2000) Reinsertion or degradation of AMPA receptors determined by activity-dependent endocytic sorting. *Neuron* 28:511-525.
- Ehlers MD, Heine M, Groc L, Lee MC, Choquet D (2007) Diffusional trapping of GluR1 AMPA receptors by input-specific synaptic activity. *Neuron* 54:447-460.
- Einstein A (1905) Über die von der molekularkinetischen Theorie der Wärme geforderte Bewegung von in ruhenden Flüssigkeiten suspendierten Teilchen. *Annalen der Physik* 322:549-560.
- El-Husseini AE, Schnell E, Chetkovich DM, Nicoll RA, Brecht DS (2000) PSD-95 involvement in maturation of excitatory synapses. *Science* 290:1364-1368.
- El-Husseini Ael D, Schnell E, Dakoji S, Sweeney N, Zhou Q, Prange O, Gauthier-Campbell C, Aguilera-Moreno A, Nicoll RA, Brecht DS (2002) Synaptic strength regulated by palmitate cycling on PSD-95. *Cell* 108:849-863.
- Erlenhardt N, Yu H, Abiraman K, Yamasaki T, Wadiche JI, Tomita S, Brecht DS (2016) Porcupine Controls Hippocampal AMPAR Levels, Composition, and Synaptic Transmission. *Cell Rep* 14:782-794.
- Ermolyuk Y, Alder FG, Surges R, Pavlov IY, Timofeeva Y, Kullmann DM, Volynski K (2013) Differential triggering of spontaneous glutamate release by P/Q-, N- and R-type Ca²⁺ channels. *Nature Neuroscience*.
- Fortin DA, Tillo SE, Yang G, Rah JC, Melander JB, Bai S, Soler-Cedeno O, Qin M, Zemelman BV, Guo C, Mao T, Zhong H (2014) Live imaging of endogenous PSD-95 using ENABLED: a conditional strategy to fluorescently label endogenous

- proteins. *The Journal of neuroscience : the official journal of the Society for Neuroscience* 34:16698-16712.
- Foster KA, Kreitzer AC, Regehr WG (2002) Interaction of postsynaptic receptor saturation with presynaptic mechanisms produces a reliable synapse. *Neuron* 36:1115-1126.
- Frank T, Rutherford MA, Strenzke N, Neef A, Pangršič T, Khimich D, Fejtova A, Gundelfinger ED, Liberman MC, Harke B (2010) Bassoon and the synaptic ribbon organize Ca²⁺ channels and vesicles to add release sites and promote refilling. *Neuron* 68:724-738.
- Franks KM, Stevens CF, Sejnowski TJ (2003) Independent sources of quantal variability at single glutamatergic synapses. *The Journal of neuroscience : the official journal of the Society for Neuroscience* 23:3186-3195.
- Freche D, Pannasch U, Rouach N, Holcman D (2011) Synapse geometry and receptor dynamics modulate synaptic strength. *PLoS One* 6:e25122.
- Frerking M, Borges S, Wilson M (1995) Variation in GABA mini amplitude is the consequence of variation in transmitter concentration. *Neuron* 15:885-895.
- Frick M, Schmidt K, Nichols BJ (2007) Modulation of lateral diffusion in the plasma membrane by protein density. *Curr Biol* 17:462-467.
- Frischknecht R, Heine M, Perrais D, Seidenbecher CI, Choquet D, Gundelfinger ED (2009) Brain extracellular matrix affects AMPA receptor lateral mobility and short-term synaptic plasticity. *Nature neuroscience* 12:897-904.
- Fromer M, Pocklington AJ, Kavanagh DH, Williams HJ, Dwyer S, Gormley P, Georgieva L, Rees E, Palta P, Ruderfer DM (2014) De novo mutations in schizophrenia implicate synaptic networks. *Nature*.
- Frost NA, Shroff H, Kong H, Betzig E, Blanpied TA (2010) Single-molecule discrimination of discrete perisynaptic and distributed sites of actin filament assembly within dendritic spines. *Neuron* 67:86-99.
- Fujiwara T, Ritchie K, Murakoshi H, Jacobson K, Kusumi A (2002) Phospholipids undergo hop diffusion in compartmentalized cell membrane. *J Cell Biol* 157:1071-1081.

- Fukata Y, Dimitrov A, Boncompain G, Vielemeyer O, Perez F, Fukata M (2013) Local palmitoylation cycles define activity-regulated postsynaptic subdomains. *J Cell Biol* 202:145-161.
- Gaertner TR, Kolodziej SJ, Wang D, Kobayashi R, Koomen JM, Stoops JK, Waxham MN (2004) Comparative analyses of the three-dimensional structures and enzymatic properties of alpha, beta, gamma and delta isoforms of Ca²⁺-calmodulin-dependent protein kinase II. *J Biol Chem* 279:12484-12494.
- Gauthier J et al. (2010) De novo mutations in the gene encoding the synaptic scaffolding protein SHANK3 in patients ascertained for schizophrenia. *Proceedings of the National Academy of Sciences of the United States of America* 107:7863-7868.
- Gerrow K, Triller A (2010) Synaptic stability and plasticity in a floating world. *Current opinion in neurobiology* 20:631-639.
- Giannone G, Hosy E, Levet F, Constals A, Schulze K, Sobolevsky AI, Rosconi MP, Gouaux E, Tampe R, Choquet D, Cognet L (2010) Dynamic superresolution imaging of endogenous proteins on living cells at ultra-high density. *Biophys J* 99:1303-1310.
- Glantz LA, Gilmore JH, Lieberman JA, Jarskog LF (2006) Apoptotic mechanisms and the synaptic pathology of schizophrenia. *Schizophr Res* 81:47-63.
- Granger AJ, Shi Y, Lu W, Cerpas M, Nicoll RA (2013) LTP requires a reserve pool of glutamate receptors independent of subunit type. *Nature* 493:495-500.
- Gray NW, Weimer RM, Bureau I, Svoboda K (2006) Rapid redistribution of synaptic PSD-95 in the neocortex in vivo. *PLoS Biol* 4:e370.
- Groc L, Heine M, Cognet L, Brickley K, Stephenson FA, Lounis B, Choquet D (2004) Differential activity-dependent regulation of the lateral mobilities of AMPA and NMDA receptors. *Nature neuroscience* 7:695-696.
- Groc L, Lafourcade M, Heine M, Renner M, Racine V, Sibarita JB, Lounis B, Choquet D, Cognet L (2007) Surface trafficking of neurotransmitter receptor: comparison between single-molecule/quantum dot strategies. *The Journal of neuroscience : the official journal of the Society for Neuroscience* 27:12433-12437.

- Gross GG, Junge JA, Mora RJ, Kwon HB, Olson CA, Takahashi TT, Liman ER, Ellis-Davies GC, McGee AW, Sabatini BL, Roberts RW, Arnold DB (2013) Recombinant probes for visualizing endogenous synaptic proteins in living neurons. *Neuron* 78:971-985.
- Hafner AS, Penn AC, Grillo-Bosch D, Retailleau N, Poujol C, Philippat A, Coussen F, Sainlos M, Opazo P, Choquet D (2015) Lengthening of the Stargazin Cytoplasmic Tail Increases Synaptic Transmission by Promoting Interaction to Deeper Domains of PSD-95. *Neuron* 86:475-489.
- Hall J, Trent S, Thomas KL, O'Donovan MC, Owen MJ (2015) Genetic risk for schizophrenia: convergence on synaptic pathways involved in plasticity. *Biol Psychiatry* 77:52-58.
- Harris KM, Stevens JK (1989) Dendritic spines of CA 1 pyramidal cells in the rat hippocampus: serial electron microscopy with reference to their biophysical characteristics. *The Journal of neuroscience : the official journal of the Society for Neuroscience* 9:2982-2997.
- Harris KM, Weinberg RJ (2012) Ultrastructure of synapses in the mammalian brain. *Cold Spring Harb Perspect Biol* 4.
- Harris KM, Jensen FE, Tsao B (1992) Three-dimensional structure of dendritic spines and synapses in rat hippocampus (CA1) at postnatal day 15 and adult ages: implications for the maturation of synaptic physiology and long-term potentiation. *The Journal of neuroscience : the official journal of the Society for Neuroscience* 12:2685-2705.
- Harrison J, Jahr CE (2003) Receptor occupancy limits synaptic depression at climbing fiber synapses. *The Journal of neuroscience : the official journal of the Society for Neuroscience* 23:377-383.
- Haselwandter CA, Calamai M, Kardar M, Triller A, da Silveira RA (2011) Formation and stability of synaptic receptor domains. *Phys Rev Lett* 106:238104.
- Hastie P, Ulbrich MH, Wang HL, Arant RJ, Lau AG, Zhang Z, Isacoff EY, Chen L (2013) AMPA receptor/TARP stoichiometry visualized by single-molecule subunit counting. *Proceedings of the National Academy of Sciences of the United States of America* 110:5163-5168.

- Hayashi Y, Shi SH, Esteban JA, Piccini A, Poncer JC, Malinow R (2000) Driving AMPA receptors into synapses by LTP and CaMKII: requirement for GluR1 and PDZ domain interaction. *Science* 287:2262-2267.
- Hebb DO (1949) *The organization of behavior; a neuropsychological theory*. New York,: Wiley.
- Heine M, Groc L, Frischknecht R, Beique JC, Lounis B, Rumbaugh G, Hugarir RL, Cognet L, Choquet D (2008) Surface mobility of postsynaptic AMPARs tunes synaptic transmission. *Science* 320:201-205.
- Henry FE, McCartney AJ, Neely R, Perez AS, Carruthers CJ, Stuenkel EL, Inoki K, Sutton MA (2012) Retrograde changes in presynaptic function driven by dendritic mTORC1. *The Journal of Neuroscience* 32:17128-17142.
- Herzog E, Nadrigny F, Silm K, Biesemann C, Helling I, Bersot T, Steffens H, Schwartzmann R, Nagerl UV, El Mestikawy S, Rhee J, Kirchhoff F, Brose N (2011) In vivo imaging of intersynaptic vesicle exchange using VGLUT1 Venus knock-in mice. *The Journal of neuroscience : the official journal of the Society for Neuroscience* 31:15544-15559.
- Hess ST, Girirajan TP, Mason MD (2006) Ultra-high resolution imaging by fluorescence photoactivation localization microscopy. *Biophys J* 91:4258-4272.
- High B, Cole AA, Chen X, Reese TS (2015) Electron microscopic tomography reveals discrete transleft elements at excitatory and inhibitory synapses. *Front Synaptic Neurosci* 7:9.
- Hirsh R (1974) The hippocampus and contextual retrieval of information from memory: a theory. *Behav Biol* 12:421-444.
- Holcman D, Triller A (2006) Modeling synaptic dynamics driven by receptor lateral diffusion. *Biophys J* 91:2405-2415.
- Holderith N, Lorincz A, Katona G, R $\sqrt{\geq}$ zsa Bz, Kulik A, Watanabe M, Nusser Z (2012) Release probability of hippocampal glutamatergic terminals scales with the size of the active zone. *Nature Neuroscience*.

- Hoze N, Nair D, Hosy E, Sieben C, Manley S, Herrmann A, Sibarita JB, Choquet D, Holcman D (2012) Heterogeneity of AMPA receptor trafficking and molecular interactions revealed by superresolution analysis of live cell imaging. *Proc Natl Acad Sci U S A* 109:17052-17057.
- Huang B, Jones SA, Brandenburg B, Zhuang X (2008) Whole-cell 3D STORM reveals interactions between cellular structures with nanometer-scale resolution. *Nat Methods* 5:1047-1052.
- Huang F, Hartwich TM, Rivera-Molina FE, Lin Y, Duim WC, Long JJ, Uchil PD, Myers JR, Baird MA, Mothes W, Davidson MW, Toomre D, Bewersdorf J (2013) Video-rate nanoscopy using sCMOS camera-specific single-molecule localization algorithms. *Nat Methods* 10:653-658.
- Huang YS, Kan MC, Lin CL, Richter JD (2006) CPEB3 and CPEB4 in neurons: analysis of RNA-binding specificity and translational control of AMPA receptor GluR2 mRNA. *EMBO J* 25:4865-4876.
- Huganir RL, Nicoll RA (2013) AMPARs and synaptic plasticity: the last 25 years. *Neuron* 80:704-717.
- Husi H, Ward MA, Choudhary JS, Blackstock WP, Grant SG (2000) Proteomic analysis of NMDA receptor-adhesion protein signaling complexes. *Nature neuroscience* 3:661-669.
- Hutsler JJ, Zhang H (2010) Increased dendritic spine densities on cortical projection neurons in autism spectrum disorders. *Brain Res* 1309:83-94.
- Inoue A, Okabe S (2003) The dynamic organization of postsynaptic proteins: translocating molecules regulate synaptic function. *Curr Opin Neurobiol* 13:332-340.
- Irier HA, Shaw R, Lau A, Feng Y, Dingledine R (2009) Translational regulation of GluR2 mRNAs in rat hippocampus by alternative 3' untranslated regions. *J Neurochem* 109:584-594.
- Jacobson K, Sheets ED, Simson R (1995) Revisiting the fluid mosaic model of membranes. *Science* 268:1441-1442.

Jones EG (1994) Santiago Ramon y Cajal and the Croonian Lecture, March 1894. *Trends Neurosci* 17:190-192.

Jullie D, Choquet D, Perrais D (2014) Recycling endosomes undergo rapid closure of a fusion pore on exocytosis in neuronal dendrites. *The Journal of neuroscience : the official journal of the Society for Neuroscience* 34:11106-11118.

Kalashnikova E, Lorca RA, Kaur I, Barisone GA, Li B, Ishimaru T, Trimmer JS, Mohapatra DP, Diaz E (2010) SynDIG1: an activity-regulated, AMPA- receptor-interacting transmembrane protein that regulates excitatory synapse development. *Neuron* 65:80-93.

Kennedy MB (2000) Signal-processing machines at the postsynaptic density. *Science* 290:750-754.

Kerr JM, Blanpied TA (2012) Subsynaptic AMPA receptor distribution is acutely regulated by actin-driven reorganization of the postsynaptic density. *The Journal of neuroscience : the official journal of the Society for Neuroscience* 32:658-673.

Kessels HW, Malinow R (2009) Synaptic AMPA receptor plasticity and behavior. *Neuron* 61:340-350.

Kharazia VN, Weinberg RJ (1997) Tangential synaptic distribution of NMDA and AMPA receptors in rat neocortex. *Neurosci Lett* 238:41-44.

Koch C, Zador A (1993) The function of dendritic spines: devices subserving biochemical rather than electrical compartmentalization. *The Journal of neuroscience : the official journal of the Society for Neuroscience* 13:413-422.

Kohn JE, Millett IS, Jacob J, Zagrovic B, Dillon TM, Cingel N, Dothager RS, Seifert S, Thiyagarajan P, Sosnick TR, Hasan MZ, Pande VS, Ruczinski I, Doniach S, Plaxco KW (2004) Random-coil behavior and the dimensions of chemically unfolded proteins. *Proceedings of the National Academy of Sciences of the United States of America* 101:12491-12496.

Konorski J (1948) *Conditioned reflexes and neuron organization*. Cambridge Eng.: University Press.

- Kopec CD, Li B, Wei W, Boehm J, Malinow R (2006) Glutamate receptor exocytosis and spine enlargement during chemically induced long-term potentiation. *The Journal of neuroscience : the official journal of the Society for Neuroscience* 26:2000-2009.
- Kucik DF, Elson EL, Sheetz MP (1999) Weak dependence of mobility of membrane protein aggregates on aggregate size supports a viscous model of retardation of diffusion. *Biophys J* 76:314-322.
- Kuriu T, Inoue A, Bito H, Sobue K, Okabe S (2006) Differential control of postsynaptic density scaffolds via actin-dependent and -independent mechanisms. *The Journal of neuroscience : the official journal of the Society for Neuroscience* 26:7693-7706.
- Kusumi A, Sako Y, Yamamoto M (1993) Confined lateral diffusion of membrane receptors as studied by single particle tracking (nanovid microscopy). Effects of calcium-induced differentiation in cultured epithelial cells. *Biophys J* 65:2021-2040.
- Kusumi A, Tsunoyama TA, Hirose KM, Kasai RS, Fujiwara TK (2014) Tracking single molecules at work in living cells. *Nature chemical biology* 10:524-532.
- Kusumi A, Nakada C, Ritchie K, Murase K, Suzuki K, Murakoshi H, Kasai RS, Kondo J, Fujiwara T (2005) Paradigm shift of the plasma membrane concept from the two-dimensional continuum fluid to the partitioned fluid: high-speed single-molecule tracking of membrane molecules. *Annual review of biophysics and biomolecular structure* 34:351-378.
- Lajoie P, Goetz JG, Dennis JW, Nabi IR (2009) Lattices, rafts, and scaffolds: domain regulation of receptor signaling at the plasma membrane. *J Cell Biol* 185:381-385.
- Lang C, Barco A, Zablow L, Kandel ER, Siegelbaum SA, Zakharenko SS (2004) Transient expansion of synaptically connected dendritic spines upon induction of hippocampal long-term potentiation. *Proceedings of the National Academy of Sciences of the United States of America* 101:16665-16670.
- Lee SH, Simonetta A, Sheng M (2004) Subunit rules governing the sorting of internalized AMPA receptors in hippocampal neurons. *Neuron* 43:221-236.
- Legant WR, Shao L, Grimm JB, Brown TA, Milkie DE, Avants BB, Lavis LD, Betzig E (2016) High-density three-dimensional localization microscopy across large volumes. *Nat Methods* 13:359-365.

- Levet F, Hosy E, Kechkar A, Butler C, Beghin A, Choquet D, Sibarita JB (2015) SR-Tesseler: a method to segment and quantify localization-based super-resolution microscopy data. *Nat Methods* 12:1065-1071.
- Levy JM, Chen X, Reese TS, Nicoll RA (2015) Synaptic Consolidation Normalizes AMPAR Quantal Size following MAGUK Loss. *Neuron* 87:534-548.
- Li TP, Song Y, MacGillavry HD, Blanpied TA, Raghavachari S (2016) Protein Crowding within the Postsynaptic Density Can Impede the Escape of Membrane Proteins. *The Journal of neuroscience : the official journal of the Society for Neuroscience* 36:4276-4295.
- Liley AW (1956) The quantal components of the mammalian end-plate potential. *The Journal of physiology* 133:571-587.
- Lin DT, Huganir RL (2007) PICK1 and phosphorylation of the glutamate receptor 2 (GluR2) AMPA receptor subunit regulates GluR2 recycling after NMDA receptor-induced internalization. *The Journal of neuroscience : the official journal of the Society for Neuroscience* 27:13903-13908.
- Lin DT, Makino Y, Sharma K, Hayashi T, Neve R, Takamiya K, Huganir RL (2009) Regulation of AMPA receptor extrasynaptic insertion by 4.1N, phosphorylation and palmitoylation. *Nature neuroscience* 12:879-887.
- Lin YC, Niewiadomski P, Lin B, Nakamura H, Phua SC, Jiao J, Levchenko A, Inoue T, Rohatgi R, Inoue T (2013) Chemically inducible diffusion trap at cilia reveals molecular sieve-like barrier. *Nature chemical biology* 9:437-443.
- Lisman J, Raghavachari S (2006) A unified model of the presynaptic and postsynaptic changes during LTP at CA1 synapses. *Sci STKE* 2006:re11.
- Lisman JE, Raghavachari S, Tsien RW (2007) The sequence of events that underlie quantal transmission at central glutamatergic synapses. *Nature reviews Neuroscience* 8:597-609.
- Liu G, Choi S, Tsien RW (1999) Variability of neurotransmitter concentration and nonsaturation of postsynaptic AMPA receptors at synapses in hippocampal cultures and slices. *Neuron* 22:395-409.

- Liu KS, Siebert M, Mertel S, Knoche E, Wegener S, Wichmann C, Matkovic T, Muhammad K, Depner H, Mettke C (2011) RIM-binding protein, a central part of the active zone, is essential for neurotransmitter release. *Science* 334:1565-1569.
- Lledo PM, Zhang X, Sudhof TC, Malenka RC, Nicoll RA (1998) Postsynaptic membrane fusion and long-term potentiation. *Science* 279:399-403.
- Lu HE, MacGillavry HD, Frost NA, Blanpied TA (2014) Multiple spatial and kinetic subpopulations of CaMKII in spines and dendrites as resolved by single-molecule tracking PALM. *The Journal of neuroscience : the official journal of the Society for Neuroscience* 34:7600-7610.
- Lucic V, Yang T, Schweikert G, Forster F, Baumeister W (2005) Morphological characterization of molecular complexes present in the synaptic cleft. *Structure* 13:423-434.
- MacGillavry HD, Kerr JM, Blanpied TA (2011) Lateral organization of the postsynaptic density. *Mol Cell Neurosci* 48:321-331.
- MacGillavry HD, Song Y, Raghavachari S, Blanpied TA (2013) Nanoscale scaffolding domains within the postsynaptic density concentrate synaptic AMPA receptors. *Neuron* 78:615-622.
- MacGillavry HD, Kerr JM, Kassner J, Frost NA, Blanpied TA (2016) Shank-cortactin interactions control actin dynamics to maintain flexibility of neuronal spines and synapses. *Eur J Neurosci* 43:179-193.
- Mainen ZF, Malinow R, Svoboda K (1999) Synaptic calcium transients in single spines indicate that NMDA receptors are not saturated. *Nature* 399:151-155.
- Makino H, Malinow R (2009) AMPA receptor incorporation into synapses during LTP: the role of lateral movement and exocytosis. *Neuron* 64:381-390.
- Malinow R, Malenka RC (2002) AMPA receptor trafficking and synaptic plasticity. *Annual review of neuroscience* 25:103-126.
- Man HY, Lin JW, Ju WH, Ahmadian G, Liu L, Becker LE, Sheng M, Wang YT (2000) Regulation of AMPA receptor-mediated synaptic transmission by clathrin-dependent receptor internalization. *Neuron* 25:649-662.

- Manley S, Gillette JM, Patterson GH, Shroff H, Hess HF, Betzig E, Lippincott-Schwartz J (2008) High-density mapping of single-molecule trajectories with photoactivated localization microscopy. *Nat Methods* 5:155-157.
- Martin SJ, Morris RG (2002) New life in an old idea: the synaptic plasticity and memory hypothesis revisited. *Hippocampus* 12:609-636.
- Masson JB, Dionne P, Salvatico C, Renner M, Specht CG, Triller A, Dahan M (2014) Mapping the energy and diffusion landscapes of membrane proteins at the cell surface using high-density single-molecule imaging and Bayesian inference: application to the multiscale dynamics of glycine receptors in the neuronal membrane. *Biophys J* 106:74-83.
- Masugi-Tokita M, Tarusawa E, Watanabe M, Molnar E, Fujimoto K, Shigemoto R (2007) Number and density of AMPA receptors in individual synapses in the rat cerebellum as revealed by SDS-digested freeze-fracture replica labeling. *The Journal of neuroscience : the official journal of the Society for Neuroscience* 27:2135-2144.
- Matsuzaki M, Honkura N, Ellis-Davies GC, Kasai H (2004) Structural basis of long-term potentiation in single dendritic spines. *Nature* 429:761-766.
- Matsuzaki M, Ellis-Davies GC, Nemoto T, Miyashita Y, Iino M, Kasai H (2001) Dendritic spine geometry is critical for AMPA receptor expression in hippocampal CA1 pyramidal neurons. *Nature neuroscience* 4:1086-1092.
- McAllister AK, Stevens CF (2000) Nonsaturation of AMPA and NMDA receptors at hippocampal synapses. *Proceedings of the National Academy of Sciences of the United States of America* 97:6173-6178.
- Mei Y, Monteiro P, Zhou Y, Kim JA, Gao X, Fu Z, Feng G (2016) Adult restoration of Shank3 expression rescues selective autistic-like phenotypes. *Nature* 530:481-484.
- Meier J, Vannier C, Serge A, Triller A, Choquet D (2001) Fast and reversible trapping of surface glycine receptors by gephyrin. *Nature neuroscience* 4:253-260.
- Michalet X, Pinaud FF, Bentolila LA, Tsay JM, Doose S, Li JJ, Sundaresan G, Wu AM, Gambhir SS, Weiss S (2005) Quantum dots for live cells, in vivo imaging, and diagnostics. *Science* 307:538-544.

- Milstein AD, Zhou W, Karimzadegan S, Bredt DS, Nicoll RA (2007) TARP subtypes differentially and dose-dependently control synaptic AMPA receptor gating. *Neuron* 55:905-918.
- Minton AP (2006) How can biochemical reactions within cells differ from those in test tubes? *J Cell Sci* 119:2863-2869.
- Missler M, Südhof TC, Biederer T (2012) Synaptic cell adhesion. *Cold Spring Harbor perspectives in biology* 4:a005694.
- Mondin M, Labrousse V, Hosy E, Heine M, Tessier B, Levet F, Poujol C, Blanchet C, Choquet D, Thoumine O (2011) Neurexin-neuroigin adhesions capture surface-diffusing AMPA receptors through PSD-95 scaffolds. *The Journal of neuroscience : the official journal of the Society for Neuroscience* 31:13500-13515.
- Moscato EH, Peng X, Jain A, Parsons TD, Dalmau J, Balice-Gordon RJ (2014) Acute mechanisms underlying antibody effects in anti-N-methyl-D-aspartate receptor encephalitis. *Ann Neurol* 76:108-119.
- Murray CJ et al. (2013) The state of US health, 1990-2010: burden of diseases, injuries, and risk factors. *JAMA* 310:591-608.
- Nair D, Hosy E, Petersen JD, Constals A, Giannone G, Choquet D, Sibarita JB (2013) Super-resolution imaging reveals that AMPA receptors inside synapses are dynamically organized in nanodomains regulated by PSD95. *The Journal of neuroscience : the official journal of the Society for Neuroscience* 33:13204-13224.
- Nakagawa T, Cheng Y, Ramm E, Sheng M, Walz T (2005) Structure and different conformational states of native AMPA receptor complexes. *Nature* 433:545-549.
- Nakamura Y, Harada H, Kamasawa N, Matsui K, Rothman JS, Shigemoto R, Silver RA, DiGregorio DA, Takahashi T (2015) Nanoscale distribution of presynaptic Ca²⁺ channels and its impact on vesicular release during development. *Neuron* 85:145-158.
- Newpher TM, Ehlers MD (2008) Glutamate receptor dynamics in dendritic microdomains. *Neuron* 58:472-497.

Nimchinsky EA, Yasuda R, Oertner TG, Svoboda K (2004) The number of glutamate receptors opened by synaptic stimulation in single hippocampal spines. *The Journal of neuroscience : the official journal of the Society for Neuroscience* 24:2054-2064.

NIMH (2002) Annual Total Direct and Indirect Costs of Serious Mental Illness. In.

Noguchi J, Nagaoka A, Watanabe S, Ellis-Davies GC, Kitamura K, Kano M, Matsuzaki M, Kasai H (2011) In vivo two-photon uncaging of glutamate revealing the structure-function relationships of dendritic spines in the neocortex of adult mice. *The Journal of physiology* 589:2447-2457.

Nuriya M, Huganir RL (2006) Regulation of AMPA receptor trafficking by N-cadherin. *J Neurochem* 97:652-661.

Nusser Z, Lujan R, Laube G, Roberts JD, Molnar E, Somogyi P (1998) Cell type and pathway dependence of synaptic AMPA receptor number and variability in the hippocampus. *Neuron* 21:545-559.

Okamoto K, Nagai T, Miyawaki A, Hayashi Y (2004) Rapid and persistent modulation of actin dynamics regulates postsynaptic reorganization underlying bidirectional plasticity. *Nature neuroscience* 7:1104-1112.

Opazo P, Choquet D (2011) A three-step model for the synaptic recruitment of AMPA receptors. *Mol Cell Neurosci* 46:1-8.

Opazo P, Sainlos M, Choquet D (2012) Regulation of AMPA receptor surface diffusion by PSD-95 slots. *Current opinion in neurobiology* 22:453-460.

Opazo P, Labrecque S, Tigaret CM, Frouin A, Wiseman PW, De Koninck P, Choquet D (2010) CaMKII triggers the diffusional trapping of surface AMPARs through phosphorylation of stargazin. *Neuron* 67:239-252.

Pantazopoulos H, Berretta S (2016) In Sickness and in Health: Perineuronal Nets and Synaptic Plasticity in Psychiatric Disorders. *Neural Plast* 2016:9847696.

Park M, Penick EC, Edwards JG, Kauer JA, Ehlers MD (2004) Recycling endosomes supply AMPA receptors for LTP. *Science* 305:1972-1975.

- Park M, Salgado JM, Ostroff L, Helton TD, Robinson CG, Harris KM, Ehlers MD (2006) Plasticity-induced growth of dendritic spines by exocytic trafficking from recycling endosomes. *Neuron* 52:817-830.
- Pastalkova E, Serrano P, Pinkhasova D, Wallace E, Fenton AA, Sacktor TC (2006) Storage of spatial information by the maintenance mechanism of LTP. *Science* 313:1141-1144.
- Peng J, Kim MJ, Cheng D, Duong DM, Gygi SP, Sheng M (2004) Semiquantitative proteomic analysis of rat forebrain postsynaptic density fractions by mass spectrometry. *J Biol Chem* 279:21003-21011.
- Penzes P, Cahill ME, Jones KA, VanLeeuwen JE, Woolfrey KM (2011) Dendritic spine pathology in neuropsychiatric disorders. *Nature neuroscience* 14:285-293.
- Perez de Arce K, Schrod N, Metzbower SW, Allgeyer E, Kong GK, Tang AH, Krupp AJ, Stein V, Liu X, Bewersdorf J, Blanpied TA, Lucic V, Biederer T (2015) Topographic Mapping of the Synaptic Cleft into Adhesive Nanodomains. *Neuron* 88:1165-1172.
- Perrin J (1909) Mouvement brownien et réalité moléculaire. *Annales de Chimie et de Physique*.
- Petersen JD, Chen X, Vinade L, Dosemeci A, Lisman JE, Reese TS (2003) Distribution of postsynaptic density (PSD)-95 and Ca²⁺/calmodulin-dependent protein kinase II at the PSD. *The Journal of neuroscience : the official journal of the Society for Neuroscience* 23:11270-11278.
- Petralia RS, Wang YX, Wenthold RJ (2003) Internalization at glutamatergic synapses during development. *Eur J Neurosci* 18:3207-3217.
- Poncer JC, Durr R, Gahwiler BH, Thompson SM (1996) Modulation of synaptic GABA_A receptor function by benzodiazepines in area CA3 of rat hippocampal slice cultures. *Neuropharmacology* 35:1169-1179.
- Racz B, Blanpied TA, Ehlers MD, Weinberg RJ (2004) Lateral organization of endocytic machinery in dendritic spines. *Nature neuroscience* 7:917-918.

- Raghavachari S, Lisman JE (2004) Properties of quantal transmission at CA1 synapses. *Journal of neurophysiology* 92:2456-2467.
- Ramón Y Cajal S (1894) The Croonian Lecture: La Fine Structure des Centres Nerveux. *Proceedings of the Royal Society of London* 55:444-468.
- Reits EA, Neefjes JJ (2001) From fixed to FRAP: measuring protein mobility and activity in living cells. *Nat Cell Biol* 3:E145-147.
- Renner ML, Cognet L, Lounis B, Triller A, Choquet D (2009) The excitatory postsynaptic density is a size exclusion diffusion environment. *Neuropharmacology* 56:30-36.
- Ryan TA, Myers J, Holowka D, Baird B, Webb WW (1988) Molecular crowding on the cell surface. *Science* 239:61-64.
- Saffman PG, Delbruck M (1975) Brownian motion in biological membranes. *Proceedings of the National Academy of Sciences of the United States of America* 72:3111-3113.
- Saglietti L, Dequidt C, Kamieniarz K, Rousset MC, Valnegri P, Thoumine O, Beretta F, Fagni L, Choquet D, Sala C, Sheng M, Passafaro M (2007) Extracellular interactions between GluR2 and N-cadherin in spine regulation. *Neuron* 54:461-477.
- Sainlos M, Tigaret C, Poujol C, Olivier NB, Bard L, Breillat C, Thiolon K, Choquet D, Imperiali B (2011) Biomimetic divalent ligands for the acute disruption of synaptic AMPAR stabilization. *Nature chemical biology* 7:81-91.
- Sako Y, Kusumi A (1995) Barriers for lateral diffusion of transferrin receptor in the plasma membrane as characterized by receptor dragging by laser tweezers: fence versus tether. *J Cell Biol* 129:1559-1574.
- Santamaria F, Gonzalez J, Augustine GJ, Raghavachari S (2010) Quantifying the effects of elastic collisions and non-covalent binding on glutamate receptor trafficking in the post-synaptic density. *PLoS computational biology* 6:e1000780.
- Santucci DM, Raghavachari S (2008) The effects of NR2 subunit-dependent NMDA receptor kinetics on synaptic transmission and CaMKII activation. *PLoS Comput Biol* 4:e1000208.

- Sargent PB, Saviane C, Nielsen TA, DiGregorio DA, Silver RA (2005) Rapid vesicular release, quantal variability, and spillover contribute to the precision and reliability of transmission at a glomerular synapse. *The Journal of neuroscience : the official journal of the Society for Neuroscience* 25:8173-8187.
- Saro D, Li T, Rupasinghe C, Paredes A, Caspers N, Spaller MR (2007) A thermodynamic ligand binding study of the third PDZ domain (PDZ3) from the mammalian neuronal protein PSD-95. *Biochemistry* 46:6340-6352.
- Savin T, Doyle PS (2005) Static and dynamic errors in particle tracking microrheology. *Biophys J* 88:623-638.
- Saxton MJ (1994) Anomalous diffusion due to obstacles: a Monte Carlo study. *Biophys J* 66:394-401.
- Saxton MJ (2010) Two-dimensional continuum percolation threshold for diffusing particles of nonzero radius. *Biophys J* 99:1490-1499.
- Saxton MJ, Jacobson K (1997) Single-particle tracking: applications to membrane dynamics. *Annual review of biophysics and biomolecular structure* 26:373-399.
- Schauder DM, Kuybeda O, Zhang J, Klymko K, Bartesaghi A, Borgnia MJ, Mayer ML, Subramaniam S (2013) Glutamate receptor desensitization is mediated by changes in quaternary structure of the ligand binding domain. *Proceedings of the National Academy of Sciences of the United States of America* 110:5921-5926.
- Schikorski T, Stevens CF (1997) Quantitative ultrastructural analysis of hippocampal excitatory synapses. *The Journal of neuroscience : the official journal of the Society for Neuroscience* 17:5858-5867.
- Schneider R, Hosy E, Kohl J, Klueva J, Choquet D, Thomas U, Voigt A, Heine M (2015) Mobility of calcium channels in the presynaptic membrane. *Neuron* 86:672-679.
- Schnell E, Sizemore M, Karimzadegan S, Chen L, Brecht DS, Nicoll RA (2002) Direct interactions between PSD-95 and stargazin control synaptic AMPA receptor number. *Proceedings of the National Academy of Sciences of the United States of America* 99:13902-13907.

- Schwenk J, Harmel N, Zolles G, Bildl W, Kulik A, Heimrich B, Chisaka O, Jonas P, Schulte U, Fakler B, Klockner N (2009) Functional proteomics identify cornichon proteins as auxiliary subunits of AMPA receptors. *Science* 323:1313-1319.
- Schwenk J, Harmel N, Brechet A, Zolles G, Berkefeld H, Muller CS, Bildl W, Baehrens D, Huber B, Kulik A, Klockner N, Schulte U, Fakler B (2012) High-resolution proteomics unravel architecture and molecular diversity of native AMPA receptor complexes. *Neuron* 74:621-633.
- Scimemi A, Diamond JS (2012) The Number and Organization of Ca²⁺ Channels in the Active Zone Shapes Neurotransmitter Release from Schaffer Collateral Synapses. *The Journal of Neuroscience* 32:18157-18176.
- Scoville WB, Milner B (1957) Loss of recent memory after bilateral hippocampal lesions. *J Neurol Neurosurg Psychiatry* 20:11-21.
- Sdrulla AD, Linden DJ (2007) Double dissociation between long-term depression and dendritic spine morphology in cerebellar Purkinje cells. *Nature neuroscience* 10:546-548.
- Serge A, Fargeaud L, Hemar A, Choquet D (2002) Receptor activation and homer differentially control the lateral mobility of metabotropic glutamate receptor 5 in the neuronal membrane. *The Journal of neuroscience : the official journal of the Society for Neuroscience* 22:3910-3920.
- Sharma K, Fong DK, Craig AM (2006) Postsynaptic protein mobility in dendritic spines: long-term regulation by synaptic NMDA receptor activation. *Mol Cell Neurosci* 31:702-712.
- Sheets ED, Lee GM, Simson R, Jacobson K (1997) Transient confinement of a glycosylphosphatidylinositol-anchored protein in the plasma membrane. *Biochemistry* 36:12449-12458.
- Shen K, Meyer T (1999) Dynamic control of CaMKII translocation and localization in hippocampal neurons by NMDA receptor stimulation. *Science* 284:162-166.
- Sheng M, Hoogenraad CC (2007) The postsynaptic architecture of excitatory synapses: a more quantitative view. *Annu Rev Biochem* 76:823-847.

- Sheng M, Kim E (2011) The postsynaptic organization of synapses. *Cold Spring Harb Perspect Biol* 3.
- Shin SM, Zhang N, Hansen J, Gerges NZ, Pak DT, Sheng M, Lee SH (2012) GKAP orchestrates activity-dependent postsynaptic protein remodeling and homeostatic scaling. *Nature neuroscience* 15:1655-1666.
- Shinohara Y, Hirase H, Watanabe M, Itakura M, Takahashi M, Shigemoto R (2008) Left-right asymmetry of the hippocampal synapses with differential subunit allocation of glutamate receptors. *Proceedings of the National Academy of Sciences of the United States of America* 105:19498-19503.
- Shipman SL, Nicoll RA (2012) Dimerization of postsynaptic neuroligin drives synaptic assembly via transsynaptic clustering of neurexin. *Proceedings of the National Academy of Sciences of the United States of America* 109:19432-19437.
- Siddiqui TJ, Craig AM (2011) Synaptic organizing complexes. *Current opinion in neurobiology* 21:132-143.
- Silver RA, Cull-Candy SG, Takahashi T (1996) Non-NMDA glutamate receptor occupancy and open probability at a rat cerebellar synapse with single and multiple release sites. *The Journal of physiology* 494 (Pt 1):231-250.
- Silverman JB, Restituito S, Lu W, Lee-Edwards L, Khatri L, Ziff EB (2007) Synaptic anchorage of AMPA receptors by cadherins through neural plakophilin-related arm protein AMPA receptor-binding protein complexes. *The Journal of neuroscience : the official journal of the Society for Neuroscience* 27:8505-8516.
- Simon CM, Hepburn I, Chen W, De Schutter E (2014) The role of dendritic spine morphology in the compartmentalization and delivery of surface receptors. *J Comput Neurosci* 36:483-497.
- Simson R, Yang B, Moore SE, Doherty P, Walsh FS, Jacobson KA (1998) Structural mosaicism on the submicron scale in the plasma membrane. *Biophys J* 74:297-308.
- Singer SJ, Nicolson GL (1972) The fluid mosaic model of the structure of cell membranes. *Science* 175:720-731.

- Smith MA, Ellis-Davies GC, Magee JC (2003) Mechanism of the distance-dependent scaling of Schaffer collateral synapses in rat CA1 pyramidal neurons. *The Journal of physiology* 548:245-258.
- Sobolevsky AI, Rosconi MP, Gouaux E (2009) X-ray structure, symmetry and mechanism of an AMPA-subtype glutamate receptor. *Nature* 462:745-756.
- Somogyi P, Tamas G, Lujan R, Buhl EH (1998) Salient features of synaptic organisation in the cerebral cortex. *Brain Res Brain Res Rev* 26:113-135.
- Song I, Huganir RL (2002) Regulation of AMPA receptors during synaptic plasticity. *Trends Neurosci* 25:578-588.
- Soto D, Coombs ID, Renzi M, Zonouzi M, Farrant M, Cull-Candy SG (2009) Selective regulation of long-form calcium-permeable AMPA receptors by an atypical TARP, gamma-5. *Nature neuroscience* 12:277-285.
- Spacek J, Hartmann M (1983) Three-dimensional analysis of dendritic spines. I. Quantitative observations related to dendritic spine and synaptic morphology in cerebral and cerebellar cortices. *Anat Embryol (Berl)* 167:289-310.
- Squire LR (1982) The neuropsychology of human memory. *Annual review of neuroscience* 5:241-273.
- Squire LR (1992) Memory and the hippocampus: a synthesis from findings with rats, monkeys, and humans. *Psychol Rev* 99:195-231.
- Steiner P, Higley MJ, Xu W, Czervionke BL, Malenka RC, Sabatini BL (2008) Destabilization of the postsynaptic density by PSD-95 serine 73 phosphorylation inhibits spine growth and synaptic plasticity. *Neuron* 60:788-802.
- Stewart MG, Medvedev NI, Popov VI, Schoepfer R, Davies HA, Murphy K, Dallerac GM, Kraev IV, Rodriguez JJ (2005) Chemically induced long-term potentiation increases the number of perforated and complex postsynaptic densities but does not alter dendritic spine volume in CA1 of adult mouse hippocampal slices. *Eur J Neurosci* 21:3368-3378.
- Sudhof TC (2008) Neuroligins and neurexins link synaptic function to cognitive disease. *Nature* 455:903-911.

- Sugiyama Y, Kawabata I, Sobue K, Okabe S (2005) Determination of absolute protein numbers in single synapses by a GFP-based calibration technique. *Nat Methods* 2:677-684.
- Sumioka A, Yan D, Tomita S (2010) TARP phosphorylation regulates synaptic AMPA receptors through lipid bilayers. *Neuron* 66:755-767.
- Takumi Y, Ramirez-Leon V, Laake P, Rinvik E, Ottersen OP (1999) Different modes of expression of AMPA and NMDA receptors in hippocampal synapses. *Nature neuroscience* 2:618-624.
- Tanaka J, Matsuzaki M, Tarusawa E, Momiyama A, Molnar E, Kasai H, Shigemoto R (2005) Number and density of AMPA receptors in single synapses in immature cerebellum. *The Journal of neuroscience : the official journal of the Society for Neuroscience* 25:799-807.
- Tang A-H, Chen H, Li TP, Metzbower SR, MacGillavry HD, Blanpied TA (2016) A transsynaptic nanocolumn aligns neurotransmitter release to receptors. *Nature*.
- Tao-Cheng JH, Crocker VT, Winters CA, Azzam R, Chludzinski J, Reese TS (2011) Trafficking of AMPA receptors at plasma membranes of hippocampal neurons. *The Journal of neuroscience : the official journal of the Society for Neuroscience* 31:4834-4843.
- Tardin C, Cognet L, Bats C, Lounis B, Choquet D (2003) Direct imaging of lateral movements of AMPA receptors inside synapses. *EMBO J* 22:4656-4665.
- Tarr TB, Dittrich M, Meriney SD (2013) Are unreliable release mechanisms conserved from NMJ to CNS? *Trends in neurosciences* 36:14-22.
- Tarusawa E, Matsui K, Budisantoso T, Molnár E, Watanabe M, Matsui M, Fukazawa Y, Shigemoto R (2009) Input-specific intrasynaptic arrangements of ionotropic glutamate receptors and their impact on postsynaptic responses. *The Journal of Neuroscience* 29:12896-12908.
- Thompson RE, Larson DR, Webb WW (2002) Precise nanometer localization analysis for individual fluorescent probes. *Biophys J* 82:2775-2783.

- Tomita S, Fukata M, Nicoll RA, Brecht DS (2004) Dynamic interaction of stargazin-like TARPs with cycling AMPA receptors at synapses. *Science* 303:1508-1511.
- Tomita S, Stein V, Stocker TJ, Nicoll RA, Brecht DS (2005) Bidirectional synaptic plasticity regulated by phosphorylation of stargazin-like TARPs. *Neuron* 45:269-277.
- Tomita S, Chen L, Kawasaki Y, Petralia RS, Wenthold RJ, Nicoll RA, Brecht DS (2003) Functional studies and distribution define a family of transmembrane AMPA receptor regulatory proteins. *J Cell Biol* 161:805-816.
- Tonnesen J, Katona G, Rozsa B, Nagerl UV (2014) Spine neck plasticity regulates compartmentalization of synapses. *Nature neuroscience* 17:678-685.
- Traynelis SF, Wollmuth LP, McBain CJ, Menniti FS, Vance KM, Ogden KK, Hansen KB, Yuan H, Myers SJ, Dingledine R (2010) Glutamate receptor ion channels: structure, regulation, and function. *Pharmacol Rev* 62:405-496.
- Triller A, Choquet D (2005) Surface trafficking of receptors between synaptic and extrasynaptic membranes: and yet they do move! *Trends Neurosci* 28:133-139.
- Triller A, Choquet D (2008) New concepts in synaptic biology derived from single-molecule imaging. *Neuron* 59:359-374.
- Trimble WS, Grinstein S (2015) Barriers to the free diffusion of proteins and lipids in the plasma membrane. *J Cell Biol* 208:259-271.
- Tsokas P, Hsieh C, Yao Y, Lesburgueres E, Wallace EJ, Tcherepanov A, Jothianandan D, Hartley BR, Pan L, Rivard B, Farese RV, Sajan MP, Bergold PJ, Hernandez AI, Cottrell JE, Shouval HZ, Fenton AA, Sacktor TC (2016) Compensation for PKMzeta in long-term potentiation and spatial long-term memory in mutant mice. *Elife* 5.
- Uchida N, Honjo Y, Johnson KR, Wheelock MJ, Takeichi M (1996) The catenin/cadherin adhesion system is localized in synaptic junctions bordering transmitter release zones. *J Cell Biol* 135:767-779.
- Usui S, Konno D, Hori K, Maruoka H, Okabe S, Fujikado T, Tano Y, Sobue K (2003) Synaptic targeting of PSD-Zip45 (Homer 1c) and its involvement in the synaptic accumulation of F-actin. *J Biol Chem* 278:10619-10628.

- Valtschanoff JG, Weinberg RJ (2001) Laminar organization of the NMDA receptor complex within the postsynaptic density. *The Journal of neuroscience : the official journal of the Society for Neuroscience* 21:1211-1217.
- Vandenberghe W, Nicoll RA, Brecht DS (2005) Interaction with the unfolded protein response reveals a role for stargazin in biosynthetic AMPA receptor transport. *The Journal of neuroscience : the official journal of the Society for Neuroscience* 25:1095-1102.
- Volk L, Chiu S-L, Sharma K, Huganir RL (2015) Glutamate Synapses in Human Cognitive Disorders. *Annu Rev Neurosci* 38:127-149.
- von Engelhardt J, Mack V, Sprengel R, Kavenstock N, Li KW, Stern-Bach Y, Smit AB, Seeburg PH, Monyer H (2010) CKAMP44: a brain-specific protein attenuating short-term synaptic plasticity in the dentate gyrus. *Science* 327:1518-1522.
- Wang X, McCoy PA, Rodriguiz RM, Pan Y, Je HS, Roberts AC, Kim CJ, Berrios J, Colvin JS, Bousquet-Moore D, Lorenzo I, Wu G, Weinberg RJ, Ehlers MD, Philpot BD, Beaudet AL, Wetsel WC, Jiang YH (2011) Synaptic dysfunction and abnormal behaviors in mice lacking major isoforms of Shank3. *Hum Mol Genet* 20:3093-3108.
- Wang XB, Yang Y, Zhou Q (2007) Independent expression of synaptic and morphological plasticity associated with long-term depression. *The Journal of neuroscience : the official journal of the Society for Neuroscience* 27:12419-12429.
- Wang Y, Cai E, Rosenkranz T, Ge P, Teng KW, Lim SJ, Smith AM, Chung HJ, Sachs F, Green WN, Gottlieb P, Selvin PR (2014) Small quantum dots conjugated to nanobodies as immunofluorescence probes for nanometric microscopy. *Bioconjug Chem* 25:2205-2211.
- Welch JM, Lu J, Rodriguiz RM, Trotta NC, Peca J, Ding JD, Feliciano C, Chen M, Adams JP, Luo J, Dudek SM, Weinberg RJ, Calakos N, Wetsel WC, Feng G (2007) Cortico-striatal synaptic defects and OCD-like behaviours in Sapap3-mutant mice. *Nature* 448:894-900.
- Whitlock JR, Heynen AJ, Shuler MG, Bear MF (2006) Learning induces long-term potentiation in the hippocampus. *Science* 313:1093-1097.

- Winckler B, Forscher P, Mellman I (1999) A diffusion barrier maintains distribution of membrane proteins in polarized neurons. *Nature* 397:698-701.
- Xie X, Liaw JS, Baudry M, Berger TW (1997) Novel expression mechanism for synaptic potentiation: alignment of presynaptic release site and postsynaptic receptor. *Proceedings of the National Academy of Sciences of the United States of America* 94:6983-6988.
- Xu W, Schluter OM, Steiner P, Czervionke BL, Sabatini B, Malenka RC (2008) Molecular dissociation of the role of PSD-95 in regulating synaptic strength and LTD. *Neuron* 57:248-262.
- Yamashita T, Ishikawa T, Takahashi T (2003) Developmental increase in vesicular glutamate content does not cause saturation of AMPA receptors at the calyx of Held synapse. *The Journal of neuroscience : the official journal of the Society for Neuroscience* 23:3633-3638.
- Yamashita T, Kanda T, Eguchi K, Takahashi T (2009) Vesicular glutamate filling and AMPA receptor occupancy at the calyx of Held synapse of immature rats. *The Journal of physiology* 587:2327-2339.
- Yang M, Bozdagi O, Scattoni ML, Wohr M, Roulet FI, Katz AM, Abrams DN, Kalikhman D, Simon H, Woldeyohannes L, Zhang JY, Harris MJ, Saxena R, Silverman JL, Buxbaum JD, Crawley JN (2012) Reduced excitatory neurotransmission and mild autism-relevant phenotypes in adolescent Shank3 null mutant mice. *The Journal of neuroscience : the official journal of the Society for Neuroscience* 32:6525-6541.
- Young SH, Poo MM (1983) Rapid lateral diffusion of extrajunctional acetylcholine receptors in the developing muscle membrane of *Xenopus* tadpole. *The Journal of neuroscience : the official journal of the Society for Neuroscience* 3:225-231.
- Yudowski GA, Puthenveedu MA, Leonoudakis D, Panicker S, Thorn KS, Beattie EC, von Zastrow M (2007) Real-time imaging of discrete exocytic events mediating surface delivery of AMPA receptors. *The Journal of neuroscience : the official journal of the Society for Neuroscience* 27:11112-11121.
- Zhang H, Etherington LA, Hafner AS, Belelli D, Coussen F, Delagrance P, Chaouloff F, Spedding M, Lambert JJ, Choquet D, Groc L (2013) Regulation of AMPA receptor surface trafficking and synaptic plasticity by a cognitive enhancer and antidepressant molecule. *Mol Psychiatry* 18:471-484.

Zhang M, Chang H, Zhang Y, Yu J, Wu L, Ji W, Chen J, Liu B, Lu J, Liu Y, Zhang J, Xu P, Xu T (2012) Rational design of true monomeric and bright photoactivatable fluorescent proteins. *Nat Methods* 9:727-729.

Zhou Q, Homma KJ, Poo MM (2004) Shrinkage of dendritic spines associated with long-term depression of hippocampal synapses. *Neuron* 44:749-757.

Ziv NE, Fisher-Lavie A (2014) Presynaptic and postsynaptic scaffolds: dynamics fast and slow. *Neuroscientist* 20:439-452.

Zoghbi HY, Bear MF (2012) Synaptic dysfunction in neurodevelopmental disorders associated with autism and intellectual disabilities. *Cold Spring Harbor perspectives in biology* 4:a009886.